AD-A044 689 CONTROL DATA CORP MELVILLE N Y TRG DIV F/G 20/1
PURVIS II SEA TRIALS PRELIMINARY DATA ANALYSIS REPORT. VOLUME I--ETC(U)
MAR 67 D CHASE, R NEWMAN NOBSR-93023
UNCLASSIFIED TRG-023-TM-67-10 NL

1 OF 2
AD A044689

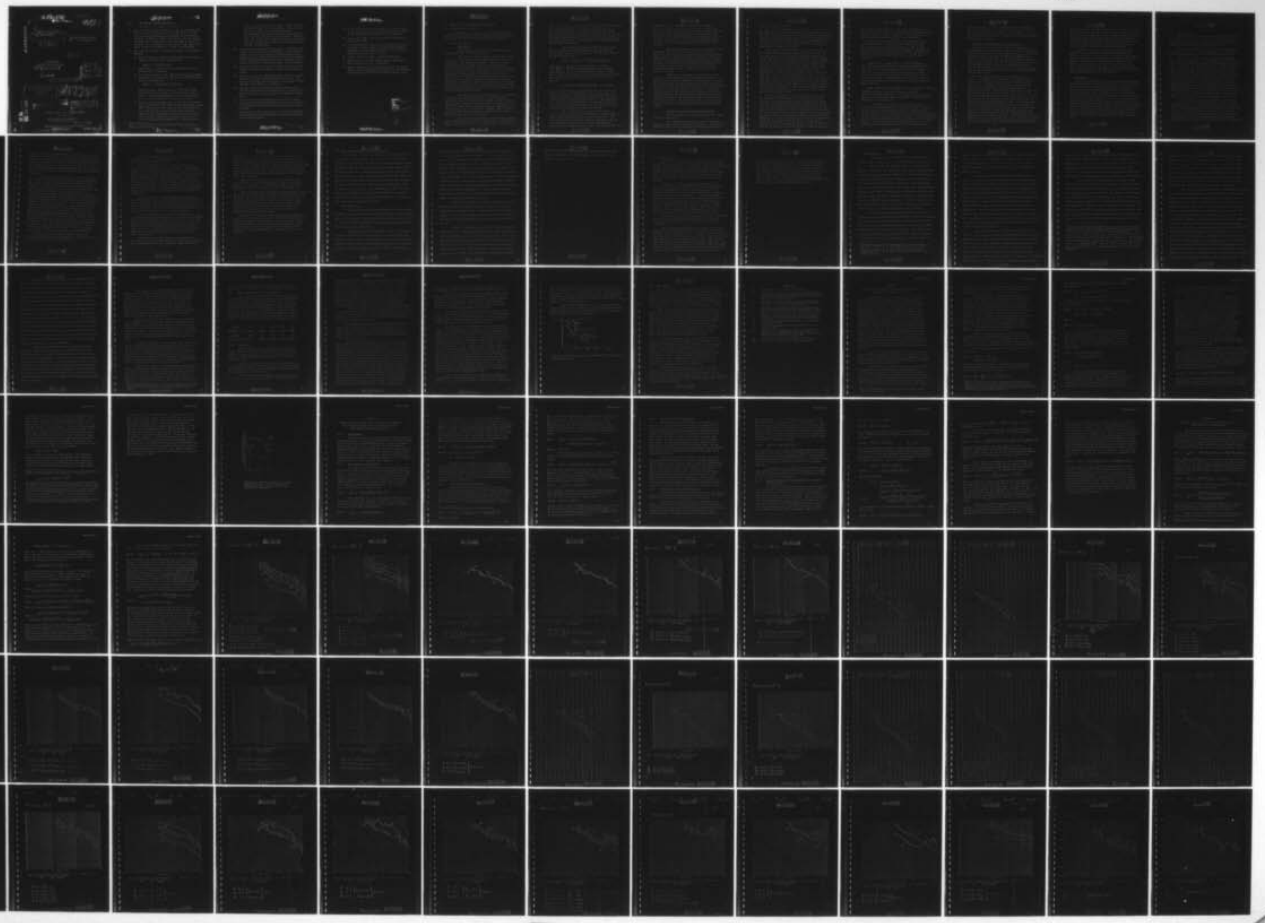

13B051-47016

MOST Project-3

(1) D.S.

DRAFT

(6) PURVIS II SEA TRIALS
PRELIMINARY DATA ANALYSIS REPORT,
VOL. II & III (U)
Volume II and III

This Document Consists of 116 Pages
No. 3 of 5 Copies Series A

(10) D. Chase,
R. Newman

(12) 110

TRG DIVISION
CONTROL DATA CORPORATION

(14) TRG-023-TM-67-10

(11) March 1967

DISTRIBUTION STATEMENT A
Approved for public release;
Distribution Unlimited

(15) Produced Under Contract NObsr-93023
for Code 2110

NAVY ELECTRONICS LABORATORY
San Diego, California

CONFORMAL/PLANAR ARRAY SONAR SYSTEM

670713-0464

0.0 Conclusions and Recommendations

We cite several salient conclusions:

1) Turbulent boundary-layer (TBL) noise appears to dominate the noise measured by flush elements of 5-in. diameter in the forward array (HF) through substantially all the frequency range 0.2 to 10 KHz at speeds 15 to 30 kt. The same appears generally true of the further aft array (LF) at speeds 20 to 30 kt. As an indication of the absolute noise levels, at 20 kt on HF-3 at 2.5 KHz it is -20 db re $(1\ \mu\text{bar})^2/\text{Hz}$.

2) Where TBL noise on these large flush elements is thought predominant:

   a) At fixed distance aft the scaling of the noise spectrum $P(\omega/2\pi)$ is fairly well represented by*

   $$P(\omega/2\pi) = \rho^2 \delta_* U_\infty^3 \pi_1(\omega\delta_*/U_\infty).$$

   With distance aft fixed, however, the appearance of δ_* in this form is arbitrary.

   b) At differing distances aft (but at fixed R_o) the scaling is fairly well represented, especially in an intermediate range of frequency, by

   $$P(\omega/2\pi) = \rho^2 \delta_* U_\infty (\omega R_o/U_\infty)^{-2} F(\omega\delta_*/U_\infty).$$

   $P(\omega/2\pi)$, however, varies roughly as ω^{-3} in this range; hence this form, so far as δ_* is concerned, merely reflects approximate independence of δ_*, and therefore its use in the scaling is not uniquely justified.

   c) Relative to the measured noise on small elements (radius r_o), in roughly the lower third of the log frequency range 0.2 to 10 KHz, where the small elements in question are not seriously affected by area averaging, the noise spectra on the large elements diverge from those on the small according roughly to a reduction factor due to area averaging given by $(\omega R_o/0.6U_\infty)^{-s}$, where R_o is the

*Here U_∞ denotes ship speed and δ_* boundary-layer displacement thickness at the element.

large element radius, with s slightly larger than two. At somewhat higher frequency, however, instead of becoming parallel, with a fixed db separation $10s \log(R_o/r_o)$, the spectra for large and small elements somewhat converge toward one another. Nevertheless, the spectra for the large elements in this region continue to scale with speed as may be expected where TBL noise predominates.

3) Regarding the G elements at the sea chest 2 location, the element flush-mounted in the fiberglass window, and especially the element recessed in a flooded cavity behind, display large speed-dependent humps in their noise spectra in a broad high-frequency range. These humps are tentatively attributed to effects of bubbles at this location.

4) Recession of elements in the water-filled cavity may have reduced flow noise more than it reduced sensitivity to a signal.

5) Recession of elements (D) behind rubber layers of varying thickness may have moderately reduced flow noise. The extent of reduction did not depend systematically on layer thickness from 59/64 in. to 5-1/32 in.

6) The noise spectra of the layer-shielded elements above 1.5 KHz varied widely and erratically from element to element. This effect may have been due to splash or bubble noise.

7) The measured in-situ calibration curves for the window-mounted and layer-covered elements in many cases varied in an unexplained fashion with time, frequency, and element identity.

On the basis of the present report we offer the following recommendations regarding further processing and analysis of the PURVIS II data.

a) Study carefully the indicated paths of natural bubbles as they depend on speed and maneuver and try to relate to the measured noise spectra for the G elements.

b) Process and analyze spectra for other G elements, including G9 or G10.

c) Investigate the variability of noise spectra for D and G elements and the dependence on turns and headings, and listen to audio noise reproductions to the end of identifying possible noise sources.

d) Further reduce and analyze in-situ calibrations.

e) With reference to the HF and LF spectra, investigate other proposed TBL noise scaling laws.

f) Analyze spectra for more HF and LF elements at various speeds and give particular consideration to the tendency of spectra to level off in the middle frequency range.

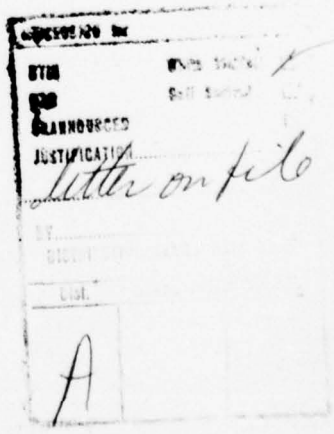

3. Analysis and Interpretation of Noise Data

3.1 Flush Wall-Mounted Elements

The hydrophones of this category are comprised by the groups designated HF, LF, and H. Flush elements G9 and G10 are considered with the other G elements in Section 3.2.

3.1.1 Autospectra

HF Elements

Noise spectra measured for several HF elements are shown in Figs. 3.1.1-1 to 3.1.1-8.

One objective of the analysis of the noise measurements is to infer the character of the noise on an element as a function of the pertinent variables. The types of noise contributing may be broadly classified as produced by an acoustic field or directly by pressure fluctuations associated with the turbulent boundary layer (TBL). The former, however, may include a component due to excitation of non-rigid boundaries by the turbulent flow; the locally generated part of this component may not be additive but correlated with the direct TBL contribution. While the acoustic noise will depend on the specific ship and element configuration, the direct TBL noise spectra at a given speed, distance aft, and element size will be substantially universal.

Referring first to the HF elements, we see from the figures that at speeds 15 kt to 30 kt, the noise spectra typically increase with speed nearly as U_∞^6. At these speeds, the frequency dependence, on the average, is roughly as $\omega^{-2.7}$ to $\omega^{-3.7}$. Below 15 kt, though the frequency dependence is not much different, the speed dependence weakens. These features accord with tentative expectation if TBL flow noise is the dominant noise source at 15 to 30 kt.

The extent of variability of measured noise spectra from one HF element to another is rather small. A typical comparison is that between HF-5 and HF-12 in Figs. 3.1.1-3 and 4.

(Since these elements are separated by 10.5 in. circumferentially, the comparison indicates an increased noise for the element nearer the water surface, if attributed to this cause rather than to mere statistical deviation, by about 3 db at 20 kt.) At the higher speeds, the small variation among elements reinforces the presumption that the dominant noise is that due directly to TBL pressure fluctuations.

According to the "outer" scaling law for the TBL pressure spectrum, which corresponds to the usual type of dimensionless plot of measured spectra, the TBL noise spectrum has the functional form

$$(3\text{-}1) \qquad P(\omega/2\pi) = \rho^2 \delta_* U_\infty^3 \pi_1(\omega\delta_*/U_\infty),$$

where π_1 is a function of the dimensionless argument $\Omega_1 \equiv \omega\delta_*/U_\infty$, ρ is the fluid density, U_∞ the asymptotic flow speed, and δ_* displacement thickness. Hence, if this form is valid, in the absence of other appreciable noise sources the measured spectra for different speeds will coalesce on plots of

$$(3\text{-}2) \qquad 10 \log [P(\omega/2\pi)/\delta_* U_\infty^3] \text{ vs. } 10 \log \Omega_1 .$$

Even if the form (3-1) is valid for the TBL noise on a point element, however, it will be valid for a large element, i.e. one where $\omega\delta_*/U_\infty \gtrsim 1$, only at fixed R_o/δ_*, since π_1 in this regime depends on R_o/δ_* as well as on Ω_1. The dependence of δ_* on U_∞ is sufficiently weak (see App. 1) that at fixed distance aft (and fixed R_o) a test of the outer scaling law (3-1) is meaningful also for large elements.

The coupled speed and frequency dependence of measured noise spectra for the HF elements is tested explicitly against the scaling law (3-1) in Figs. 3.1.1-7 and 8. The measured data agree fairly well with the suppositions that in the speed range 15 to 30 kt the principal contribution to noise spectra on the HF elements is due to the TBL and that this

contribution, at fixed δ_*/R_c, satisfies the scaling law (3-1), at least in an extensive middle range of frequency. According to these suppositions, at the lower speeds 5 and 10 kt, on the other hand, the TBL noise contribution is small relative to other noise, being lower than the total noise in the case of element HF-3, for example, by about 3 to 14 db, depending on frequency, at 10 kt and by about 18 to 25 db at 5 kt.

Alternative possible scaling laws for TBL pressure that differ from (3-1) can be proposed (e.g. see Ref. 3). Applied to the instance of a large element, these would yield speed dependences that differ only moderately from that given by (3-1). Hence, while our conclusion regarding the relative magnitude of the TBL noise contribution is not subverted, we must maintain an open mind as to whether (3-1) correctly represents the TBL scaling. Further pertinent comparisons will be made below.

Regarding the dependence of noise spectra of HF elements on heading and turning conditions, Fig. 3.1.1-5 shows results for HF-3 at 20 kt for headings 0°, 90°, and 270°. The result at 180° is nearly identical with that at 0° and is therefore omitted. At this speed the noise is evidently nearly independent of heading except for local peaks in the high-frequency range in the instance of 90° heading. Fig. 3.1.1-6 shows results also for HF-3 at 20 kt at heading 0° and during a full right rudder turn. The level in the turn is about 1 to 3 db above the other. In a full left rudder turn the result for this element is nearly identical with that for full right rudder.

LF Elements and Comparison with HF Elements

Measured spectra for various LF elements are shown in Figs. 3.1.1-9 to 13.

The variation of noise level among LF elements is perhaps somewhat greater than among HF elements. Measured noise spectra for LF-6, for the most part, lie below those for the

other processed LF elements.

Figs. 3.1.1-9 and 10 show that the noise spectra for LF-6 and LF-7 first rise appreciably above the zero-speed level at 15 kt. (Indeed, the measured spectra at 10 kt in the high-frequency region unaccountably lie below those at 0 kt.) Nevertheless, no appreciable increase in noise spectra is measured between 15 and 20 kt. At 25 kt and especially 30 kt the measured increments in noise, however, are large.

Noise spectra for LF-6 and LF-7 are compared with those for a typical HF element, HF-3, in Figs. 3.1.1-14 to 16. At zero speed the levels for the LF's are higher than that for the HF, which has a more secluded, forward position, by about 18 db. At 20 kt, by which the LF levels have surmounted their high values for zero speed, LF-7 lies several db above HF-3 and LF-6 at moderate frequencies, and all three differ only modestly above 3 kHz. At 30 kt the level for LF-7 lies above HF-3 by a few db and by more above 5 kHz. LF-6, on the other hand, lies somewhat below HF-3 up to 3 kHz. In Fig. 3.1.1-16a, spectra for both LF-7 and HF-3 at 20 kt are compared with that measured on the 3-in. diameter element 5E111 flush-mounted at Sea Chest 2 in the PURVIS I test, a location comparable with that of the LF's. The spectrum for 5E111, which is somewhat less reduced by area averaging, still lies for the most part between the others.

Dimensionless plots of the type (3-2) are given at 10, 20, and 30 kt for LF-7 in Fig. 3.1.1-18 and LF-6 in Figure 3.1.1-17. On these plots the spectrum for 10 kt lies above the others by a substantial frequency-dependent margin in the case of LF-6 and by a larger but less variable amount of the order of 15 db in the case of LF-6. The spectra for 20 and 30 kt in each instance do not closely approach coalescence, though the curves for LF-6 remain close in the interval up to 10 log $(\omega\delta_*/U_\infty) = 13$, and the 20-kt curves do not lie systematically above the 30-kt curves nor hence suggest a large acoustic component at 20 kt. Similar dimensionless plots are given for LF-4 at 10, 20 and 30 kt and for LF-12 at 5, 10, 15, 20, and

30 kt in Figs. 3.1.1-19 and 20. For HF-1 at 5 kt the curve lies far above the others, as would be expected, but for speeds 15 kt and above the curves, though again not coalescing in detail, do display comparable average levels and slopes.

To compare HF and LF elements, corresponding as they do to different values of R_o/δ_*, we must suitably generalize the conjectured outer scaling law (3-1). In App. 1 it is pointed out that for large elements ($\omega R_o/U_\infty \gtrsim 2\pi$, $R_o \gtrsim \delta_*$) the analog of the outer scaling law (3-1) for point elements consists in the following functional form for the TBL noise spectrum:

$$(3\text{-}3)\quad P(\omega/2\pi) = (R_o/\delta_*)^{-s}\, \rho^2 \delta_* U_\infty^3\, \tilde{\pi}_1(\omega\delta_*/U_\infty),$$

where $\tilde{\pi}_1$ is a function not necessarily simply related to π_1 in Eq. (3-1) for the point spectrum (if the latter holds at all) and, so far as the indicated area dependence of TBL noise for large elements corresponds to R_o^{-2}, we must have $s = 2$. The scaling law (3-3) would imply coalescence of plots for different R_o/δ_*, as well as different U_∞, provided the plot is taken as

$$(3\text{-}4)\quad 10 \log [P(\omega/2\pi)/\delta_* U_\infty^3] + 10\, s \log (R_o/\delta_*) \text{ vs. } 10 \log \Omega_1$$

in place of (3-2). If in some range of $\omega\delta_*/U_\infty$ the spectrum $P(\omega/2\pi)$ should vary as ω^{-3} while conforming to (3-3) with $s = 2$, we note, then the spectrum would be independent of δ_* and hence of distance aft.

Dimensionless plots of the type (3-4) with $s = 2$ are given for elements HF-3 at 15 and 20 kt and LF-7 at 20 and 30 kt in Fig. 3.1.1-21 and again with LF-6 in place of LF-7 in Fig. 3.1.1-22. In the instance of HF-3 and LF-7 the coalescence is quite good in the middle frequency range $8 < 10 \log (\omega\delta_*/U) < 13$. At lower and especially higher values of $\omega\delta_*/U_\infty$ the coalescence is poor. In the instance of HF-3 and LF-6 the coalescence is poorer in the middle range and better in the extreme ranges,

being fairly good, in fact, in the lower range. A similar dimensionless plot for HF-3 and LF-6 is made in Fig. 3.1.1-23 on assumption that s = 3 instead of 2. For this value of s, the coalescence of the curves for the two elements in the middle range becomes very poor.

Comparison of HF Elements with Small Elements

The noise spectra measured for HF-3 are compared in a dimensionless plot with those measured in other tests on certain small elements in Fig. 3.1.1-24. The small elements chosen are the 1/8-in. diameter FS-1 number 1666 of the PURVIS I test series and two 0.11-in. diameter elements of Franz's Albacore noise measurements (Ref. 9). The FS-1 was located in Sea Chest 1 of the PURVIS I test at a distance aft nearly the same as HF-3 (27 ft), and the two chosen elements of the Albacore test were located at distances 21 and 46 ft. aft, which straddle the distance aft of HF-3.

The 5-in. diameter element HF-3 constitutes a large element, i.e. $\omega R_o/U_\infty >> \pi$, throughout the frequency range in question; the FS-1 and Albacore elements constitute small elements, i.e. $\omega R_o/U_\infty \lesssim 1$, at 20 kt up to about 1 kHz, or in the case of the FS-1 up to about 10 log $(\omega\delta_*/U_\infty) = 7$ independently of U_∞. At sufficiently high frequency that even the smaller elements would consistute large elements, the spectrum for the HF-3, if the area-averaging effect is as R_o^{-2}, should lie below the spectrum on the smaller elements by an amount increasing asymptotically to 32 db. In the lower range where the smaller elements behave as point sensors there is some prior empirical basis to think the spectrum on the large element of radius R_o would be equal to that on the smaller multiplied by $(\omega R_o/\eta U_\infty)^{-2}$, where $\eta \sim 0.6$ (Ref. 10); this relation has also a theoretical basis if the dominant contributing wavenumber range in the TBL pressure spectrum is of the order of the convective value $\sim\omega/U_\infty$ for both large and small elements.

The relation between the HF-3 and FS-1 spectra in Fig. 3.1.1-24 is seen roughly to correspond to this supposition. On the other hand, at larger $\omega\delta_*/U_\infty$ the spectrum for HF-3 begins to decrease less, rather than more rapidly with frequency than the FS-1, and the difference in the spectra is reduced to a fairly small one at the higher frequencies. This circumstance does not accord with prior expectation for TBL noise spectra.

The Albacore spectra, we note, lie further above the spectra for the large elements than do the FS-1 spectra. These too, however, decline as least as rapidly as the large-element spectra in a wide frequency range. Digressing to the question of the difference between the measured FS-1 and Albacore noise levels, we observe that the FS-1 used for Fig. 3.1.1-24 is quieter than most; in Fig. 3.1.1-25 we give dimensionless spectra for this element and another FS-1, number 1638, along with the two Albacore spectra.

H Elements

Spectra are available for one of the far-aft, flush, hull-mounted H elements, namely H-5, and are shown in Fig. 3.1.1-26 and compared with HF and LF elements in Figs. 3.1.1-27 to 30. At 0, 10, and, in run 340B, 20 kt the spectra for H5 are nearly coincident. It is concluded that, on account of the proximity of this element to machinery spaces, the levels up to this speed are dominated by this noise source. At 30 kt and, in disagreement with run 340A, also to a lesser degree in run 340B at 20 kt, the spectra lie higher. In the comparison of these levels with those for HF and LF elements, however, the H levels lie above the latter. It thus appears that spectra for this element, except possibly at 30 kt, cannot be used in making inferences concerning the dependence of TBL noise on distance aft.

3.1 ? Cross-spectra

The magnitude and phase of the normalized cross-spectral density of noise measured on various pairs of HF elements are shown in low and high-frequency bands for a number of different runs and ship speeds in Figs. 3.1.2-1 to 82, Vol.I.

Regarding the magnitude $\gamma(\bar{\mathcal{S}}, \omega)$ of the cross-spectra, where $\bar{\mathcal{S}} = (\mathcal{S}_1, \mathcal{S}_3)$ denotes the center-to-center separation vector between elements, we make the following observations.

At zero knots, the magnitudes, apart from relatively narrow-band irregularities and a pronounced dip as frequency decreases toward 0.5 kHz, generally are substantial (e.g. $\gtrsim 0.3$) up to a frequency $\omega (= 2\pi f)$ whose value is roughly consistent with the formula $\omega\mathcal{S}/c \sim 2$ to 3 for the upper frequency limit above which an acoustic noise field incident with a distribution in azimuth is expected to yield a substantially decreased cross-spectral magnitude [see Eq. (A3-8) and related discussion in App. 3]. Superimposed on several of the plots of cross-spectral magnitude is the function $|J_o(\omega\mathcal{S}/c)|$ that would apply (App. 3) if the pressure were due to an acoustic field that is isotropic, uncorrelated in direction, and propagating in the plane of the elements. Detailed correspondence does not ordinarily occur, nor should be expected, but some similarity is noted for element pairs HF5-HF12, HF12-HF6, and HF12-HF8.

At 10 kt the cross-spectral magnitudes are generally reduced relative to zero kt, especially in the lower frequency interval ($\lesssim 2$ kHz). In some instances the pattern of variation remains somewhat similar, in most rather changed. At 20 kt the magnitudes are decidedly further reduced (except for pairs and frequencies where the magnitude at 10 kt was already low). An exception occurs for the adjacent-element pairs HF5-HF12 and HF5-HF4 at high frequency; for the former pair at frequencies

$\gtrsim$ 5.5 kh the magnitude is noticeably higher than at 10 kt, rising to a peak at 8 kHz, and for the latter there is a band of substantial magnitude at $\sim$ 8.5 kHz.

At 30 kt, however, the magnitudes, at least in the high-frequency range ($\gtrsim$ 5 kHz), are generally somewhat higher than at 20 kt. The magnitude in this high range, in fact, on the average is higher than in the frequency range just below. In narrow frequency intervals, peaks of relatively high magnitude occur at such high frequencies also in some instances at lower speed.

We offer the following inferences from the described behavior of the cross-spectral magnitudes.

At zero speed the pattern broadly corresponds to what might be expected for an acoustic field with a fairly complex and frequency-dependent angular distribution. We are unable, however, to account for the dip in the magnitude at frequencies $\lesssim$ 0.5 kHz.

The observed decrease in magnitude with increasing ship speed can reasonably be attributed only to an increased relative contribution to the noise autospectra of the element pair due to a pressure field whose individual normalized cross-spectral magnitude at the frequencies and separations in question is much smaller than that of an acoustic field. In terms of Eq. (A3-14) of App. 3, some $\Psi_i(\omega)$ in the denominator becomes increasingly large relative to the others, but the numerator is not correspondingly affected, since the γ_i multiplying this particular Ψ_i is supposed relatively small. The only likely such contribution to the pressure field is that due to the turbulent boundary layer. Assuming this in fact to be the cause, we conclude that the TBL contribution to the noise autospectra of the HF elements is roughly comparable with the acoustic noise at 10 kt and predominates over the latter at 20 kt at least up to a frequency $\sim$ 3 kHz. This conclusion is based mainly on the evidence of the pairs of adjacent elements, since the acoustic field itself yields a relatively lower cross-spectral magnitude when the elements are further separated.

At the same time, at frequencies $\gtrsim 5$ kHz, in certain bands at least, it appears that the acoustic contribution to autospectra exceeds the TBL at 20 kt, and in fact that acoustic sources are present in this range that are absent or weaker at 0 and 10 kt. Such a source seems especially strong at ~ 8 kHz; referring to the measured autospectra on HF elements at 20 kt, we note a corresponding hump at about this frequency. (On the other hand, the pronounced hump in the autospectra at ~ 0.9 kHz for 20 kt seems correlated, if at all, with a dip and not a rise in the cross-spectral magnitude.)

At 30 kt the apparent increase of acoustic noise in the high-frequency range becomes much more pronounced. The humps in the measured autospectra in this range, however, are no more pronounced than at 20 kt, and indeed similar humps occur also for the lower speeds.

The additional high-frequency acoustic noise inferred from the increase in cross-spectral magnitude at 20 kt and especially 30 kt appears to derive from sources in a relatively well defined direction. We conclude this from the fact that $\omega\mathcal{S}/c \gg 1$ in the range in question, and an azimuthally isotropic distribution, for example, would therefore yield a magnitude $|J_0(\omega\mathcal{S}/c)| \ll 1$, whereas a unidirectional wave, at the other extreme, would yield a magnitude unity. It is suggested that this increase in the cross-spectral magnitude at 20 kt and especially 30 kt may be due to some incipient cavitation.

Thus far in this discussion of cross-spectra we have considered only the magnitude and ignored the phase. If only an acoustic field is present, as noted in App. 3, we expect a relatively slow variation of phase with a change of 2π occurring only over frequency intervals in which $\omega\mathcal{S}/c$ changes by at least roughly 2π, except that abrupt changes in phase by as much as π can occur at intervals in $\omega\mathcal{S}/c$ equal to ~ 2.4 to π [e.g., see App. 3, Eq. (A3-16)]. If another noise field is present,

notably one due to the TBL, but has a normalized cross-spectral magnitude small compared to that of the acoustic noise, as noted in App. 3, the phase will still be approximately that for the acoustic field alone, and this may be so even if the contribution of the TBL to the noise autospectra exceeds the acoustic one. Hence the type of phase variation just described may be expected to apply to the measured spectra in question at most speeds and frequencies.

In actuality, the measured phase variation is seen to be more rapid and erratic in many instances than suggested by this account. This irregular behavior is largely confined to frequency intervals where the cross-spectral magnitude is small, but is scarcely less noticeable at zero speed, where the TBL contribution is absent, than at higher speed. It is tentatively suggested that the true phase is well behaved, as expected, but that the numerical computation procedure produces spurious and rather random results when the cross-spectral magnitude is as low as it frequently is. This conjecture is susceptible to investigation, but no answer can be given in the present report. In addition, it is worth pointing out, the phase curves as drawn to connect adjacent computed values are presumably frequently unjustified when these adjacent values differ by nearly 2π; i.e., since the phase values π and $-\pi$ must be identified, the connecting line from a computed phase $\pi - \delta_1$ to $-\pi + \delta_2$, say, where $\delta_1 \lesssim 1$, $\delta_2 \lesssim 1$, should not be the direct line, but rather one leading from $\pi - \delta_1$ to π and then one leading from $-\pi$ to $-\pi + \delta_2$. Some violent apparent phase variations in the plots are thus eliminated.

In any case, we have not been able to employ the measured phase plots for these large-element cross-spectra of the Purvis II tests for any useful inference.

The magnitude and phase of the normalized cross-spectral density of noise measured on various pairs of LF elements are shown in Figs. 3.1.2-83 to 164, Vol. I.

We may compare these cross-spectral magnitudes with those for pairs of HF elements discussed above. Pairs LF3-LF2 and LF12-LF11, for example, have the minimum spacing of 30.5 in. of the LF array, and this separation is comparable with (slightly smaller than) the spacing of the pair HF12-HF8. For the most part, the cross-spectral magnitude at the various speeds have much the same character for these comparable pairs of elements in the LF and HF arrays. On a few of the plots of cross-spectral magnitude for zero speed is superposed the function $|J_o(\omega j/c)|$ of App. 3, Eq. (A3-8). A few particularities of the LF pairs may be cited.

For several LF pairs a pronounced peak in the cross-spectral magnitude appears at about 7.5kHz and persists through speeds up to 20 kt. A corresponding hump in the autospectra of most of the LF elements likewise occurs near this frequency. It is inferred that an acoustic noise source with relatively well defined effective direction exists at this frequency.

The perceptible though oscillatory increase in the cross-spectral magnitude at high frequency at 30 kt which was exhibited by the HF element pairs even when the separation was comparable to that of these LF pairs does not occur for these latter. If that rise was due to cavitation, then either the cavitation source was more acoustically accessible to the HF than the LF elements or else its effect on the LF's remains masked by other acoustic noise.

In two 10-kt runs with no change in controlled run variables, the cross-spectral magnitudes for LF pairs in Run 345 were substantially lower than in Run 858. This difference is

attributed to the fact that the movable strut near the LF array was extended during the 800-series runs but not during the 300-series. As indicated by comparison of autospectra and confirmed by these cross-spectral magnitudes, the strut produced spurious added acoustic noise on the LF elements. Hence it is more appropriate to use the 300-series results. On the basis of Run 345 it would appear that TBL noise predominates through most of the frequency range already at 10 kt.

Concerning the variation among results for the various runs at 20 kt, we note, pronounced peaks in the cross-spectral magnitude for LF3-LF2 appear at 0.8 and 1.7 kHz in Run 543 at 180° heading which are not prominent in the other 20-kt runs.

Figs. 3.1.2-165 to 184 show cross-spectra for a pair of elements, HF2 and H5, which are located at widely separated positions along the hull. The results give some indication of results to be expected when the crossed elements have more or less the least possible correlation. We note, however, in Run 340B at 20 kt, a local peak in the magnitude at ~ 8 kHz, presumably corresponding to an acoustic wave at this frequency propagating roughly along the length of the ship.

Recalling the conclusions based on HF and LF autospectra, we note that the cross-spectra appear to indicate that TBL noise begins to dominate acoustic noise at somewhat lower speed than inferred previously. In view of the complex influences on the cross-spectra we tentatively regard this discrepancy as not serious and consider the indications from autospectra as more reliable.

3.2 Flush and recessed elements in sea chest 2

Among the G elements, auto- or cross-spectra are available involving G5 through G10. The pair G5 and G6 are recessed behind a flooded cavity covered by the fiberglass window of sea chest 2 and are mounted flush in the air-backed rear face of this cavity, which is likewise fiberglass. The front window is 9/16 in. thick and the rear window 3/4 in. thick. The lateral dimensions of the cavity are about 36 in. longitudinally and 21 in. circumferentially. The pair of elements G7 and G8 are set flush in the outer fiberglass window of this sea chest. Over some area surrounding this pair there is a 1/2-in. steel doubler plate attached to the inside of the window. The pair G9 and G10 are flush-mounted in the hull above the window. The center spacing of the pairs is 8 in.

3.2.1 Autospectra

Measured spectra are presently available only for elements G5 and G7 and are shown in Figs. 3.2.1-1 to 5 together with comparisons with a neighboring LF element. Spectra presently available for the G elements are limited, including only speeds 15 and 25 kt for the flush window-mounted element G7.

The speed and frequency dependence for the recessed element G5 differs strikingly from the dependence observed for flush hull-mounted elements. In the range of frequency up to about 1.5 kH, the spectra decrease regularly and similarly, apart from minor humps, at an average rate given roughly by ω^{-2} to $\omega^{-3.4}$. In this region

the spread among the various speeds from 0 to 30 kt is $\lesssim$ 11 db, and the variation with speed is not monotonic. At frequencies ranging from 1.4 to 3 kHz depending on speed, the spectra for 10, 15, 20, and 25 kt turn upward and reach broad peaks of varying height at about 7.5 kHz with a tendency to a secondary peak in the same broad rise at about 4 kHz. This broad high-frequency peak develops and declines in a rather regular way with speed. Thus, at 0 kt no such peak occurs, at 10 kt the peak is pronounced, at 15 kt decidely higher, at 20 kt somewhat lower again, at 25 kt still lower, and at 30 kt the peak has degenerated to a minor leveling trend. At the 7.5-kHz peak, the measured noise level at 15 kt is actually 20 db above that at 30 kt, while the latter is 16 db above that at 0 kt.

Relative to a typical LF element, the spectra for G5 in the range of lower frequency distinguished above are much lower, especially at the higher speeds. In the range of the high-frequency maxima, however, the G5 spectra rise well above the LF spectra at 10 through 25 kt, but the G5 spectrum at 30 kt is again much below the LF.

As for the flush window-mounted element G7, the spectra at 15 and 25 kt are substantially higher than for G5, especially at 15 kt in the valley preceding the high-frequency rise. The spectrum approaches more nearly the spectrum for an LF element in the lower frequency range but, as with G5, greatly exceeds it in the higher range. The broad humps at high frequency still occur but are less pronounced than for G5. Fig. 3.2.1-2 shows also that the position

and height of the high-frequency peak for 15 kt was considerably different for runs at 0° and 90° headings, but at 25 kt no such difference was observed.

3.2.2 Cross-spectra

The magnitude and phase of the normalized cross-spectral density of noise measured on three pairs of G elements are shown in Figs. 3.2.2-1 to 60, Vol. I. These pairs, namely G5-G6, G7-G8, and G9-G10, represent pairs of G elements of the three types, respecively recessed behind a flooded cavity behind the fiberglass window, flush-mounted in this window, and flush-mounted in the hull1 above the window. All pairs have the same 8-in. center spacing.

On the plot of the magnitude for the G9-G10 pair at zero speed, the function $|J_0(\omega f/c)|$ of App. 3, Eq. (A3-8) is once more superposed. We may compare the magnitude for G9-G10 at the various speeds with that for the pair of adjacent HF elements HF5-HF4 shown previously. . At zero speed the magnitude for the former pair is substantially higher than for the latter in the high-frequency band above 2 kHz. The pairs are more similar at 10 kt, apart from a strong peak for the G pair at 5 kHz For the G pair at 20 kt, unlike the HF pair, there is no rise at frequencies $\gtrsim$ 8 kHz, and at 30 kt the average magnitude is considerably below that for the HF pair.

The magnitude for the flush, window pair G7-G8 at zero speed is lower than for the flush,hull pair G9-G10. At 30 kt, for G7-G8, unlike G9-G10, there is a gradual rise to a peak at $\sim$1.6 kHz.

For the recessed pair G5-G6 at zero speed, the average magnitude in the high and low bands is of the same order as for HF5-HF4. There is, however, a notable failure of the computed magnitudes in the two frequency bands to join continuously at $\sim$ 1.4 kHz. Though the data used for one band is only a subset of the data used for the other, a joining discrepancy of the order computed should be grossly unlikely statistically. (The joining is rather poor also for G7-G8 at zero speed and very poor for G5-G6 again at 20 kt.) At 10 kt, the average magnitude for G5-G6

is somewhat higher than for G9-G10 or HF5-HF4, with a build-up to a high-frequency peak at ~ 8 kHz. At 20 kt the magnitude is much reduced, though still higher than for G7-G8 and G9-G10 or even HF5-HF4. At 30 kt, the magnitude drastically increases for frequencies $\lesssim$ 2 kHz, where the curve greatly resembles that for zero speed. This increase at 30 kt suggests increased relative prominence of some acoustic field that affects the recessed elements and to a lesser degree the flush window-mounted elements, but not the flush hull-mounted elements.

3.2.3 Analysis

We may seek an explanation for the measured G5 and G7 spectra, employing also the measured G5-G6 and G7-G8 cross-spectra.

If we regard only the lower frequency range where the spectra lie below the LF spectra and depend weakly and irregularly on speed, we might suppose the following. The direct flow noise due to the TBL is drastically reduced for the recessed G5 element by the acoustic wavelength-filtering action of the intervening water between the element and the flow (e.g., see App. 2). Thus the high-wavenumber noise will be attenuated to a negligible level and white low-wavenumber noise will be reduced, at frequencies $\lesssim$ 1.2 kHz, by a factor $\sim R_o^2/8L^2$, i.e., with depth $L = 6$ in. and $R_o = 2.5$ in., by $\sim$ 16 db.* This reduction of flow noise then leaves the element dominated by the residual acoustic noise at its location.

Even without confronting the high-frequency behavior, this explanation is challenged by consideration of the cross-spectral magnitude for the pair G5-G6 measured at 0, 10, and 20 kt. In the low-frequency range under discussion there is, in fact, a striking similarity among the cross-spectral magnitudes at 0, 10, and 30 kt, and the magnitude is rather high. On the other hand, at 20 kt the cross-spectral magnitude is quite different, being much lower in

*This estimate neglects the difference between the impedance of the window and that of an equal thickness h_o of water; this neglect is valid at the pertinent low wavenumbers, since $(\omega h_o/c)(\rho_o/\rho - 1) \ll 1$, where ρ_o/ρ is the relative density of the windown material.

average magnitude. (The runs for which the cross-spectra are available, it is noted, are unfortunately not the same as the runs at the corresponding speeds for which the autospectra are available, but one would hope that the behavior in question is reproducible between runs.)

In addition, the supposition that flow noise on G5 is reduced in a more or less expected way in the lower frequency range without further anomaly would suggest that the spectrum on the flush G7 should have nearly the same speed dependence and roughly the same level as for neighboring flush hull-mounted elements. From the data at 15 and 25 kt, there is little speed dependence for G7 through much of this range. At the same time, the contribution of the local acoustic field is rather uncertain, so that there is no clearcut discrepancy. The level for G7 and 25 kt is appreciably below that for most LF elements at this speed, whereas at 15 kt from $\sim$ 0.4 to $\sim$ 1.5 kHz the level is nearly as high as for the LF's, suggesting some possible acoustic cancellation of low-wavenumber flow noise on account of low baffle impedance.

In particular, despite the 1/2-in. steel doubler plate attached to the window surrounding element G7, the effective acoustic impedance of the baffle may be substantially less than for the hull-mounted elements. Some indication should be given by comparison of in situ calibration measurements for the two types of mounting. Comparison of Figs. 4-4 and 4-6 referring respectively to the LF and the flush G elements shows, in fact, that the apparent sensitivities in situ for the LF elements is greater than the measured absolute

sensitivity by an amount approaching the theoretical limit of 6 db for an infinite rigid baffle at normal incidence, except at very low frequency, whereas the sensitivities in situ for the G elements are lower than the absolute sensitivities by a few db at most frequencies. It is not clear, however, why this result obtains also for elements G9 and G10, inasmuch as these elements are hull-mounted.

From theoretical considerations we may point out the expected character of the effect of a low-impedance air-backed baffle on the noise measured by a flush element (e.g., see Ref. 4). First, the high-wavenumber part of the direct TBL noise on a flush element in a rigid baffle will remain nearly the same for the low-impedance baffle, provided $\omega R_o/U_\infty \gg 1$. By virtue of non-rigidity, however, there will exist a resonant acoustic field due to excitation by TBL pressure on the baffle, or by mechanical shaking, of modes with wave numbers $k_n \simeq k_r(\omega)$, where $k_r(\omega)$ is the wavenumber for free bending waves in the water-loaded plate (baffle) at frequency ω.* If the

---

* For a thin plate with water loading on one side (m=1) or two sides (m=2), if the mechanical damping is small, this wavenumber of free bending waves is given approximately by $k_r(\omega) \simeq k_o(m/k_o h)^{1/5}$ for $k_o h \ll 1$ or by $k_r(\omega) \simeq k_o$ for $k_o h \gg 1$, where k_o is the wavenumber of the bending waves in the absence of water loading and $h\left[=(\rho_o/\rho)h_o\right]$ is the fluid-equivalent plate thickness. k_o is given by $k_o = (\omega/a_o)^{1/2}$, where $a_o = c_t h_o/\left[6(1-\sigma)\right]^{1/2}$ with c_t the shear sound velocity in the bulk plate material, σ its Poisson ratio, and h_o the plate thickness.

baffle stiffness is rather low, as for the fiberglass window proper, the modes excited in the frequency range of concern are high modes, and the k_n are closely spaced relative to the effective width of the resonance peak in wavenumber. If $k_r(\omega)R_o \gg 1$, the contribution of these resonant modes to noise is substantially reduced by area averaging. Also, for $\omega/U_{\infty} \gtrsim k_r(\omega)$, excitation of these modes by the high-wavenumber part of the TBL pressure spectrum produces modal pressures that tend to cancel one another alternately.

With regard to non-resonant acoustic contributions resulting from excitation of the baffle locally by TBL pressure, the contribution due to the high-wavenumber part of the TBL spectrum, in some indicative regime at least, is of the order of the high-wavenumber contribution to the TBL noise on a flush element of area equal to the free (unsupported) area of the baffle plate, and hence is small. As for the contribution due to the low-wavenumber part of the TBL spectrum, if $k_r(\omega)R_o \gg 1$, the baffle impedance there is mass-dominated and, where $\omega R_o/c \lesssim 1$, this contribution depends mainly on h/R_o, where h is the effective water-equivalent plate thickness of the baffle. This contribution is opposite in sign and proportional to the low-wavenumber direct TBL pressure, and tends to cancel the latter; in the extreme limit of $h/R_o \ll 1$ and $\omega R_o/U_{\infty} \ll 1$, for example, this part of the acoustic field just cancels the corresponding part of the TBL pressure field, i.e. in the limit where the baffle is a pressure-release surface and the radiation impedance of the element is negligible, the element face is likewise nearly a pressure release surface. This

tendency toward cancellation for low baffle impedance naturally applies also to a radiated acoustic noise field transmitted to the element directly through the water.

Thus the effect of finite baffle impedance on the noise measured by a flush element depends not only on complex frequency-dependent relations involving the resonance parameters and boundary conditions of the loaded and supported baffle, but also on the size of the element and the incompletely established character of the wave-number spectrum of TBL pressure at low wavenumbers.

We return now to the question of the speed-dependent increase in measured noise on G5 (and G7) at high frequency. The character of this effect strongly suggests some type of resonance phenomenon. Referring to G5, we recall that the water-filled cavity separating the pair of elements G5 and G6 from the flow is covered by a fiberglass window of 9/16-in. thickness, and the opposite face in which the elements themselves are flush-mounted is an air-backed fiberglass plate of thickness 3/4 in.

Since the noise spectra near the maxima do not increase at all monotonically with flow speed, if the effect to be explained is real, we apparently have to deal with a response of the interior acoustic field that depends at each frequency not only on the magnitude of the source spectrum, but also on some other speed-dependent property of the source, unless we suppose that the speed-dependent noise source in question, e.g. bubble noise, decreases in some interval with increasing speed. It is natural to think of the condition

of hydrodynamic coincidence, at which the wavenumber of free bending waves in the cover bounding the flow coincides with the wavenumber where the TBL spectrum for a given frequency has a maximum, i.e. $k_r(\omega) \simeq \omega/u_c$ where u_c is a large fraction of U_ω. For the window, however, the stiffness would have to be unreasonably low to yield coincidence at frequencies so high and flow velocities so low as those involved. Moreover, coincidence should occur for each speed but at a changing frequency, whereas the maxima in the spectra occur at a relatively speed-independent frequency for speeds where they appear at all.

Indeed, even apart from the speed dependence of the maxima, we are unable to propose a reason why such a high broad maximum should occur, with a level there greatly exceeding the level on a flush hull-mounted element. We cannot suppose, for example, that the peak is associated with coincidence of the bending-wave resonance wavenumber with a modal wavenumber, i.e. $k_n \simeq k_r(\omega)$, since, among other reasons, for the applicable magnitudes of parameters, such resonances, if observable, would be narrow and closely spaced in frequency. Likewise, the interior acoustic field due to modes that propagate normal to the baffle and are excited by the pressure field outside the window cannot be substantially more intense than the corresponding exciting exterior field, since a resonant build-up of this sort can occur only to the extent that $(\omega h_o/c)(\rho_o/\rho) >> 1$, where h_o is the thickness of the outer window and ρ_o, ρ are respectively the mass density of this window and of water. In the subject regime this parameter is instead less than unity, and the effective "Q" of the supposed resonant cavity is small.

In addition, the inner fiberglass face in which elements G5 and G6 are mounted is air-backed, and, having moderate impedance itself at the predominant wavenumbers of the interior acoustic field, it constitutes a baffle of relatively low impedance. Since this impedance is lower than that of the baffle containing the flush G7 and G8, we might expect lower noise and also lower in situ sensitivity. From Figs. 4-7 and 4-6 we see that the in situ sensitivity of G5, for example, at the higher frequencies is rather less than that of G7 relative to the respective absolute sensitivities, but the opposite is true in the frequency range from 1 kHz to 2 kHz. In attempting to account for the noise measured by the window-mounted G elements, it may be pertinent to bear in mind the wider variations from element to element and the more erratic frequency dependence found in the in situ calibrations for these elements relative to those for hull-mounted elements. Likewise, the in situ calibrations of G elements, though mutually consistent, are often unrepeatable.

We may attempt to correlate the speed-dependent high-frequency behavior of the G5 autospectra with indications of the G5-G6 cross-spectra at 0, 10, 20, and 30 kt (Figs. 3.2.2.41 to 60). The rises in the autospectra, we recall, occurred among these speeds at 10 kt and especially 20 kt. The cross-spectral magnitudes at high frequency are largets at 10 and 30 kt, with a build-up for 10 kt to a moderate peak at 8 kHz. At 20 kt the magnitude at high frequency is somewhat lower with no notable broad maxima. We thus derive from these cross-spectra no clue to an account of the G5 and G7 autospectra at high frequency.

In the absence of any other likely explanation of the high-frequency behavior of the G5 and G7 autospectra, it naturally suggests itself that the increased high-frequency noise is due to bubbles. These elements are so located that indeed the bubble stream may have passed over them, and furthermore the proximity of the stream might depend on ship speed in a nonmonotonic fashion related to that of the magnitude of the high-frequency humps in the autospectra. The pronounced dependence of the high-frequency hump in the G7 spectrum at 15 kt on heading reinforces this supposition.

On the other hand, earlier analog data for autospectra of G9 and G10, the nearby elements flush in the hull above the window, indicated no anomalous high-frequency behavior, whereas it would seem likely that these too would be affected by bubbles at some ship speeds. Also, there is no tie-in between an account of the anomalous G5 and G7 spectra by bubble noise and the erratic results of the in-situ calibrations for these window elements.

Nevertheless, bubbles seem most likely to be implicated, and this hypothesis should be thoroughly pursued in further analysis. In this regard it will be desired to examine more of the G spectra, including G9 and G10, when available, investigate the variation of the high-frequency humps between runs under nominally identical conditions, study carefully the photographic evidence regarding bubble paths as a function of ship speed, and listen to audio reproductions of the recorded noise.

Apart from the region of the high-frequency humps, the G5 noise spectra at the higher speeds are well below those for the flush LF elements. Relative to LF-7, for example, at 25 kt. the noise was lower by at least 10 db up to 3 KHz. Hence, it appears that recession of elements from the flow does decrease flow noise. As pointed out, however, this effect in the present

*A new correct spectrum for G5 at zero speed shows a noise level which, from 0.8 to 2 KHz, lies well above that at 15 kt. Hence more than mere attenuation of flow noise by the dome is involved.

configuration was attended by a partially compensatory decrease in the in-situ sensitivity of the recessed element to a signal

3.3 Layer-shielded Elements in Sea Chest 1

The D elements of sea chest 1 were covered, and thus shielded from direct TBL pressure fluctuations, by rubber layers of maximum thicknesses given in the table below. The layers covering elements D1, D5, D6, and D10 were roughly planar and integral with a rubber window covering the entire sea chest. The layers covering the other elements were limited in lateral extent to a cone diverging from the element periphery at 60° from the normal but merging into the window layer of thickness ~1/2 in. The D elements had sensing faces of diameter 1.5 in.

ELEMENT	D1	D2	D3	D4	D5
Thickness (in.)	1-5/32	1-47/64	2-51/64	4-59/64	5/8
ELEMENT	D10	D9	D8	D7	D6
Thickness (in.)	59/64	5-1/32	2-25/32	1-23/32	13/16

3.3.1 Autospectra

Measured noise spectra for D elements are shown in various groupings and compared with flush element HF-3, which occupied a similar position aft, in Figs. 3.3.1-1 to 16. Results of in-situ calibrations of the D elements are shown in Figs. 4-9, 4-10.

It is a conspicuous fact, for non-zero speed, that in no appreciable frequency interval do the measured noise spectra lie nearly in the inverse (or direct) order of thickness of the layers interposed over their faces.

At zero speed the noise spectra are comparable except in a range ~4 to 7 KHz and near 1.2 KHz. This result obtains

despite the fact that the apparent sensitivities of the elements given by the in-situ (overside) calibrations differ greatly among elements. These apparent sensitivites likewise bear no notable relation to the thickness of the respective layers. In some instances and frequency intervals the measured in-situ sensitivites lie above, in others below, the free-field sensitivites. The order of the calibration curves undergoes decided reversals with changing frequency. The noise spectra at zero speed lie well above that for element HF-3, and, in fact, the spectra do not emerge appreciably from this zero-speed level until a speed of 20 kt.

The noise spectra on the various D elements do not differ greatly from one another in the low-frequency range up to ~1.3kHz at any speed through 30 kt. In this range, at 20 kt the spectra for the most part are a few db below that for the flush element HF-3, and somewhat further below at 30 kt.

In the higher frequency range the spread among the spectra is larger and increases with speed at 20 and 30 kt. As stated, the relative levels are not simply related to the order of layer thickness or type of layer installation (planar or conical). At 30 kt, from ~1.3 KHz to ~3.5 KHz the spectra lie 10 db or more below that for HF-3.

We may wish to consider the consequences of the supposition that the intrinsic sensitivities of some of the D elements were altered in the process of installation, or the similar supposition that the installation produced some peculiarity of the in-situ condition, e.g., air bubbles between sensitive face and covering layer, such that the apparent sensitivity of an element to both noise and to a calibration signal differed from its value in a satisfactory final configuration of interest. In such event it would be more appropriate to use the in-situ sensitivities in place of the nominal absolute sensitivities actually employed for the reduction of the noise data. (The measured sensitivities must be corrected for the angle of incidence and distance from the calibration source.) Inspection of the noise spectra with this point in mind, however, does not produce a more likely or sensible ordering of levels. If we take the same approach but discount the overside calibrations, we might employ relative

noise spectra measured at zero speed to adjust the relative spectra at high speeds; this course also produces uncompelling results.

Possibly the erratic variation among noise spectra at the higher frequencies is attributable to splash or bubble noise. The D elements are at least more accessible to these sources than are the HF elements, though they would seem still relatively remote from the main bubble stream. As in the case of the C elements, further analysis of this possibility is warranted.

If we look apart from the high-frequency anomalies of the noise spectra and the erratic character of the in-situ calibrations, we may suggest rather uncertainly on the basis of the comparisons at 20 and 30 kt that the layers on the D elements have somewhat reduced the flow noise relative to flush elements.

We recall once more the character of the anticipated effect of a covering layer on noise (App. 2), where three components of the noise are distinguished: (1) high-wavenumber, (2) low-wavenumber, (3) acoustic. If the layers were all planar and of sufficiently large extent, we would expect component (1) to be greatly reduced at all frequencies $\geq$0.2 KHz for all the layer thicknesses considered, since even at U_∞ = 30 kt we have $\omega L/U_\infty > 2$ for $\omega/2\pi > 0.2$ KHz if L $\geq$ 1 in. In the instances of those elements where a large portion of the thickness L has only the lateral extent of a conical plug, the reduction of this component, however may be much less than for a planar layer of the full thickness. The component (2), on assumption that it is roughly white noise in wave number, would be reduced somewhat as shown in the accompanying sketch, the maximum reduction being 25 db for L = 5 in. In the instances of a conical plug the reduction factor may be somewhat less than for an equally thick planar layer. The component (3) would not be appreciably reduced at all.

These expectations based on a fluid layer, however, are questionable in the present instance of a cover made of rubber, which has a low shear sound velocity. With reference to components

(1) and (2), it was assumed, in particular, that $U_\infty \ll c$, where c presumably should be considered of the order of the shear sound velocity in the case of a solid layer. If the sketch pertaining to reduction of components (2) does apply, the upper frequency limit for appreciable reduction, we note, is given by $\omega/2\pi \sim c/\pi R_0$, which decreases with decreasing c.

Though the design plan for the D elements called for a thinnest layer of 1/4 in. thickness, in fact the thinnest was of 5/8 in. thickness. It is unfortunate that there was not also a flush-mounted element of the same type.

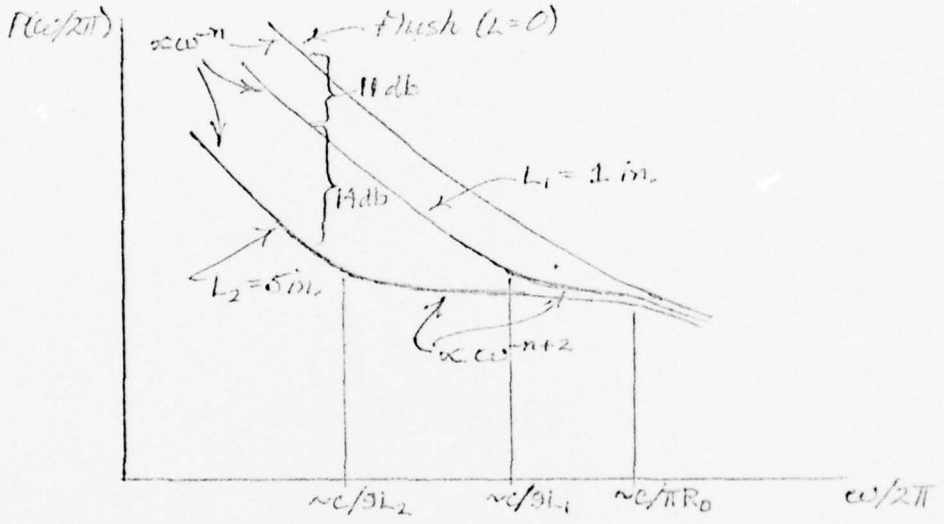

Spectra of wavenumber-white noise beneath planar fluid layers of various thicknesses.

3.3.2 Cross-spectra

The magnitude and phase of the normalized cross-spectral density of noise measured on three pairs of D elements are shown in Figs. 3.3.2-1 to 52, Vol. I. These pairs, namely D2-D1, D3-D8, and D4-D9, consist of elements at roughly the same depth, increasing in the order given. Among these elements, we recall, the covering layers diverge conically from the peripheries of all but D1. The center spacings of the respective pairs are 20, 12, and 43 in.

There is no conspicuously uniform change in the behavior of the cross-spectral magnitude with increasing element depths (and spacings) from pair to pair. The average magnitude in the high-frequency range ($\gtrsim$ 2 kHz) at 10 kt does increase with this progression, and the magnitude is very high for the pair D4-D9. The magnitudes in various instances display strong peaks and dips. In several of the plots the continuity at the joining of the curves computed for the low-and high-frequency ranges is poor. Overall, the cross-spectral magnitudes are somewhat higher than for the flush pair HF5-HF4, for example.

It is not unambiguously clear what effect the recession of the elements ideally should have on the cross-spectra. Certainly the high-wavenumber TBL noise, which has a cross-spectral magnitude appreciable over a relatively limited extent in $\omega\mathcal{Y}$ [e.g., see App. 3, Eq. (A3-3)], will contribute less to the autospectra on recessed elements, so that the magnitude of the normalized total cross-spectral density might be higher for such elements. This result should hold at least if true acoustic noise and not low-wavenumber TBL noise is the chief additional contributor to the noise autospectra.

For the D3-D8 pair at zero speed, the cross-spectral phase, it is noted,has an unusually regular linear dependence in two frequency intervals extending from 4 to 10 kHz. An effective phase velocity can be computed from the slope and corresponds to an acoustic wave with wave vector at a particular angle relative to the element separation.

REFERENCES

1. G.M. Corcos, J. Fluid Mech. 18, 353(1964).
2. L. Freeman, J. Watral, and M. Johnson, "Flush-Mounted-Array Investigations of Turbulent Boundary-Layer Noise on the USS ALBACORE," 24th Navy Symposium on Underwater Acoustics, 1966 (Confidential).
3. D.M. Chase, 23rd Navy Symp. on Underwater Acoustics 1965, ONR Symp. Rept. ACR-115 (Confidential), p.51; TRG tech. memo 011-TN-65-8 (Unclassified).
4. D.M. Chase, "Flow Noise Transmitted Through Domes or Acoustically Modified by Non-Rigid Boundaries," TRG Rept. 011-TN-66-1, Contract Nonr 4385(00), Jan., 1966.
5. D.M. Chase, "Space-Time Correlations of Velocity and Pressure and the Role of Convection for Homogeneous Turbulence in the Universal Range," to be published.
6. H. Schlichting, Boundary Layer Theory, Pergamon Press Ltd., London, 1955.
7. J.O. Hinze, Turbulence, McGraw-Hill Book Co., Inc., New York, 1959.
8. D. Chase and H. Steinberg, "Effect of Inter-Element Correlation of Turbulent Boundary-Layer Noise on Signal-To-Noise Ratio for a Flush Planar Sonar Array," TRG Tech. Memo 023-USL-67-1, Jan, 1967.
9. G.J. Franz, JUA (USN) 12, 5(1962) (Confidential).
10. G.M. Corcos, J.Acoust.Soc.Am. 35, 192 (1963).

APPENDIX 1

DIMENSIONLESS SPECTRA AND POSSIBLE SCALING LAWS FOR TURBULENT BOUNDARY-LAYER PRESSURE

It has become customary, with reference both to laboratory measurements of TBL noise and to ship measurements of self-noise on flush elements at non-vanishing ship speed, to present noise autospectra in dimensionless form vs. frequency in dimensionless form where the forms used are those defined by taking boundary-layer displacement thickness δ_* as the length parameter and asymptotic flow speed U_∞ as the velocity parameter. Presentation in this form is obviously equivalent in information value to the raw measured spectra, entailing no assumptions, but the utility and appropriateness of this form is measured by the extent to which noise spectra due to the TBL scale in such a way that spectra for different values of U_∞ and δ_* (i.e. of speed and distance aft) tend to coalesce on such a plot. The degree of coalescence, however, may well suffice to render this method convenient for presentation of data referring to different speeds without inspiring confidence in the optimality or even adequacy of the associated scaling law for extrapolation of results to an unmeasured regime*.

If one is assured that TBL noise spectra do coalesce on some form of dimensionless plot, we note, then if measured spectra, e.g. sea-test data, are so plotted, they must lie above the basic TBL curve by an amount that measures the contribution of noise sources other than the TBL.

A theoretical discussion can be advanced (e.g. Ref.3) suggesting that at sufficiently high frequency (perhaps for $\omega\nu/v_*^2 \geq 0.1$) the appropriate TBL pressure scaling parameters may be not δ_* and U_∞ but rather the length and speed parameters characteristic of the inner part of the boundary layer, namely ν/v_* (proportional to the thickness of the viscous sublayer) and v_*, where ν denotes kinematic viscosity and v_* the friction

*This is particularly true with regard to dependence of TBL noise on distance aft.

velocity. We refer to the pressure scaling form corresponding to parameters ν/v_* and v_* as the inner scaling law and to that corresponding to parameters δ_* and U_∞ as the outer.

For the Purvis data processing reported here, some noise autospectra were plotted in both inner and outer dimensionless forms, defined specifically below. The form taken in each case refers to point pressure and, even if the pertinent scaling law for TBL pressure is valid, TBL spectra measured by elements of radii R_o therefore cannot be expected to coalesce unless $\omega R_o/U_\infty \lesssim 1$. Since the appropriate area correction factor, at fixed R_o and δ_*, may depend almost solely on $\omega\delta_*/U_\infty$, however, *the outer form of dimensionless plot* (though not the inner), if valid for $\omega R_o/U_\infty \lesssim 1$, may yield coalescing plots for varying U_∞ but fixed R_o even when $\omega R_o/U_\infty \gtrsim 1$.* Accordingly, the outer form of plot is useful and has been computed for elements of all sizes.

Various alternative possible scaling forms may be conjectured also for large elements ($\omega R_o/U_\infty >> \pi$)(e.g. Ref.3), which would take account of the area-averaging factor. Thus far these have not been computed in the Purvis data processing. apart from hand-computed results in Sec. 2 based on Eq. (A1-10) below.

The outer and inner forms of dimensionless plot are respectively

(A1-1) $10 \log\pi_1$ vs. $10 \log\Omega_1$

$10 \log\pi_2$ vs. $10 \log\Omega_2$

with π_i, Ω_i defined as follows. Let $P(f)$ denote the spectrum of noise pressure on a given element, so normalized that the mean squared noise pressure is given by

$$(A1\text{-}2) \qquad \langle p^2 \rangle = \int_0^\infty df P(f) \equiv (2\pi)^{-1} \int_0^\infty d\omega P(\omega/2\pi).$$

*Since δ_* depends weakly on U_∞ and strongly on distance aft, coalescence for given large R_o at differing U_∞ would be only approximate, and no coalescence would be expected for elements at varying distances aft. The appropriate generalization for dependance on R_o/δ_* is considered further on.

The dimensionless frequency and pressure-spectra variables are defined by

$$(A1\text{-}3)\qquad \Omega_1 = \omega\delta_*/U_\infty, \pi_1 = P(\omega/2\pi)/\rho^2\delta_* U_\infty^3,$$

$$\Omega_2 = \omega\nu/v_*^2, \pi_2 = P(\omega/2\pi)/\rho^2\nu v_*^2,$$

in which U_∞ is identified with ship speed. These definitions may be rewritten as

$$(A1\text{-}4)\qquad \Omega_1 = (\omega\nu/U_\infty^2)R_*, \quad \pi_1' = P(\omega/2\pi)/\rho^2\nu U_\infty^2 R_*,$$

$$\Omega_2 = \Omega_1/g^2 R_*, \quad \pi_2 = \pi_1(R_*/g^2),$$

where

$$(A1\text{-}5)\qquad R_* = U_\infty\delta_*/\nu, \quad g = v_*/U_\infty.$$

R_* and g are considered to be given adequately by the corresponding quantities for the TBL on a flat plate (at zero angle of attack) at a distance x from the leading edge equal to distance aft of the bow (taken as Frame 0). R_* and g have been computed from the following formulas, applicable at the high Reynolds numbers of concern, as discussed below:

$$(A1\text{-}6)\qquad R_* = 1.30(10^5)(R_x/10^8)^{0.842},$$

$$g = 0.03023(R_x/10^8)^{-0.066},$$

where

$$R_x = U_\infty x/\nu.$$

Expression (A1-6) for g represents a power-law fit over the interval $0.97(10^7) < R_x < 0.77(10^9)$ to the values tabulated in Table 21.1, p. 540, of Ref. 6, with the fit made exact at $R_x = 10^8$. That Table was computed from a logarithmic velocity profile with constants determined empirically and provided an excellent fit to g up to the

maximum value $R_x = 0.45(10^9)$ for which a measured value is available from Fig. 21.2 of Ref. 6. Eq. (A1-6) for g fits the tabulated values very closely for $10^7 \leq R_x \leq 10^9$.

Expression (A1-6) for R_*, giving the displacement thickness δ_* as a function of distance aft x and flow speed U_∞, was obtained as follows. The momentum equation was integrated to give the increase in momentum thickness δ_m with downstream distance from x_o to x. In the integrand, the friction coefficient was taken to be that yielded by formula (A1-6) for g. The lower limit x_o was taken to correspond to $R_{x_o} = 10^7$, and the corresponding value of δ_m was computed from the relation $R_m = U_\infty \delta_m / \nu = 0.045 R_x^{0.79}$ given by Ref.7, Eq.(7-80), p.487, as valid in this range. R_* was computed from the R_m obtained by integration by the relation $R_* = HR_m$; the shape coefficient H was taken as $H = (1-6.1g)^{-1}$, given in Ref. 7, Fig. 7-6, p. 483, as a fit to experimental data (at somewhat lower Reynolds numbers, however, than those in question), and g was once more computed by (A1-6). Finally, as in the instance of g, a power law was fitted to the resulting computed R_* over the interval $10^7 < R_x < 0.77(10^9)$, with the fit made exact at $R_x = 10^8$.

We extend consideration of the outer pressure scaling law to the case of large elements ($\omega R_o / U_\infty \gtrsim 1$) to permit a comparison with measured noise spectra on elements at differing distance aft. If the point pressure spectrum scales according to the outer law (i.e., if the measured π_1 defined by (A1-3) depends only on Ω_1), and possibly even if it does not, for $R_o \gg \delta_*$ the spectrum of area-averaged TBL pressure on a large element is expected to have approximately the form (Ref. 3)

$$(A1\text{-}7) \qquad P(\omega/2\pi) = (\omega R_o / U_\infty)^{-2} \rho^2 \delta_* U_\infty^3 N(\delta_*/R_o, \omega\delta_*/U_\infty),$$

where N is some function of the indicated dimensionless arguments. If, in addition, the wavenumber spectrum of TBL pressure varies little in most of the low-wavenumber range defined by $K \lesssim 2\pi R_o^{-1}$,

which can be true (if at all) only for $\omega R_o/U_\infty \gtrsim 2\pi \gtrsim \omega R_o/c$, then (A1-7) reduces to the more restricted form

$$(A1\text{-}8) \qquad P(\omega/2\pi) = (\omega R_o/U_\infty)^{-2} \rho^2 \delta_* U_\infty^3 F(\omega\delta_*/U_\infty),$$

where F is another function. This form, unlike (A1-7), implies a unique area dependence, namely as R_o^{-2}. If the wavenumber spectrum does not satisfy the restriction leading to (A1-8) but increases more or less smoothly with wavenumber, the general outer form (A1-7) may nevertheless hold and be approximated by the form

$$(A1\text{-}9) \qquad P(\omega/2\pi) = (\omega R_o/U_\infty)^{-s} \rho^2 \delta_* U_\infty^3 F(\omega\delta_*/U_\infty),$$

where s is regarded as roughly constant and lies between 2 (as in (A1-8)) and 3; (A1-9) may be rewritten as

$$(A1\text{-}10) \qquad P(\omega/2\pi) = (R_o/\delta_*)^{-s} \rho^2 \delta_* U_\infty^3 G(\omega\delta_*/U_\infty),$$

where $G(x) \equiv x^{-s} F(x)$. Now we define a modified dimensionless spectrum $\tilde{\pi}_1$ by

$$(A1\text{-}11) \qquad \tilde{\pi}_1 = \pi_1 (R_o/\delta_*)^s,$$

with π_1 still defined in terms of a measured spectrum $P(\omega/2\pi)$ by (A1-4). Hence, if TBL pressure dominates the measured noise on a large element in some regime and this pressure satisfies the outer scaling law (A1-10), then plots of 10 log $\tilde{\pi}_1$ vs. 10 log Ω_1 will coalesce, and, unlike the instance of plots employing the unmodified π_1, the comparison of these plots has a basis even where the values of R_o/δ_* differ, since the form (A1-10) takes proper account of this dependence on R_o/δ_*.

APPENDIX 2*

REDUCTION OF FLOW NOISE BY A COVERING LAYER

We review briefly the basic points relevant to the question of noise reduction by a layer or a fluid dome with negligible cover impedance.** At a given frequency, three contributions to the noise on a large flush element (radius R_o, $\omega R_o/U_\infty >> \pi$) are distinguished. The first two are due directly to pressure fluctuations associated with the turbulent boundary layer (TBL). Of these, the first is a high-wave number part ($K > \omega/U_\infty$) which is the only kind that would be present if the pressure were generated by "frozen" eddies convected down-stream at velocities not exceeding the ship speed (U_∞). This part varies with radius as R_o^{-3}. Any additional pressure fluctuations due to surface roughness may be predominantly also of this high-wavenumber character. The second is a low-wavenumber component ($K \lesssim 2\pi R_o^{-1}$); the amplitude of this component is no doubt much smaller than that of the former, but it is more heavily weighted in the average pressure on the element, since its contribution is much less reduced by area averaging. The third contribution to noise is understood to include all other sources; it is presumed to have the character of a radiated sound field (modified by interaction with the flow-bounding hull and including any sound due to compressibility of the fluid of the TBL).

Shielding the given element by a layer of depth L is expected to have the following effects on the three contributions. The first (high-wavenumber) part will be reduced to negligibility provided roughly $L >> U_\infty/\omega$ and the lateral dimensions of the layer

---

* This appendix is based on Refs. 3 and 4.

** The explicit mathematical analysis that has been done pertains to a fluid, not a solid, layer. We expect, subject to experimental test, that an elastic solid behaves similarly provided the transverse sound velocity is of the order of the sound velocity for the fluid analog and large compared to the ship speed.

are large compared to the element diameter (and perhaps larger than the wave length $\lambda (= 2\pi c/\omega)$ of sound in the layer material). In some parameter regime, more specifically, this part is reduced rather as though averaged, not over the element area, but over the lateral area of the layer.* The second (low-wavenumber TBL) part will be reduced to an extent depending mainly on the ratios R_o/λ and R_o/L. For example, if the wavenumber spectrum of the TBL pressure at frequency ω is constant** in the range in question (whence this part of the average-pressure spectrum for the flush element would vary as R_o^{-2}), this part for the shielded element is reduced as if averaged, not over the element area, but over an area πR_e^2, if $R_e \gtrsim R_o$, where:

$$R_e^{-2} = (\pi/\lambda)^2 + 1/8L^2$$

i.e., roughly over an area of radius equal to the smaller of three times the layer thickness or one third the sound wave length in the material; if $R_e \lesssim R_o$, however, (as becomes true at sufficiently high frequency) this part is not appreciably reduced. The third (radiative) part will not be substantially

---

* When the lateral sheath size (nominal radius = a) is sufficiently large and the depth is not too small, i.e., roughly when

$$\pi/a \ll \omega/U_\infty - (\omega^2/c^2 + L^{-2})^{1/2},$$

for sheathed elements the contribution corresponding to this high-wavenumber component may be composed approximately as the sum of a component arising from sheath modes with $k_n \simeq K$ and nearly equal to the entire high-wavenumber contribution for an infinite sheath ($a = \infty$), and a component arising from relatively unattenuated sheath modes [$k_n \lesssim (\omega^2/c^2 + L^{-2})^{1/2}$]; these may be designated the infinite-sheath and the low-mode components, respectively.

** I.e., when averaged over wave-vector direction in the boundary, constant per unit area in two-dimensional wave-vector space.

reduced for any L, except that if the material is such as to introduce an acoustic impedance mismatch with respect to the water outside, both a signal and this part of the noise will be reduced similarly (such mismatch is thus not desired). The reduction factors, S_i say, representing the effect of the layer on these (1) high-wavenumber, (2) low-wavenumber, and (3) acoustic radiative components of the average-pressure spectrum, each normalized to unity for $L = 0$, are thus expected to depend on thickness L at fixed frequency somewhat as shown in Figure A2-1. It is assumed in Figure A2-1 that $R_o \lesssim \lambda/\pi$. The asymptotic level approached by S_2 decreases with decreasing R_o/λ, and, in fact, if the low-wavenumber spectrum is constant, we have approximately $S_2 \to (\pi R_o/\lambda)^2$. S_1 at large L depends mainly on the superficial extent of the sheath (e.g., on a) but also somewhat on ω and L.

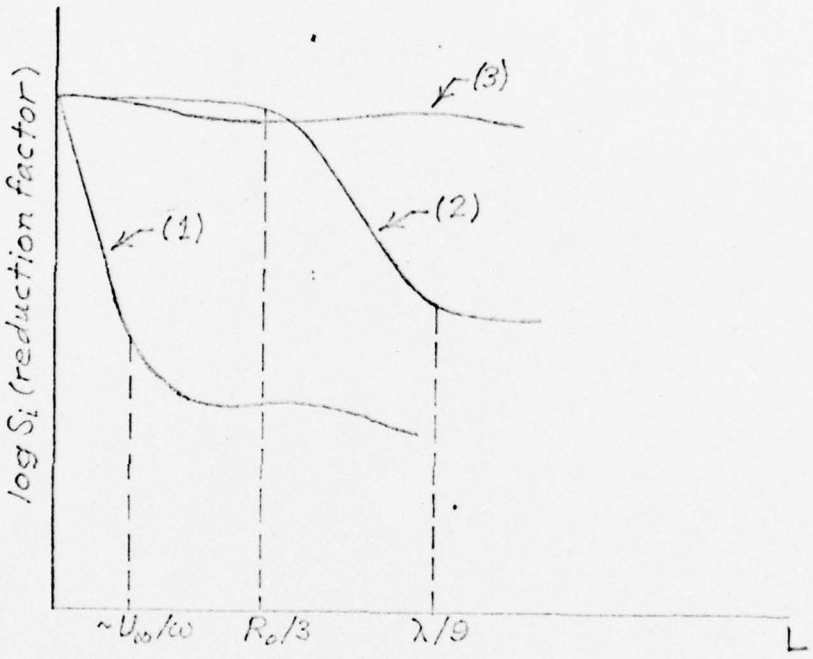

Figure A2-1. Schematic dependence of noise-reduction factors on layer thickness for (1) high-wavenumber, (2) low-wavenumber, (3) acoustic components.

APPENDIX 3

NORMALIZED CROSS-SPECTRAL DENSITY OF NOISE FOR ACOUSTIC AND TURBULENT BOUNDARY-LAYER PRESSURE FIELDS AND FOR UNCORRELATED SUPERPOSED FIELDS

A.3.1 Introduction

The measured noise cross-spectra between flush elements ordinarily involve a frequency-dependent mixture of pressure fields with characteristic and differing properties, namely a turbulent boundary-layer (TBL) field, an acoustic field, and perhaps a bending-wave field. Here we shall note the cross-spectra expected for each of these individually, and draw inferences about normalized cross-spectra associated with the superposed fields in pertinent idealized examples. We thereby provide a basis for analysis and interpretation of the measured cross-spectra.

A.3.2 Cross-Spectrum for TBL Noise

Let $\tilde{\Psi}_1(\overline{\zeta},\omega)$ denote the frequency transform of the cross-correlation of the average pressures on a pair of flush elements, where $\overline{\zeta} = (\zeta_1,\zeta_3)$ is the center-to-center separation vector, with ζ_1 streamwise, and the subscript 1 on $\tilde{\Psi}_1$ is used to distinguish the TBL as the pressure field being considered. Likewise, let $\Psi_1^{(1)}(\omega), \Psi_1^{(2)}(\omega)$ denote the respective average-pressure spectra due to the TBL on the elements individually. The normalized corss-spectral density is then given by

$$\text{(A3-1)} \qquad \psi_1(\overline{\zeta},\omega) = \tilde{\Psi}(\overline{\zeta},\omega)/[\Psi_1^{(1)}(\omega)\Psi_1^{(2)}(\omega)]^{1/2}.$$

For small elements, i.e., for $\omega R_o/U_\infty \ll 1$ where U_∞ is the asymptotic flow velocity and R_o the radius of either element, laboratory measurements on the TBL of a flat plate have yielded, in a broad regime, the similarity form

$$\text{(A3-2)} \qquad \psi_1(\overline{\zeta},\omega) = \exp(i\omega\zeta_1/u_c)F(\omega\overline{\zeta}/u_c),$$

where F is a positive function of the indicated dimensionless argument [with $F(0) = 1$] and the effective convection velocity u_c decreases from $\sim 0.8U_\infty$ at low frequency to $\sim 0.58U_\infty$ at relatively high frequency (e.g., see Ref. 1). The measurements have determined F for $\bar{\zeta} = (\zeta_1, 0)$, $\bar{\zeta} = (0, \zeta_3)$, and for some intermediate values of ζ_3/ζ_1. Similar results have been obtained in sea tests on the TBL of a ship's hull (e.g., Ref. 2 and Purvis I phase of the tests reported here). As a simple approximation that roughly matches these results, for indicative purposes we may take

$$(A3\text{-}3) \qquad F(\omega\bar{\zeta}/u_c) = \exp(-\alpha_1\omega\zeta_1/u_c)\exp(-\alpha_3\omega\zeta_3/u_c),$$

provided $\alpha_1\zeta_1 \gg \alpha_3\zeta_3$ or $\alpha_1\zeta_1 \ll \alpha_3\zeta_3$,* with

$$\alpha_1 \cong 0.105, \quad \alpha_3 \cong 0.714.$$

In App. 4 a rough estimate is made of the change in $\Psi_1(\bar{\zeta},\omega)$ from that given for small areas by (A3-2) when the elements (assumed equal and circular) are not small ($\omega R_o/U_\infty \gtrsim 1$). It is indicated that the phase factor in Ψ_1 is relatively insensitive to this effect and that the magnitude $|\Psi_1|$ may be increased in some regime by a factor ~ 2 but does not likely differ in order of magnitude or general behivior.

A.3.3 Cross-Spectra for Acoustic Noise

We consider now pure acoustic noise having the wave number ω/c and spatial coherence of a radiated field, and incident on the pair of correlated elements with some angular distribution but no correlation of the noise from different directions. Let $N(\theta,\varphi,\omega)$ denote the spectral density of net noise pressure per unit solid angle due to waves incident from azimuth φ relative to

*For arbitrary $\alpha_1\zeta_1/\alpha_3\zeta_3$ we may reasonably presume

$$(A3\text{-}4) \qquad F(\omega\bar{\zeta}/u_c) \cong \exp\left\{-(\alpha_3\omega/u_c)\left[\zeta_3^2 + (\alpha_1/\alpha_3)^2\zeta_1^2\right]^{1/2}\right\}$$

(see also App. 4).

the ζ_1 direction and polar angle θ relative to the normal to the plane of elements. We confine consideration to a regime where the elements are small compared to the sound wave length ($\omega R_o/c \lesssim 1$), where c is the speed of sound in water). Using a subscript 2 to denote the acoustic field being considered and forming the normalized cross-spectrum $\psi_2(\bar{\zeta},\omega)$ as at (A3-1), we obtain

$$\text{(A3-5)} \qquad \psi_2(\bar{\zeta},\omega) = [\int d\Omega N(\theta,\varphi,\omega)]^{-1} \int d\Omega N(\theta,\varphi,\omega) \times \exp[i(\omega/c)\sin\theta(\zeta_1\cos\varphi + \zeta_3\sin\varphi)],$$

where $d\Omega = d\varphi d\theta \sin\theta$.

For orientation, we may examine special cases. First, if the noise derives from a unique direction θ_o,φ_o, we have simply

$$\text{(A3-6)} \qquad \psi_2(\bar{\zeta},\omega) = \exp[i(\omega/c)\sin\theta_o(\zeta_1\cos\varphi_o + \zeta_3\sin\varphi_o)] \equiv e^{i\bar{k}_c\cdot\bar{\zeta}}$$

where $\bar{k}_c$ is the incident wave vector ($|\bar{k}_c| = \omega/c$). In this instance we have $|\psi_2| = 1$, and the phase of ψ_2 advances by 2π only as $\omega\zeta/c$ changes by an amount $\geq 2\pi$ depending on the angle between $\bar{k}_c$ and $\bar{\zeta}$. A second special case is that of hemispherical isotropy; from (A3-5) we then obtain

$$\text{(A3-7)} \qquad \psi_2(\bar{\zeta},\omega) = \sin(\omega\zeta/c)/(\omega\zeta/c)$$

($\zeta^2 \equiv \zeta_1^2+\zeta_3^2$). A further case is that of azimuthal independence with the wave vectors constrained to parallel the plane of $\bar{\zeta}$ (two-dimensional isotropy, $\theta = \pi/2$); we obtain

$$\text{(A3-8)} \qquad \psi_2(\bar{\zeta},\omega) = J_o(\omega\zeta/c).$$

In the cases of (A3-7) and (A3-8), unlike (A3-6), $|\psi_2|$ is oscillatory and small ($\ll 1$) for $\omega\zeta/c \gg \pi$; likewise, the phase of ψ_2 is sectionally constant, jumping from zero to π and back again as ψ_2 changes sign with increasing $\omega\zeta/c$.

A.3.4 Cross-Spectra for Bending Waves

Along with the acoustic radiation field from sources well removed from the elements in question, the total acoustic pressure will be affected by the field due to such sources but mediated by the hull or other bounding surface with bending-wave response, and likewise due to more local excitation of bending-waves by the TBL pressure field. At a given frequency, many wave numbers (or wave speeds) will contribute to this bending-wave field. The principal dependence on wave number will be inversely as the impedance of the water-loaded plate. The distribution of wave numbers and wave directions will not be continuous but rather spaced in accord with the modes of the finite local mechanical structure.

The previous discussion of the cross-spectrum for an incident radiation field may be regarded as roughly applicable also to the present field where, however, there is a distribution of wave speeds c with a peak near the speed of free bending waves in the loaded plate (and $\sin\theta = 1$). These waves may produce jumps in the phase similar to those associated with (A3-8), but more closely spaced in frequency, since the pertinent c will ordinarily be much smaller than the speed of sound in water. The magnitude of this pressure field and hence its influence on the actual measured normalized cross-spectra will depend on the impedance of the local plate or window surrounding the elements.

A.3.5 Cross-Spectra for Shielded Elements

We consider briefly the implication for the cross-spectra of component fields discussed above where the elements are not flush but shielded from the flow boundary by a layer or dome.

The TBL cross-spectrum, given for a flush element by (A3-2), is drastically altered; for a layer of large lateral extent the high-wavenumber part of the pressure on each element, which largely determines the form of the cross-spectrum for flush-mounted elements, is greatly attenuated for depths $L \gg U_\infty/\omega$, as

discussed in App. 2. Some contribution from TBL pressure at low wave numbers may remain, modified by the impedance of the dome cover, if any. Assuming a white wavenumber spectrum, which may be roughly valid in the pertinent range if the cover impedance is small, we can readily find the normalized cross-spectrum for such a pressure field on shielded elements in a rigid baffle at depth L in a fluid of sound speed c in the particular regime $\omega L/c \gg 1, (\omega L/c)^{-1}(\zeta/L) \ll 1$; we obtain

$$\psi_1(\zeta,\omega) \cong 2J_1(\omega\zeta/c)/(\omega\zeta/c). \quad \text{(A3-9)}$$

The fluid dome has been treated as laterally infinite in deriving this result, which is strictly justified only if the lateral dimensions, say a, satisfy $(\omega L/c)(\omega a/c)^{-1/2} \ll 1$. The result in the more interesting regime where $\omega L/c \lesssim 1$ and $\zeta \sim L$ is less readily evaluated and depends sensitively on the assumed wavenumber spectrum.

The results for cross-spectra of acoustic fields given above apply equally to fluid-shielded elements, but the actual effective angular distribution no doubt is conditioned greatly by the local structure and geometry.

A.3.6 Characteristic Normalized Cross-Spectra for Mixed Pressure Fields

We consider now the behavior of the magnitude and phase of the normalized cross-spectrum where the pressure on either element is due to a superposition of fields of the idealized types discussed above. We assume that the component fields considered are uncorrelated with one another. This is likely to be a good, though imperfect, approximation in the application in question. Accordingly, the (unnormalized) cross-spectrum of area-averaged noise pressure on a pair of elements, $\bar{\psi}(\bar{\zeta},\omega)$, may be written as a sum of the cross-spectra, $\bar{\psi}_i(\bar{\zeta},\omega)$, due to

the component pressure fields i:

$$\text{(A3-10)} \qquad \bar{\psi}(\bar{\zeta},\omega) = \Sigma_i \bar{\psi}_i(\bar{\zeta},\omega).$$

The autospectrum of average pressure for the ν-th element of the pair, $\psi^{(\nu)}(\omega)$, may likewise be written as a sum of the component autospectra:

$$\text{(A3-11)} \qquad \psi^{(\nu)}(\omega) = \Sigma_i \psi_i^{(\nu)}(\omega) \qquad (\nu = 1,2).$$

We denote the magnitude and phase of the normalized cross-spectrum due to the total field by $\gamma(\bar{\zeta},\omega)$, $\varphi(\bar{\zeta},\omega)$, respectively, choosing $-\pi < \varphi \leq \pi$; we denote the magnitudes and phases for the normalized cross-spectra due to the individual component fields similarity by $\gamma_i(\bar{\zeta},\omega)$, $\varphi_i(\bar{\zeta},\omega)$ $(-\pi < \varphi_i \leq \pi)$. Hence we have

$$\begin{aligned} \psi_i(\bar{\zeta},\omega) &\equiv \gamma_i(\bar{\zeta},\omega)\exp[i\varphi_i(\bar{\zeta},\omega)] \\ &= \bar{\psi}_i(\bar{\zeta},\omega)/[\psi_i^{(1)}(\omega)\psi_i^{(2)}(\omega)]^{1/2} \end{aligned} \qquad \text{(A3-12)}$$

and by (10) and (11)

$$\begin{aligned} \psi(\zeta,\omega) &\equiv \gamma(\bar{\zeta},\omega)\exp[i\varphi(\bar{\zeta},\omega)] \\ &= \psi(\zeta,\omega)/[\psi^{(1)}(\omega)\psi^{(2)}(\omega)]^{1/2} \\ &= \Sigma_i \bar{\psi}_i(\zeta,\omega)/[\Sigma_i \psi_i^{(1)}(\omega)]^{1/2}[\Sigma_j \psi_j^{(2)}(\omega)]^{1/2} \\ &= \frac{\Sigma_i \gamma_i(\bar{\zeta},\omega)[\psi_i^{(1)}(\omega)\psi_i^{(2)}(\omega)]^{1/2}\exp[i\varphi_i(\bar{\zeta},\omega)]}{[\Sigma_i \psi_i^{(1)}(\omega)]^{1/2}[\Sigma_j \psi_j^{(2)}(\omega)]^{1/2}} \end{aligned} \qquad \text{(A3-13)}$$

In the special case of equal autospectra, $\psi_i^{(1)}(\omega) = \psi_i^{(2)}(\omega) \equiv \psi_i(\omega)$, (13) becomes

$$\text{(A3-14)} \qquad \psi(\bar{\zeta},\omega) = [\Sigma_i \psi_i(\omega)]^{-1}\Sigma_o \gamma_i(\bar{\zeta},\omega)\psi_i(\omega)\exp[i\varphi(\bar{\zeta},\omega)].$$

This form holds also if $b\psi_i^{(2)}(\omega) = \psi_i^{(1)}(\omega) = \psi_i(\omega)$, where b is independent of i.

We note the idealized example of perfect correlation in the sense that $\gamma_i(\bar{\zeta},\omega) = 1$, $\varphi_i(\bar{\zeta},\omega) = 0$. In this instance, (13) reduces to

$$\text{(A3-15)} \qquad \psi(\bar{\zeta},\omega) = \Sigma_i[\psi_i^{(1)}(\omega)\psi_i^{(2)}(\omega)]^{1/2}/[\Sigma_i\psi_i^{(1)}(\omega)]^{1/2}[\Sigma_j\psi_j^{(2)}(\omega)]^{1/2}.$$

By Schwartz's inequality, this yields $\psi(\bar{\zeta},\omega) \leq 1$. If $b\psi_i^{(2)}(\omega) = \psi_i^{(1)}(\omega)$, then the equality holds, but if instead the mixture of noise spectra differs for the two elements, then the magnitude $\gamma_i(\bar{\zeta},\omega)$ is less than unity even though $\gamma_i(\bar{\zeta},\omega) = 1$ for each i.

Let us imagine a superposition of an azimuthally isotropic acoustic field, with normalized cross-spectrum $\psi_2(\bar{\zeta},\omega)$ of (A3-8) and a unidirectional acoustic field, with cross-spectrum $\psi_3(\bar{\zeta},\omega)$, say, given by (A3-6). Eq. (A3-14), then yields

$$\text{(A3-16)} \qquad \psi(\zeta,\omega) = (\psi_2 + \psi_3)^{-1}\left[\psi_2 J_o(\omega\zeta/c) + \psi_3 e^{i\omega\zeta_p/c}\right],$$

where ψ_i denotes the autospectra $\psi_i(\omega)$ and ζ_p is the projection of $\bar{\zeta}$ along the wave vector of the field i = 3. The magnitude $\gamma(\zeta,\omega)$ of ψ has a form intermediate between $\gamma_2 = |J_o(\omega\zeta/c)|$ and $\gamma_3 = 1$; where $J_o(\omega\zeta/c) = 0$, in particular, we have $\gamma = \psi_3/(\psi_2 + \psi_3)$. In a range of $\omega\zeta/c$ such that $J_o(\omega\zeta/c) < 0$, if ψ_2/ψ_3 has an appropriate value, the phase φ of ψ may assume any value; so long as $\omega\zeta/c < 2.4$ so that $J_o(\omega\zeta/c) > 0$, however, φ remains a small angle.

Let us now consider a superposition of a TBL pressure field (i = 1) and an acoustic field (i = 2), where we no longer specify a particular idealized form for the latter. We regard the possible frequency dependence of γ and φ at fixed $\bar{\zeta}$. Suppose

the elements are sufficiently small that provided the frequency is not too high, at least, the TBL contribution dominates the autospectra, i.e., $\psi_1(\omega) \gg \psi_2(\omega)$. In the low-frequency range where $\alpha_1\omega\zeta_1/u_c \leq 1$ and $\alpha_3\omega\zeta_3/u_c \leq 1$, according to (A3-3) for $\gamma_1(=F)$ we will then have also $\gamma_1(\bar{\zeta},\omega)\psi_1(\omega) \gg \gamma_2(\bar{\zeta},\omega)\psi_2(\omega)$; by (A3-14) the magnitude and phase γ,φ will there be given approximately by the corresponding TBL functions γ_1,φ_1 of (A3-3) and (A3-2). In view of the rapid decrease of the TBL cross-spectral magnitude $\gamma_1(=F)$ implied by (A3-3) relative to the decrease of the acoustic magnitude γ_2 exemplified by (A3-6) and (A3-8), we see however, that in some frequency range where $\omega\zeta/u_c \gg 1$ but $\omega\zeta/c \lesssim 1$ we will have $\gamma_1(\bar{\zeta},\omega)\psi_1(\omega) \ll \gamma_2(\bar{\zeta},\omega)\psi_2(\omega)$. In this regime Eq. (A3-14) yields rather

$$\text{(A3-17)} \qquad \psi(\bar{\zeta},\omega) \cong \gamma_2(\bar{\zeta},\psi)\left\{\psi_2(\omega)/[\psi_1(\omega) + \psi_2(\omega)]\right\}\exp[i\varphi_2(\bar{\zeta},\omega)].$$

So long as $\psi_1(\omega) \gg \psi_2(\omega)$, therefore, the magnitude γ of the normalized cross-spectrum will be small, but the phase φ will be approximately the phase φ_2 of the acoustic field, which varies slowly and remains small for $\omega\zeta/c \lesssim 1$. It may happen that the acoustic contribution to the autospectra decreases less rapidly than the TBL contribution and, at some higher frequency, becomes comparable with and then larger than the latter [$\psi_2(\omega) \gtrsim \psi_1(\omega)$]. In such a range, according to (A3-17) the magnitude γ will again increase and approach the acoustic value γ_2 while the phase will continue to be nearly equal to φ_2.

APPENDIX 4*

CROSS-SPECTRAL DENSITY OF TURBULENT BOUNDARY-LAYER PRESSURE FOR NON-VANISHING AREAS

We indicate here to what degree the normalized inter-element cross-spectral density of area-averaged TBL pressure depends on element area. We take the elements to be circular and of equal radii R_o and denote the normalized cross-spectral density of area-averaged pressure by $\psi_{R_o}(\bar{\zeta},\omega)$ (indentifiable with $\psi_1(\bar{\zeta},\omega)$ of App. 3). In general, this normalized cross-spectrum is related to the (unnormalized) cross-spectrum for point pressure, $\tilde{\psi}_o(\bar{\zeta},\omega)$,

$$(A4.1) \qquad \psi_{R_o}(\bar{\zeta},\omega) = \int d^2\bar{R}_1 \int d^2\bar{R}_2 \tilde{\psi}_o(\bar{R}_2-\bar{R}_1,\omega) \;/\; \int d^2R_1 \int d^2R_1' \tilde{\psi}_o(\bar{R}_1'-\bar{R}_1,\omega),$$

where $\int d^2\bar{R}_1$ and $\int d^2\bar{R}_1'$ run over the area of a single element a and $\int d^2\bar{R}_2$ over that of the other. We denote the autospectrum of average pressure on either element by $Q_{R_o}(\omega)$ (identifiable with $\psi_1^{(v)}(\omega)$ of App. 3), whence $Q_o(\omega)$ is the spectrum of point pressure. In terms of the wavenumber-frequency spectrum of TBL pressure, $P(\bar{K},\omega)$, we have

$$(A4.2) \qquad \tilde{\psi}_o(\bar{\zeta}',\omega) = \int d^2\bar{K}\, e^{i\bar{K}\cdot\bar{\zeta}'} P(\bar{K},\omega) \quad [\bar{K} = (k_1,k_3)].$$

(Thus we may write $Q_o(\omega) = \tilde{\psi}_o(0,\omega)$.) Inserting this in (A4.1) and performing the area integrals we obtain

$$(A4.3) \qquad \psi_{R_o}(\bar{\zeta},\omega) = \frac{\int d^2\bar{K}\, e^{i\bar{K}\cdot\bar{\zeta}} \left[2J_1(KR_o)/KR_o\right]^2 P(\bar{K},\omega)}{\int d^2\bar{K} \left[2J_1(KR_o)/KR_o\right]^2 P(\bar{K},\omega)} .$$

In the approximation of point elements ($\omega R_o/U_\infty << 1$), we replace the area-averaging factor $[2J_1(KR_o)/KR_o]^2$ by unity in both numerator and denominator [recall App. 3, Eq. (A3-2)].

Suppose first that $P(\bar{K},\omega)$ contains a non-convective, low-wavenumber contribution, say $P_<$, that, with reference to

*This appendix is an edited version of App. A of Ref. 8.

non-vanishing R_o, may be regarded as independent of wavenumber $\bar{K}$. Such a component is found to yield a vanishing contribution to the numerator in (A4.3), reflecting the fact that a flat wavenumber spectrum corresponds to zero correlation distance and hence no cross-correlation between elements. We therefore expect that the major contribution to the numerator, if not to the denominator ($Q_{R_o}(\omega)$), in (A4.3) arises from the region of the convective peak (where $k_1' \sim \omega/u_c$) in $P(\bar{K},\omega)$. Accordingly, we assume a form for $P(\bar{K},\omega)$ that is thought to represent correctly the character of this peak, though it cannot be expected to have validity in the "tail" where $k_1 \ll \omega/U_\infty$. In this way, we probably overestimate, if anything, the normalized cross-spectrum $\Psi_{R_o}(\bar{\zeta},\omega)$, a course preferable to underestimating it. We may expect also that the error from our crude representation of $P(\bar{K},\omega)$ in the region of its peak will in part be cancelled on account of its appearance in both numerator and denominator of (A4.3).

For reasons we shall not pursue*, we assume that $P(\bar{K},\omega)$ may be taken for present purposes as

$$(A4.4) \qquad P(\bar{K},\omega) = B^2 v_e^{-1}\left[K^2+(\omega-u_o k_1)^2/v_e^2+a^2\right]^{-(\nu+1/2)},$$

($K^2 = k_1^2+k_3^2$), where u_o is a certain average convection velocity (not to be identified precisely with u_c in Eq. (A3-2) of App. 3; v_e is an effective rms local convection velocity associated with turbulence and shear, of the order of $3v_*$, or perhaps somewhat larger, with v_* the usual friction velocity; B^2 is a suitably dimensional factor regarded as constant; the constant ν may be related to the high frequency dependence of the convective contribution to the point spectrum given by (A4.4) according to $Q_o(\omega) \propto \omega^{-2\nu+1}$ (see Eq. (A4.6) below), and we presume $\nu \sim 5/3$; a^{-1} represents a mean spatial scale of the pressure fluctuations, perhaps $a^{-1} \sim \delta_*$ at moderate frequencies.

Referring first to point areas ($\omega R_o/u_o \ll 1$), from (A4.4)

*The explicit form (A4.4) has its origin in a treatment of homogenous turbulence (Ref. 5), but in general character is thought correct for the present purpose.

and (A4.2) we find*

$$\tilde{\Psi}_o(\bar{\zeta},\omega) = 2^{-\nu+3/2}\pi[\Gamma(\nu+1/2)]^{-1}B^2u_e^{-1}(\omega^2/u_e^2+a^2)^{-(\nu-1/2)/2}$$

(A4.5)

$$\times \exp(i\omega\zeta_1/u_c)(\zeta_3^2+\mu^2\zeta_1^2)^{(\nu-1/2)/2}$$

$$\times K_{\nu-1/2}((\omega^2/u_e^2+a^2)^{1/2}(\zeta_3^2+\mu^2\zeta_1^2)^{1/2}),$$

where

$$u_e^2 = u_o^2+v_e^2, \qquad u_c = u_e^2/u_o, \qquad \mu = v_e/u_e,$$

and K_α denotes a modified Bessel function of the exponentially decreasing sort. Likewise, we obtain

$$(A4.6) \qquad Q_o(\omega) \equiv \tilde{\Psi}_o(0,\omega) = \pi(\nu-1/2)^{-1}B^2u_e^{-1}(\omega^2/u_e^2+a^2)^{-(\nu-1/2)}.$$

Division of (A4.5) by (A4.6) yields the normalized cross-spectrum $\psi_o(\bar{\zeta},\omega)$ for point areas implied by (A4.4). We write $\psi_o(\bar{\zeta},\omega)$ explicitly in the approximation valid for $(\omega^2/u_e^2+a^2)^{1/2}(\zeta_3^2+\mu^2\zeta_1^2)^{1/2}\gtrsim 1$ when $K_{\nu-1/2}$ is replaced by its asymptotic form:

$$\psi_o(\bar{\zeta},\omega) \simeq \pi^{1/2}(\nu-1/2)2^{1-\nu}\Gamma(\nu+1/2)^{-1}\exp(i\omega\zeta_1/u_c)$$

(A4.7)

$$\times\left[(\omega^2/u_e^2+a^2)(\zeta_3^2+\mu^2\zeta_1^2)\right]^{(\nu-1)/2}\exp\left[-(\omega^2/u_e^2+a^2)^{1/2}(\zeta_3^2+\mu^2\zeta_1^2)^{1/2}\right].$$

For $\zeta_3 = 0$ or $\zeta_1 = 0$, we note, with appropriate ν, this form is closely similar to form (A3-2) and (A3-3) or A3-4) in App. 3.

We now get to the point of treating non-vanishing R_o in certain tractable regimes. In conceiving such regimes we are cognizant that, since $\zeta > 2R_o$, the factor $e^{i\bar{K}\cdot\bar{\zeta}}$ has a shorter period of oscillation in K than does the area-averaging factor except along a direction of $\bar{K}$ nearly normal to $\bar{\zeta}$. First, we assume $\omega R_o/u_e \lesssim 1$ and consider corrections in $\psi_{R_o}(\bar{\zeta},\omega)$ to lowest order in R_o. We therefore use the first two terms of the expansion

*Here and subsequently we have performed quadratures by aid of the Bateman project's Tables of Integral Transforms.

$$\left[2J_1(K\kappa_c)/KR_o\right]^2 = 1-(1/4)(KR_o)^2+ \ldots$$

and assume $\nu > 3/2$ in (A4.4), in which case the contribution of the second term to the numerator and denominator of (A4.3) converges and yields the correction asymptotically in the subject limit. The numerator may be written as

$$\left[1+(1/4)R_o^2(\partial^2/\partial\zeta_1^2+\partial^2/\partial\zeta_3^2)\right]\tilde{\Psi}_o(\bar{\zeta},\omega)$$

with $\tilde{\Psi}_o$ given by (A4.5). We assume $\mu \equiv v_e/u_e << 1$ (a reasonable approximation) but $\omega\mu\zeta_1/u_e \gtrsim 1$ (which implies $\zeta_1 >> R_o$). We restrict consideration to $\zeta_3 = 0$ for simplicity, as the case of greatest concern. To the order considered, we find

$$\tilde{\Psi}_{R_o}(\zeta_1,0,\omega) \simeq \left\{1-(1/4)(\omega R_o/u_c)^2 - (1/4)(R_o/\mu\zeta_1)^2\left[(\omega^2/u_e^2+a^2)^{1/2}\mu\zeta_1-\nu+1\right]\right\}\tilde{\Psi}_o(\zeta_1,0,\omega). \tag{A4.8}$$

Similarly, for the denominator of (A4.3) we find

$$Q_{R_o}(\omega) \simeq \left\{1-(1/4)(\nu-3/2)^{-1}R_o^2\left[(\nu-1)\omega^2/u_e^2+(1/2)a^2\right]\right\}Q_o(\omega). \tag{A4.9}$$

The ratio yields, to the order considered,

$$\Psi_{R_o}(\zeta_1,0,\omega) \simeq \left\{1+(1/8)(\nu-3/2)^{-1}\left[(\omega R_o/u_c)^2+(aR_o)^2\right] - (1/4)(R_o/\mu\zeta_1)^2\left[(\omega^2/u_e^2+a^2)^{1/2}\mu\zeta_1-\nu+1\right]\right\}\Psi_o(\zeta_1,0,\omega). \tag{A4.10}$$

This result indicates that the correlation is enhanced ($\Psi_{R_o}/\Psi_o > 1$) as R_o increases within the domain of applicability. It indicates also that the phase of Ψ_{R_o}, i.e., the effective convection velocity, remains unaffected in this approximation. The range of R_o to which (A4.10) applies, however, is explicitly limited to that where the enhancement being investigated is small.

We can successfully consider a second, more interesting limit. This is defined by the conditions

(A4.11) $\omega R_o/u_o >> 1$, $\mu(\omega R_o/u_o) << 1$, $\zeta_3 = 0$, $\omega\mu\zeta_1/u_o >> 1$, $\omega/u_e >> a$.

These conditions are crudely satisfied in much of the domain of interest. The second of conditions (A4.11) ensures that $J_1(KR_o)$ in (A4.3) varies little as k_1 varies through the convective peak, so that the k_1 integration may be performed; the first of (A4.11) then permits use of the asymptotic form for $J_1((k_3^2+\omega^2/u_e^2)^{1/2}R_o)$; the first and third permit a local average value of 1/2 to be used for the resulting factor $\cos^2((k_3^2+\omega^2/u_e^2)^{1/2}R_o - 3\pi/4)$; the fourth permits K_ν to be replaced by $K_{\nu+3}$, which has the same asymptotic form, with regard to a factor $K_\nu((k_3^2+\omega^2/u_e^2+a^2)^{1/2}\mu\zeta_1)$ from the k_1 integration in the numerator, and, when $\underline{a}$ is neglected by the fifth condition, the k_3 integration can also be carried out. Ultimately we obtain for the normalized cross-spectrum*

$$\psi_{R_o}(\zeta_1,0,\omega) \simeq \pi^{1/2}2^{1-\nu}\,\frac{\nu+1/2}{\nu}\,\frac{\Gamma(\nu+1/2)}{[\Gamma(\nu)]^2}\,\exp(i\omega\zeta_1/u_c)$$

(A4.12)

$$\times\,(\omega\mu\zeta_1/u_e)^{\nu-1}\exp(-\omega\mu\zeta_1/u_c).$$

Comparing with $\psi_o(\zeta_1,0,\omega)$ as given by (A4.7) with $a = 0$, we see that (A4.12) differs only by having the constant coefficient $(\nu-1/2)/\Gamma(\nu+1/2)$ of (A4.7) replaced by $[(\nu+1/2)/\nu]\Gamma(\nu+1/2)/[\Gamma(\nu)]^2$. If $\nu = 5/3$, the ratio of the latter to the former is 1.61. In the subject limits, the normalized cross-spectrum is thus increased relative to the instance of elements with vanishing area by 1.6 (and the phase is unchanged). The exact value computed may not be considered reliable in view of the many approximations. Nevertheless, the analysis suffices to indicate that the finite-area effect increases the inter-element cross-spectral density of average pressure by only a modest factor.

*The denominator of (A4.3) is given in the present approximation by

$$Q_{R_o}(\omega) \simeq 4\left(\frac{\nu}{\nu+1/2}\right)\left[\frac{\Gamma(\nu)}{\Gamma(\nu+1/2)}\right]^2 B^2 R_o^{-3} u_e^{-1}(\omega/u_e)^{-2\nu-2}.$$

CONFIDENTIAL

ELEMENT: HF-3

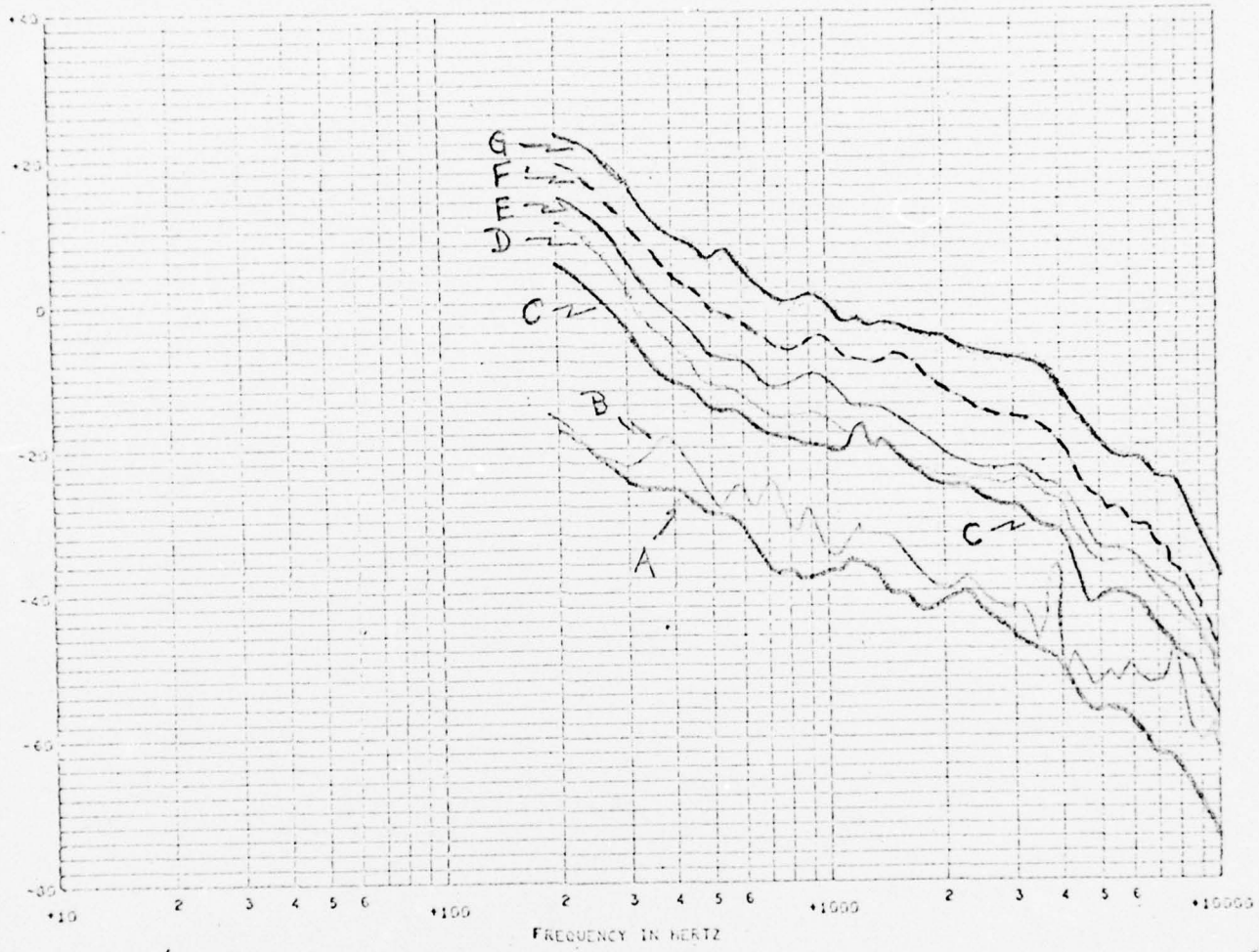

SPECTRUM DB REF 1 MICROBAR SQUARED TIMES SEC GXX LOW BAND CF56 - 598 - HIGH BAND CF56 - 616
RUN 342 START TIME 13047800.0 SPEED 30 HEADING 000
TYPE SER NO FT FROM EOW
TRG HF-3 026 09.75

A: 0 KTS - Run 336 - ORANGE
B: 0 KTS - Run 860 = BLUE
C: 10 KTS - Run 338 = Red
D: 15 KTS - Run 339A - GREEN
E: 20 KTS - Run 340A - PURPLE
F: 25 KTS - Run 341A = BLACK DOTTED
G: 30 KTS - Run 342 - BLACK

FIG. 3.1.1-1

ELEMENT: HF-5

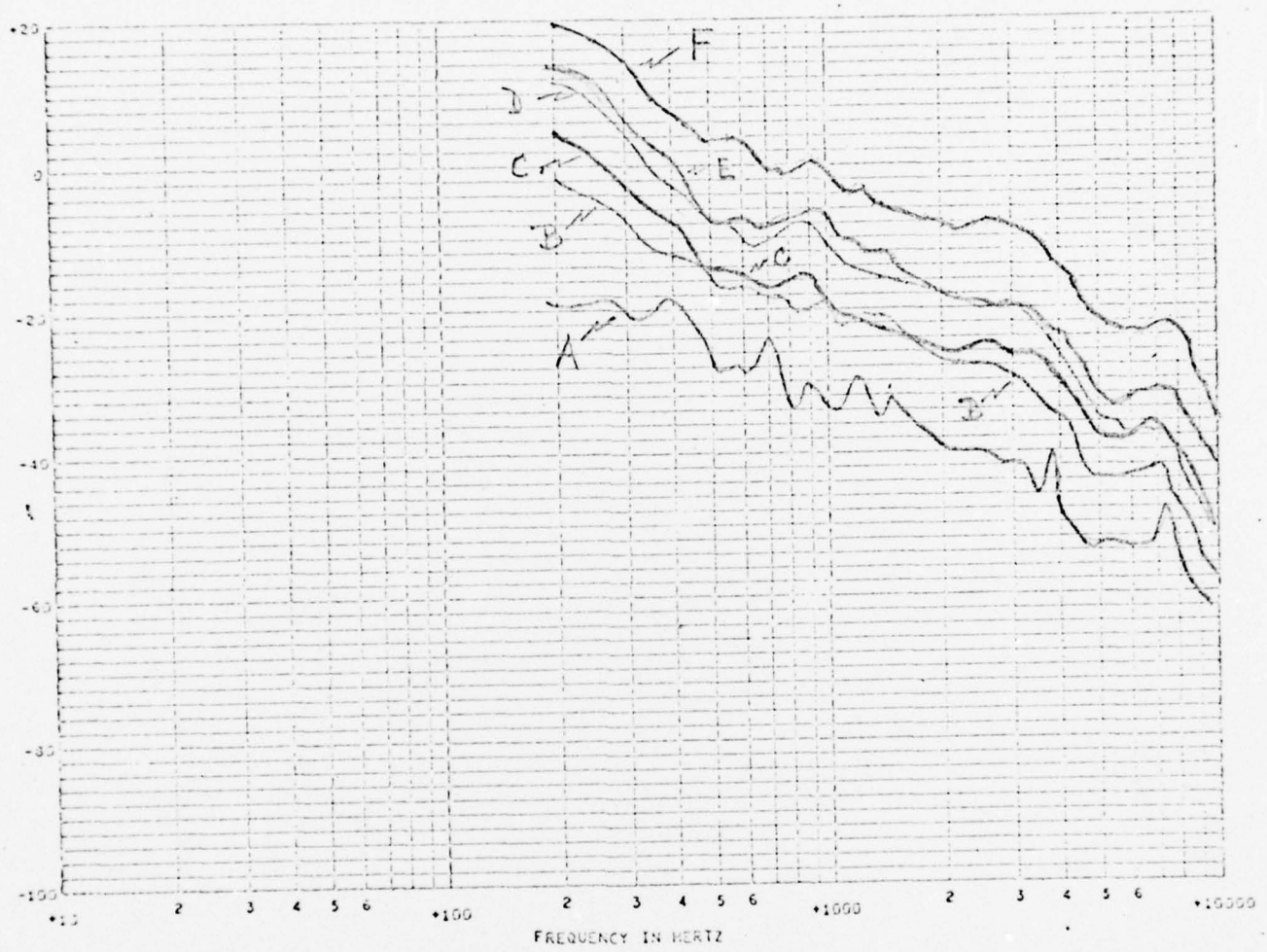

SPECTRUM DB REF 1 MICROBAR SQUARED TIMES SEC GXX LOW BAND CPSG - 80D - HIGH BAND CPSG - 62D
RUN 342 START TIME 13047900.0 SPEED 30 HEADING 000

TYPE	SER NO	FT FROM BOW
TRG	HF-5	023 06.75

A. = 0 KTS - Run 860
B. = 10 KTS - Run 338
C. = 15 KTS - Run 339A
D. = 20 KTS - Run 340B
E. = 22 KTS - Run 862
F. = 30 KTS - Run 341

FIG. 3.1.1-2

2a.

CONFIDENTIAL

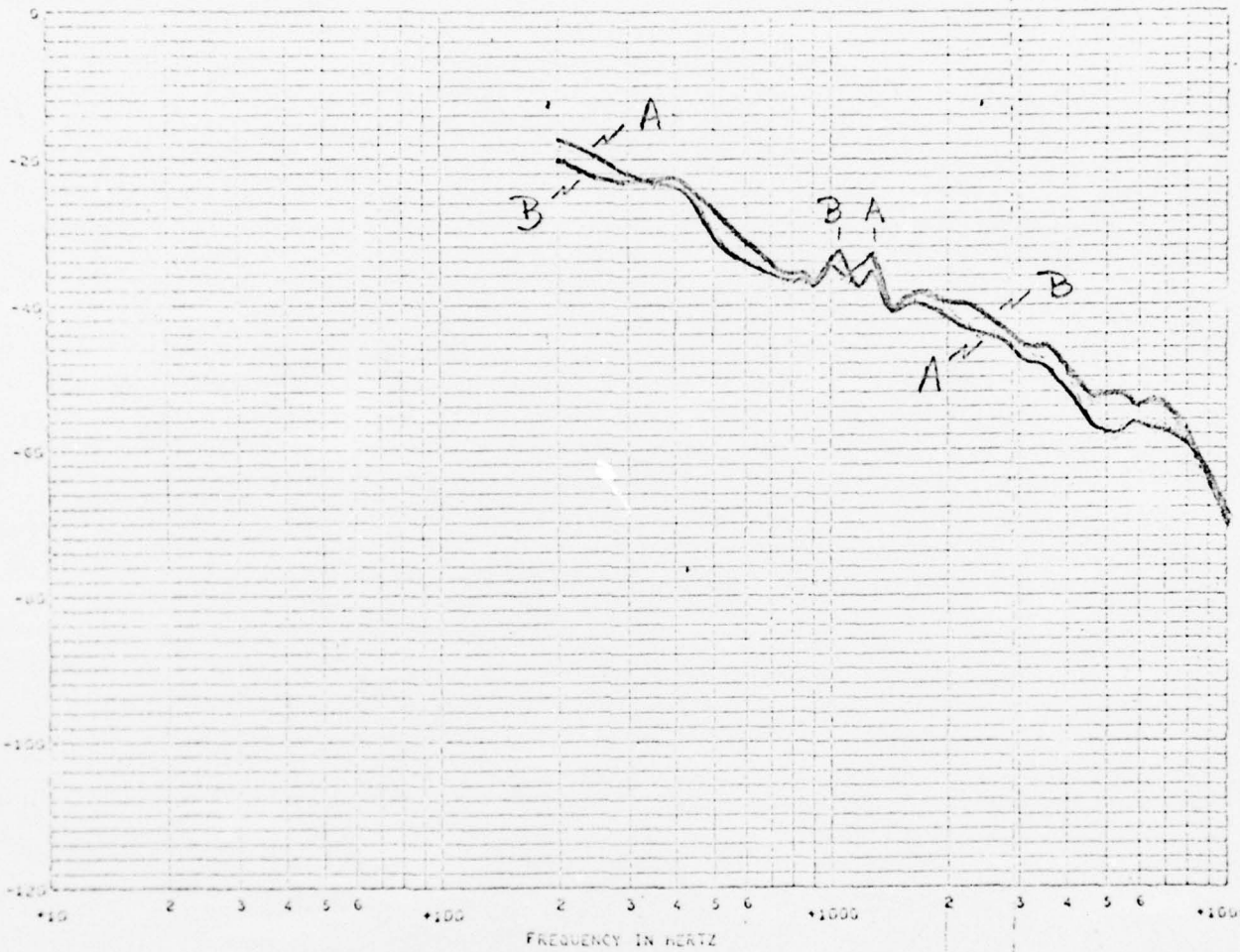

SPECTRUM DD REF 1 MICRODAR SQUARED TIMES SEC 0XX LOW BAND CPSG - 20 - HIGH BAND CPSG - 40
RUN 336 START TIME 1490291G.0 SPEED DD HEADING DDD
TYPE SER NO FT FROM DOW
TAG HF-5 020 00.75

A = HF-5
B = HF-12
} Run 336 - 0 KTS

FIG. 3.1.1-3

CONFIDENTIAL

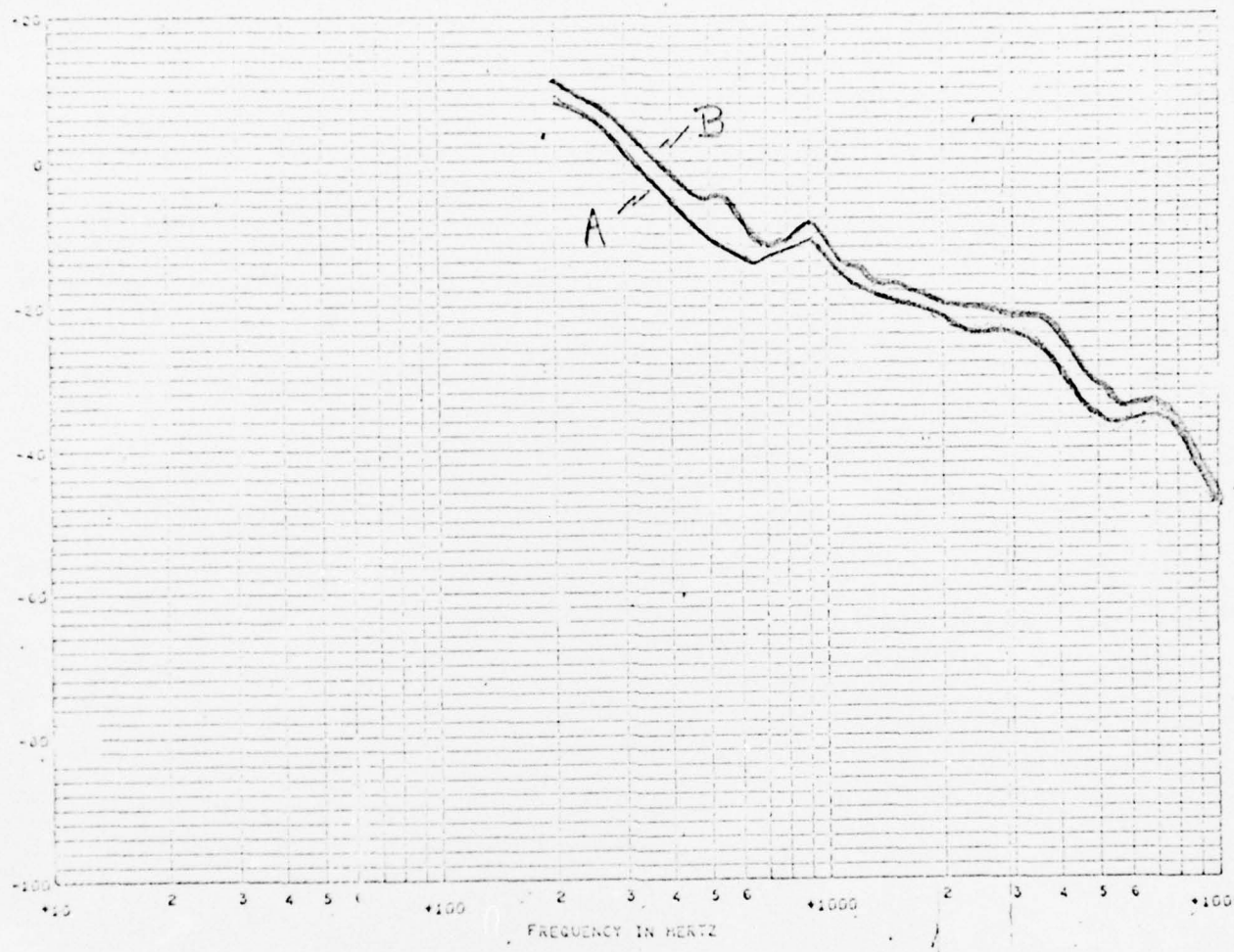

SPECTRUM DD REF 1 MICROBAR SQUARED TIMES SEC 0XX LOW BAND CPSD - 94D - HIGH BAND CPSD - 93D
RUN 340A START TIME 1640840.0 SPEED 20 HEADING 000
TYPE SER NO FT FROM DOW
TRD HF-5 028 00.75

A = HF-5
B = HF-12
} Run 340A - 20 KTS

Fig. 3.1.1-4

CONFIDENTIAL

ELEMENT: HF-3

1791

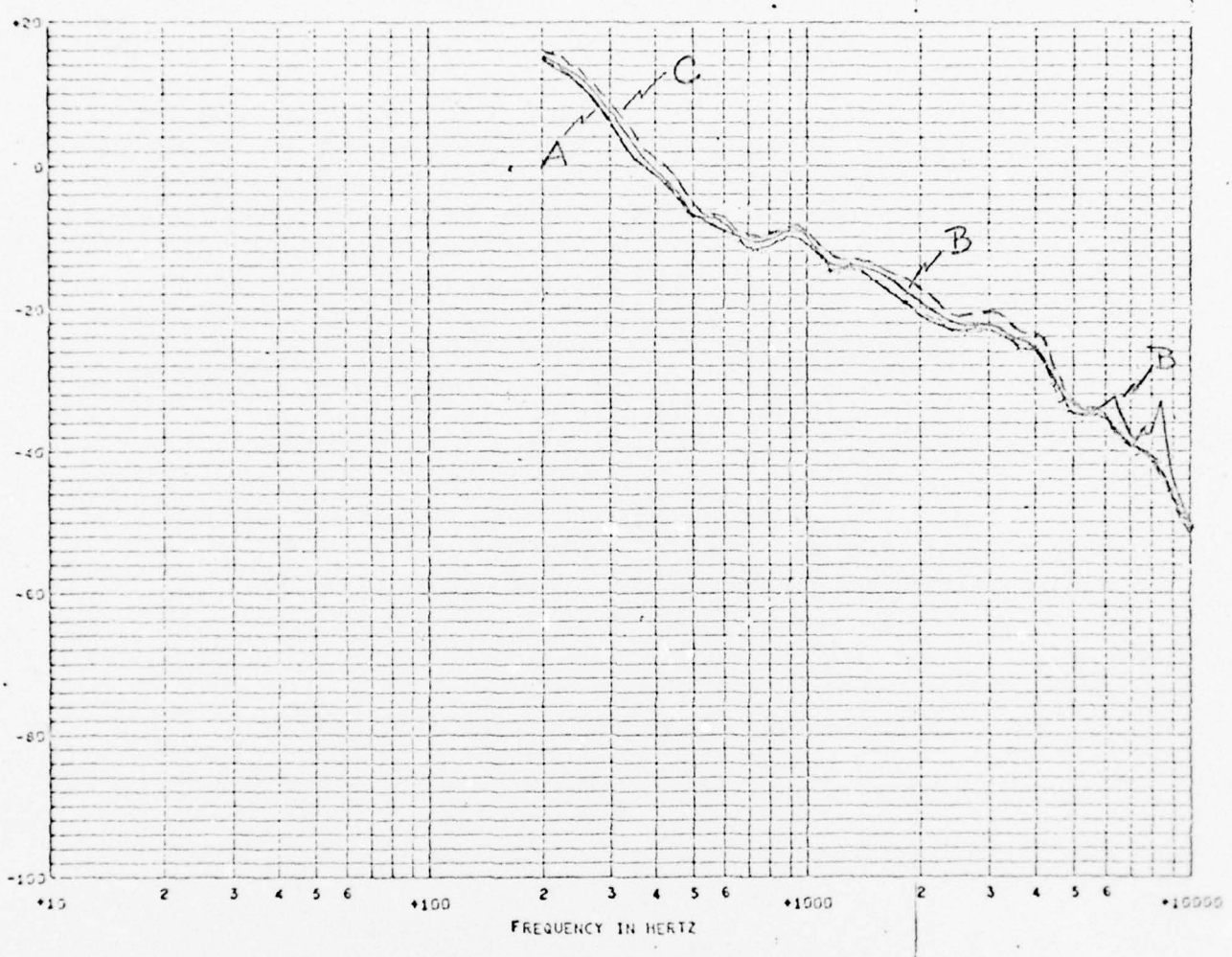

SPECTRUM DB REF 1 MICROBAR SQUARED TIMES SEC GXX LOW BAND CF56 - 338 - HIGH BAND CF56 - 348
RUN 340A START TIME 16946940.0 SPEED 20 HEADING 000

TYPE	SER NO	FT FROM BOW
TRG	HF-3	026 09.75

A= 20 KNOTS - RUN 340A, 0°
B= 20 KNOTS - RUN 436, 90°
C= 20 KNOTS - RUN 637, 270°

FIG. 3.1.1-5

CONFIDENTIAL

ELEMENT: HF-3

1731

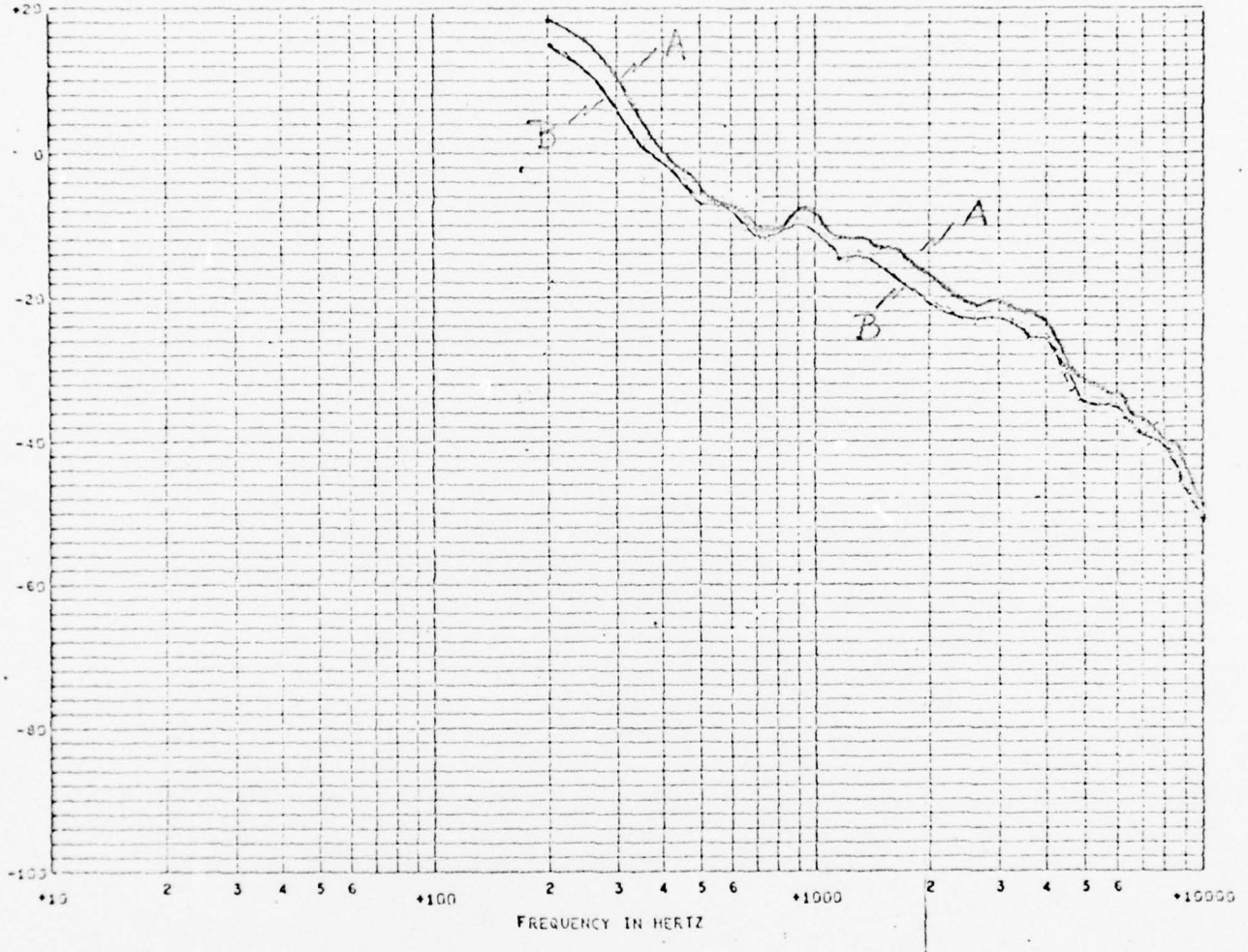

SPECTRUM DD REF 1 MICROBAR SQUARED TIMES SEC GXX LOW BAND CF56 - 33B - HIGH BAND CF56 - 34B
RUN 340A START TIME 16946#40.0 SPEED 20 HEADING 0°
TYPE SER NO FT FROM BOW
TRG HF-3 026 09.75

A. = RUN 822 - 20KTS - HEADING FRR

B. = RUN 340A - 20KTS - HEADING 0°

NOTE: RUN 823 - FLR ≅ FRR

FIG. 3.1.1-6

CONFIDENTIAL

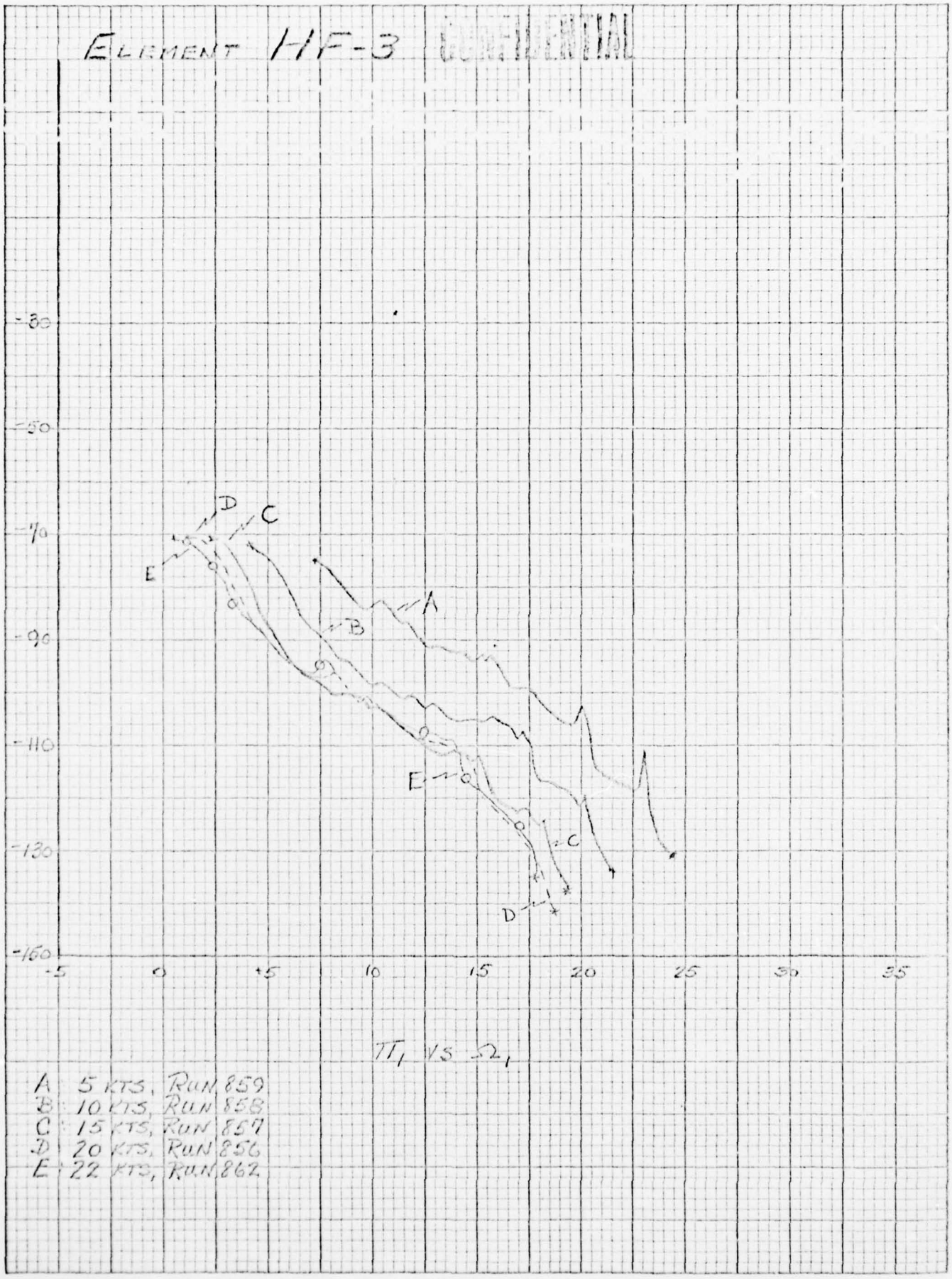

FIG. 3.1.1-7

ELEMENT - HF-8

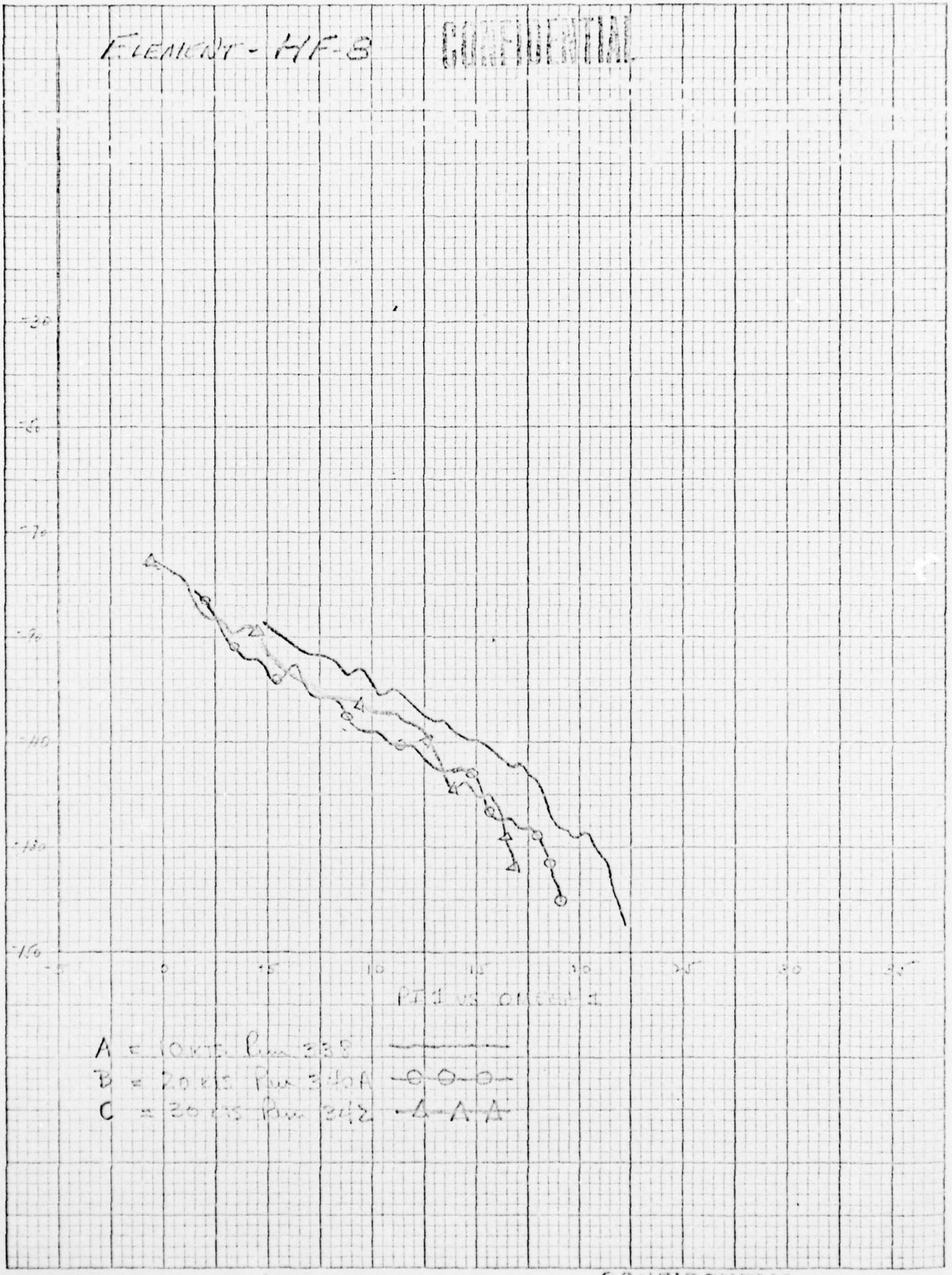

FIG. 3.1.1-8

ELEMENT: LF 6

1017

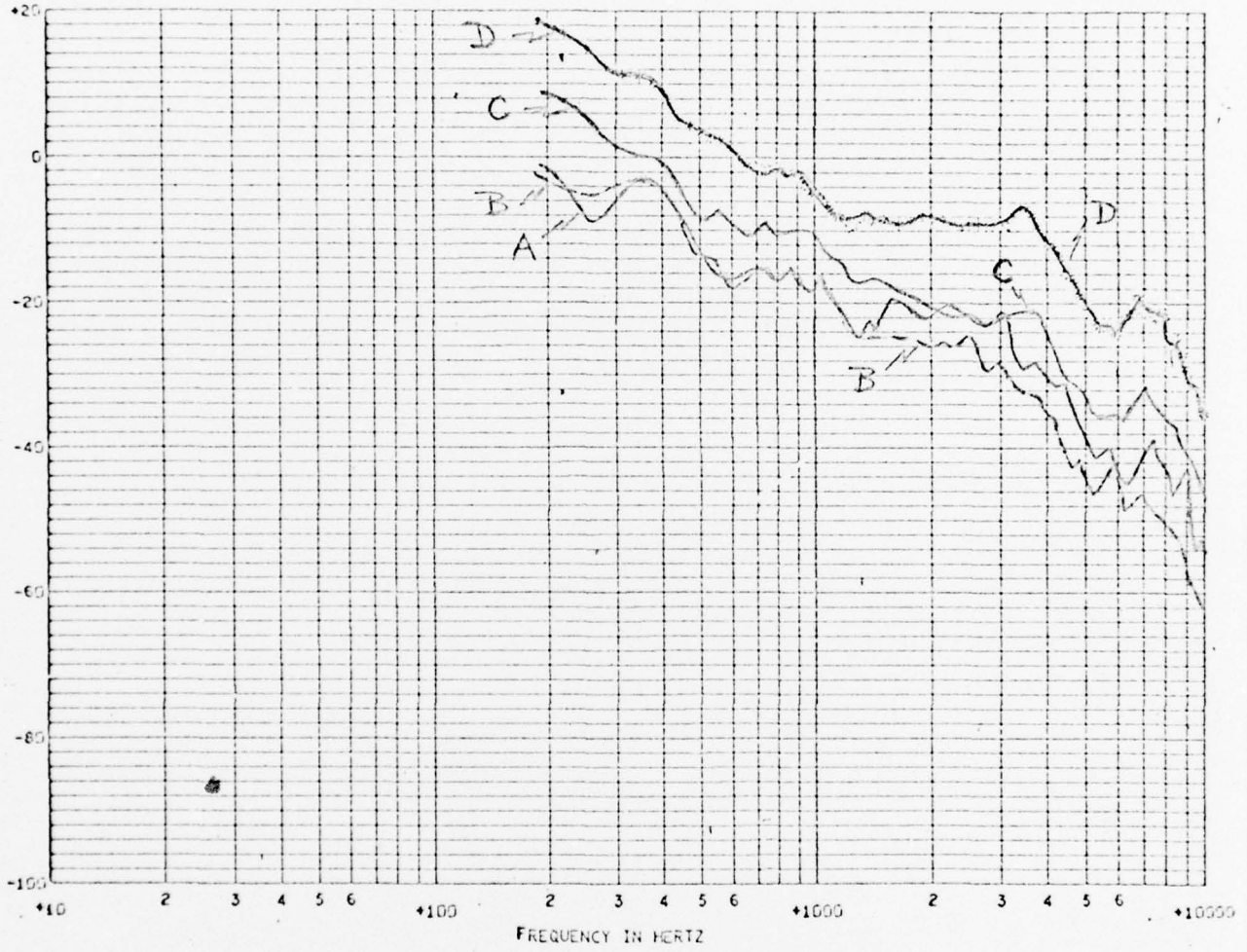

SPECTRUM DB REF 1 MICROBAR SQUARED TIMES SEC GXX LOW BAND CF222 - 43B - HIGH BAND CF222 - 45B
RUN 349 START TIME 13:56:00.0 SPEED 30 HEADING 000
TYPE SER NO FT FROM DOW
TRG EF-5 087 11.75

LF-6

A: 0 KTS, RUN 343
B: 10 KTS, RUN 345
C: 20 KTS, RUN 347A
D: 30 KTS, RUN 349

FIG. 3.1.1-9

1038

ELEMENT: LF-7

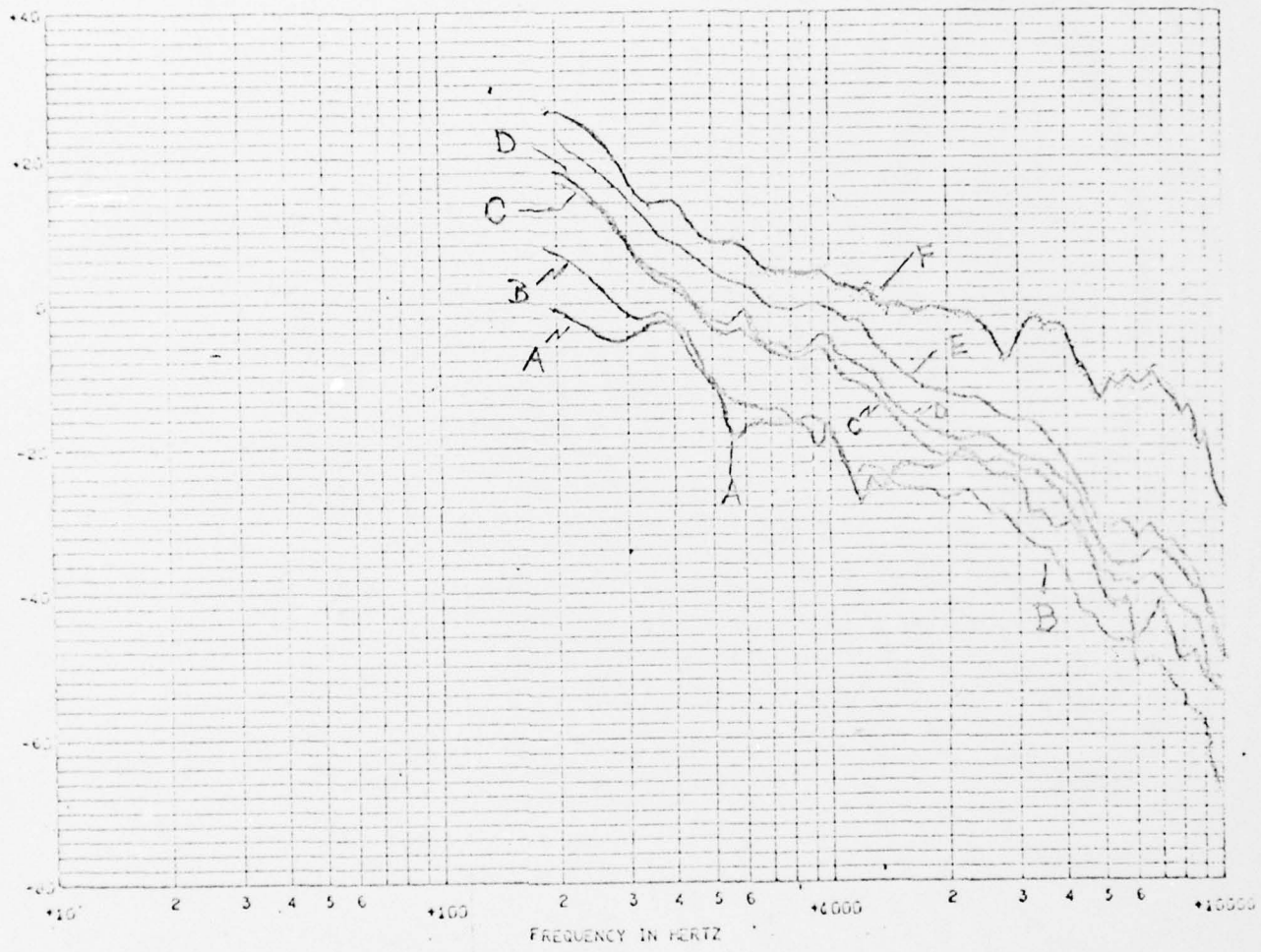

SPECTRUM DB REF 1 MICROBAR SQUARED TIMES SEC GXX LOW BAND CF222 - 44B - HIGH BAND CF222 - 46B
RUN 345 START TIME 13456000.0 SPEED [illegible] HEADING 000

TYPE	SER NO	FT FROM BOW
TRG	LF-7	000 02.75

A= 0 KTS Run 343
B= 10 KTS Run 345
C= 15 KTS Run 346A
D= 20 KTS Run 347A
E= 25 KTS Run 348A
F= 30 KTS Run 349

FIG. 3.1.1-10

1538

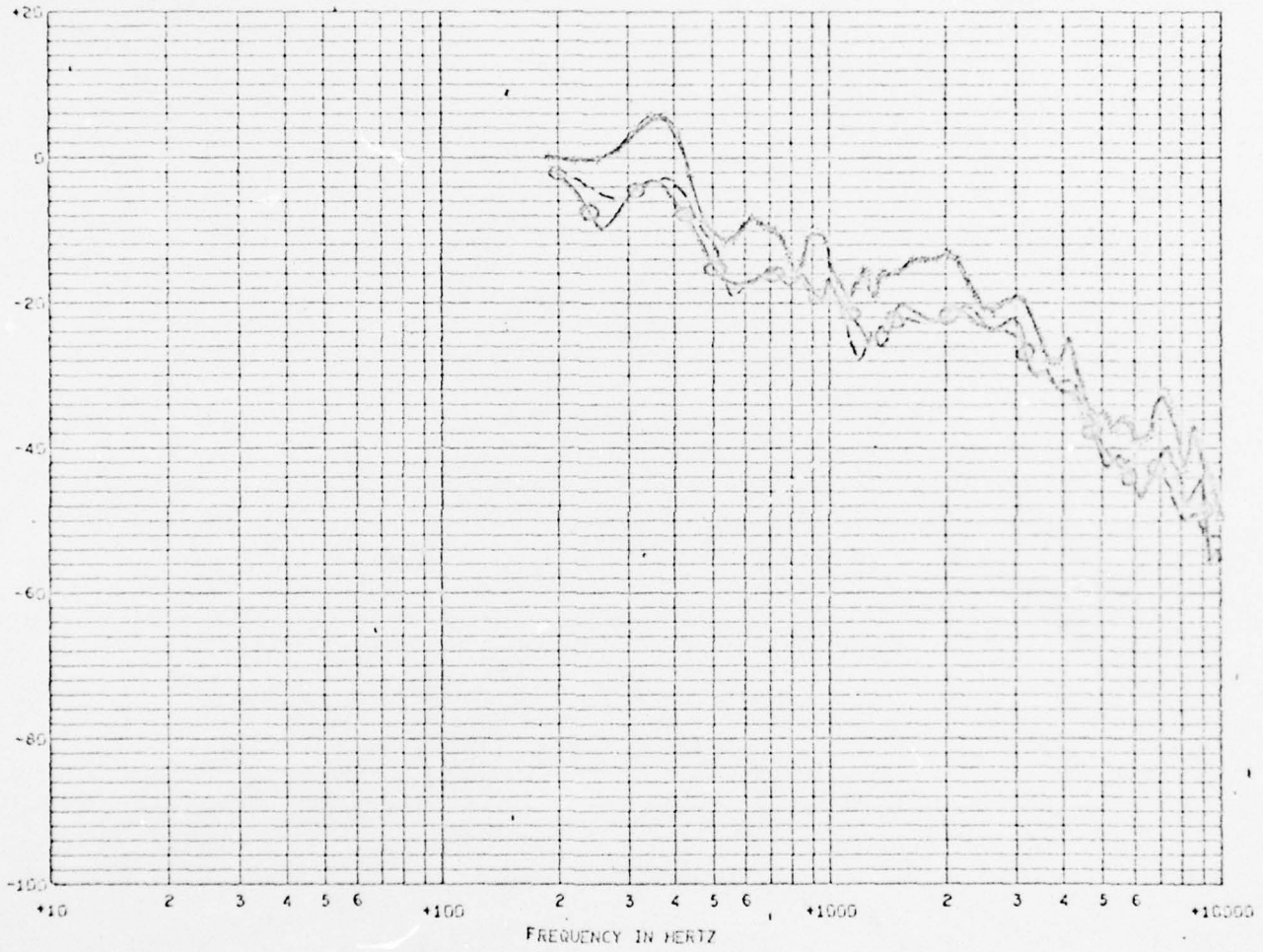

SPECTRUM DB REF 1 MICROBAR SQUARED TIMES SEC GXX LOW BAND CF222 - 20A - HIGH BAND CF222 - 28A
RUN 343 START TIME 14914915.0 SPEED 00 HEADING 000
TYPE SER NO FT FROM DOW
TRG [redacted]A 085 05.75

LF-4 RUN 343, 0 KTS ——————

LF-6 RUN 343, 0 KTS -o-o-o-

LF-7 RUN 343, 0 KTS - - - - -

FIG. 3.1.1-11,

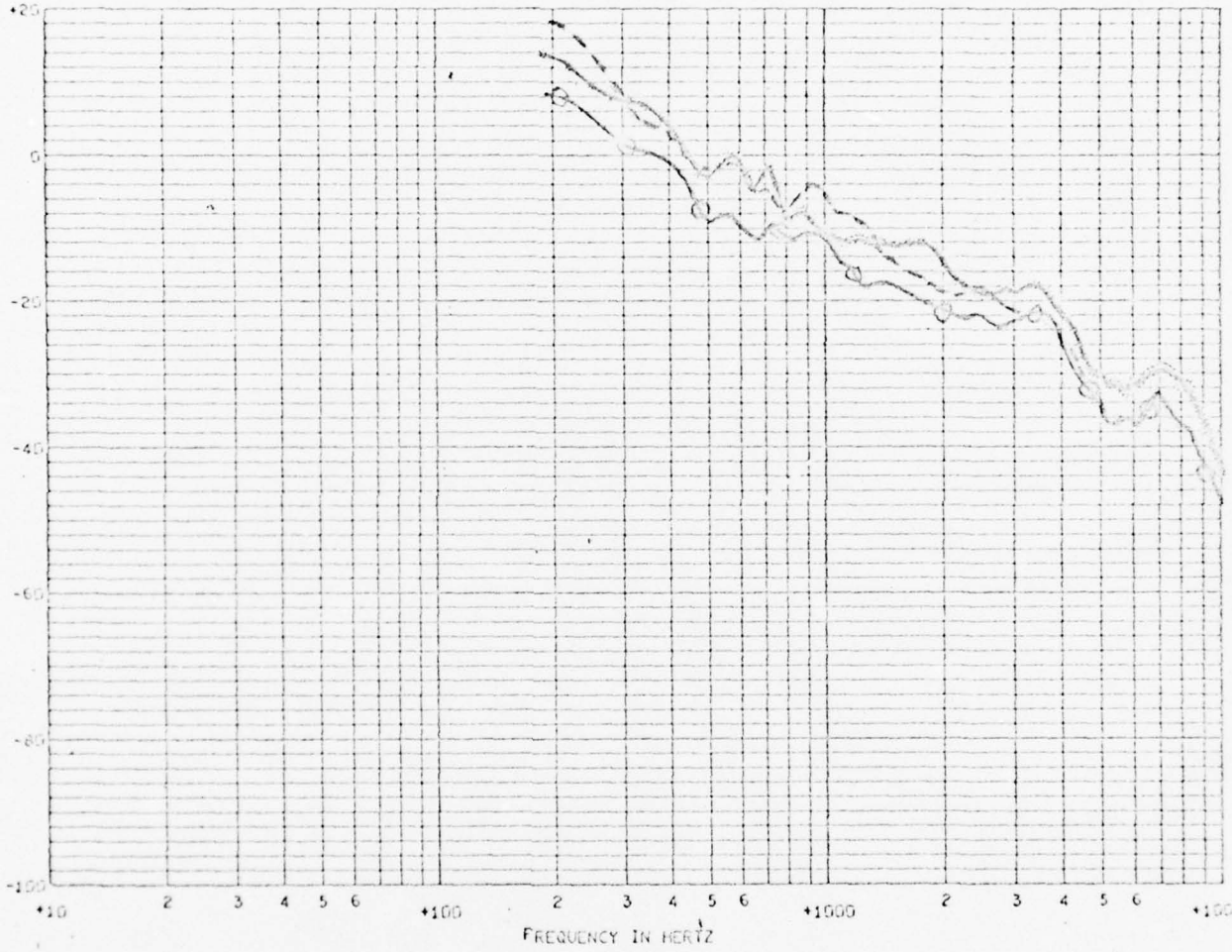

SPECTRUM DB REF 1 MICROBAR SQUARED TIMES SEC GXX LOW BAND CF222 - 38A - HIGH BAND CF222 - 110A
RUN 347A START TIME 16940830.0 SPEED 20 HEADING 000
TYPE SER NO FT FROM BOW
TRG LF-4 085 05.75

LF-4, RUN 347A, 20 KTS ——————

LF-6, RUN 347A, 20 KTS —o—o—o—

LF-7, RUN 347A, 20 KTS - - - - -

FIG. 3.1.1-12

1600

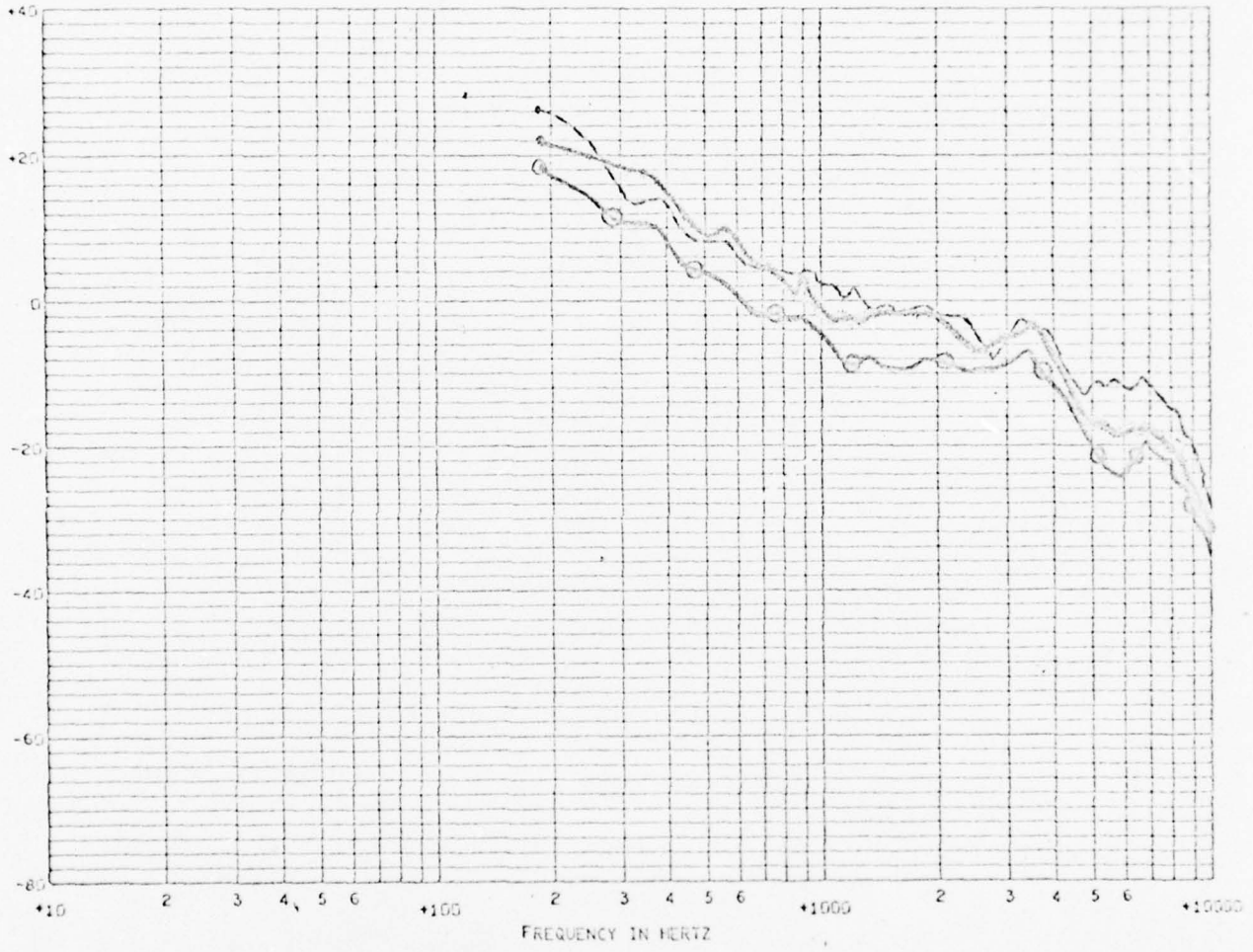

SPECTRUM DB REF 1 MICRODAR SQUARED TIMES SEC GXX LOW BAND CF222 - 44A - HIGH BAND CF222 - 40A
RUN 349 START TIME 134560O0.0 SPEED 30 HEADING 000

TYPE	SER NO	FT FROM DOW
TRG	LF-4	085 05.75

LF-4, RUN 349, 30 KTS ——————

LF-6, RUN 349, 30 KTS —o—o—o—

LF-7, RUN 349, 30 KTS - - - - -

FIG. 3.1.1-13

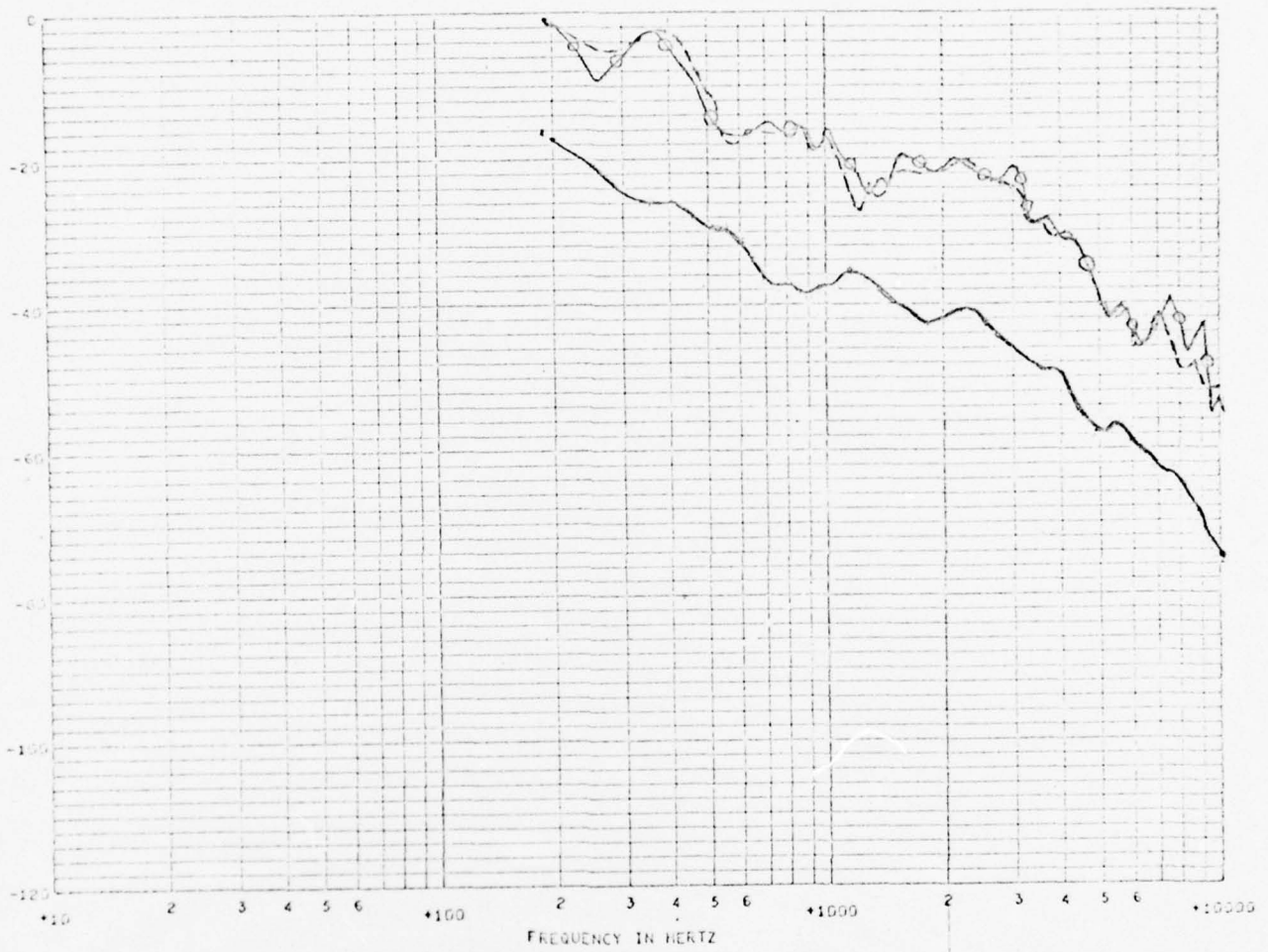

SPECTRUM DB REF 1 MICROBAR SQUARED TIMES SEC GXX LOW BAND CF56 - 1B - HIGH BAND CF56 - 3E
RUN [redacted] START TIME 149023010.0 SPEED 00 HEADING 000
TYPE SER NO FT FROM BOW
TRG [redacted] 026 09.75

HF-3, RUN 336, 0 KTS ——————

LF-6, RUN 343, 0 KTS —o—o—o—

LF-7, RUN 343, 0 KTS – – – – –

FIG. 3.1.1-14

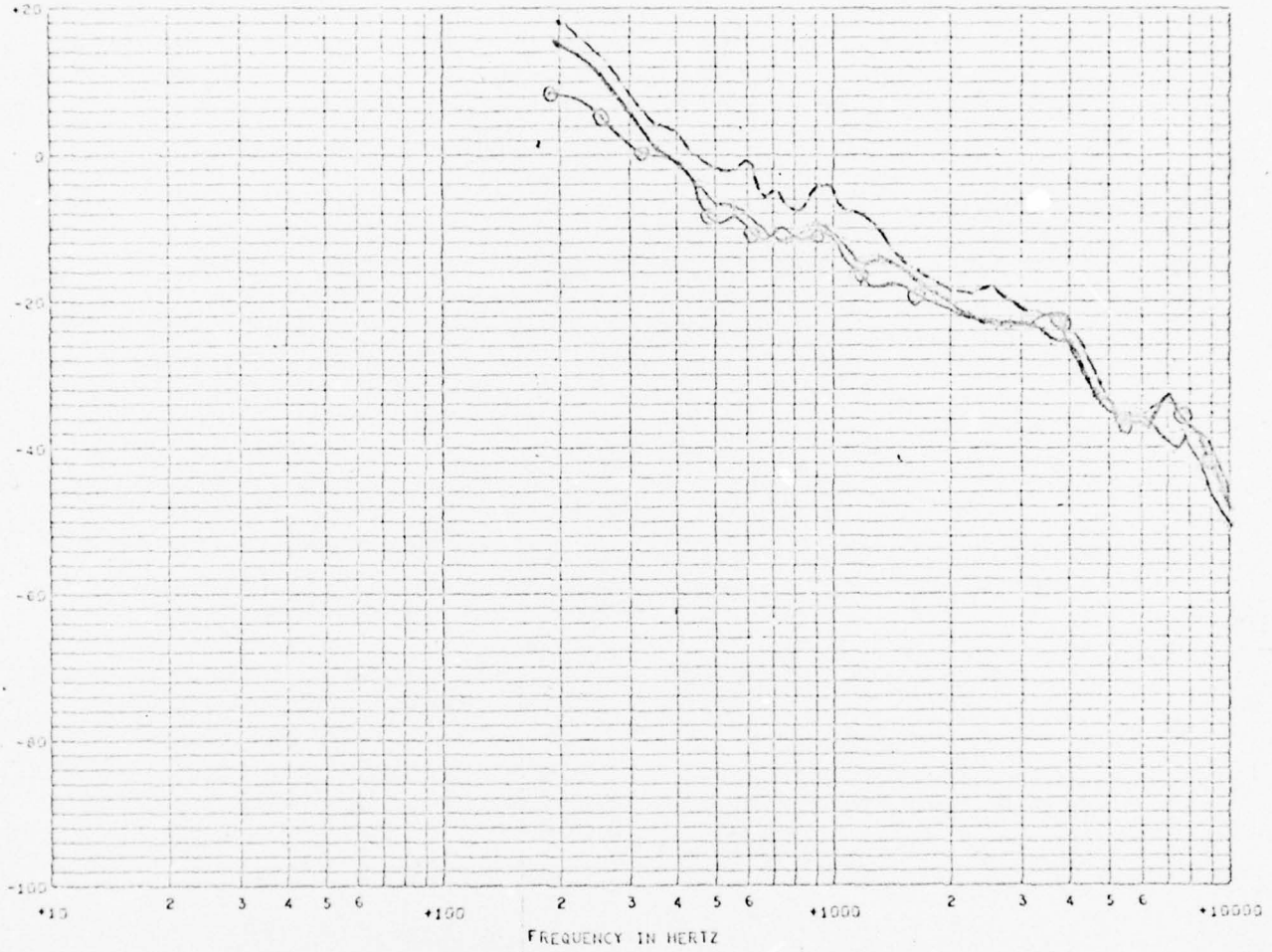

SPECTRUM DB REF 1 MICROBAR SQUARED TIMES SEC GXX LOW BAND CF56 - 33B - HIGH BAND CF56 - 34B
RUN 340A START TIME 16946940.0 SPEED 20 HEADING 000

TYPE	SER NO	FT FROM BOW
TAG	HF-3	026 09.75

HF-3, RUN 340A, 20 KTS ————

LF-6, RUN 347A, 20 KTS —o—o—o—

LF-7, RUN 347A, 20 KTS - - - - -

FIG. 3.1.1-15

1693

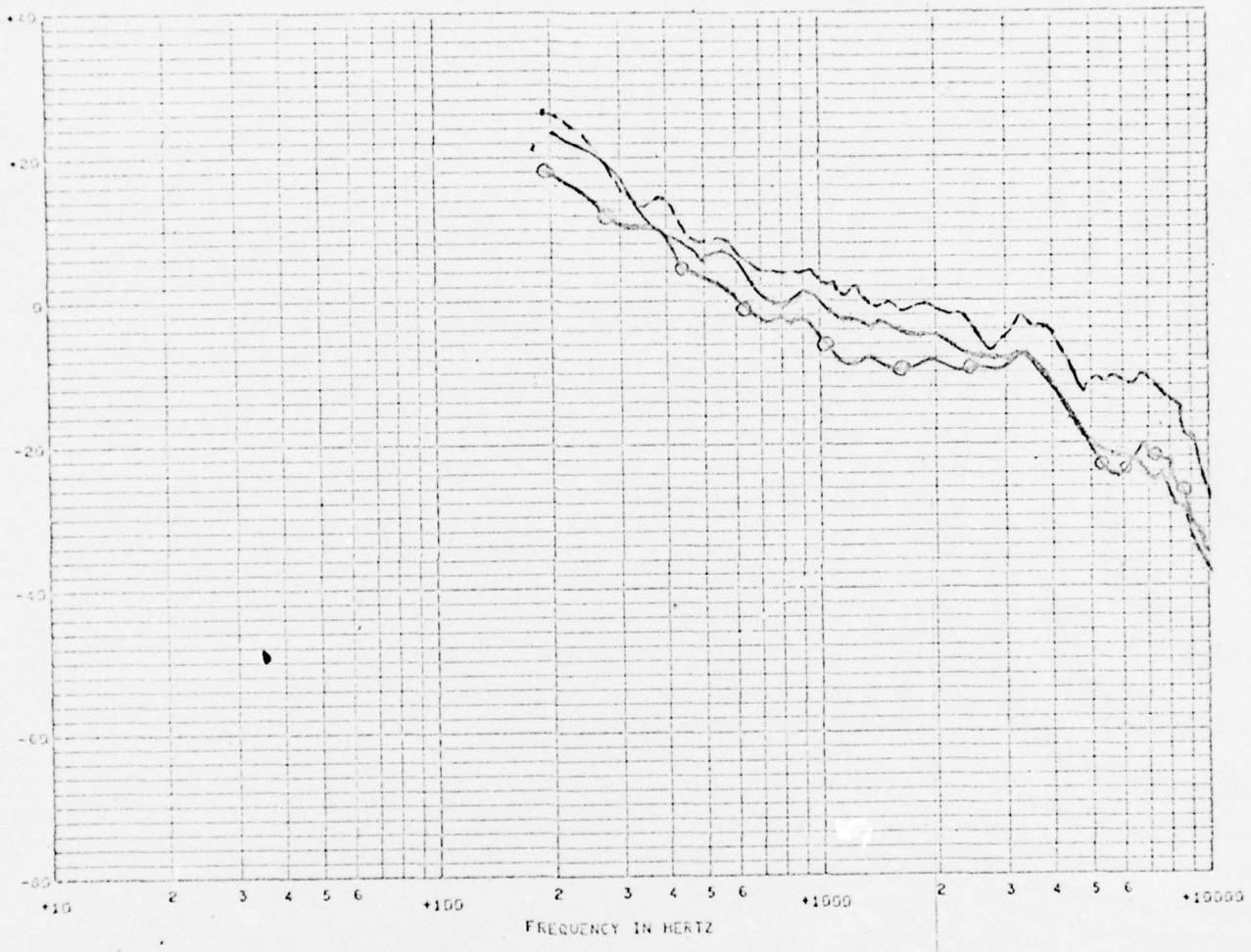

SPECTRUM DD REF 1 MICRODAR SQUARED TIMES SEC 6XX LOW BAND CF56 - 598 - HIGH BAND CF56 - 618
RUN 342 START TIME 1304700.0 SPEED 30 HEADING 000

TYPE	SER NO	FT FROM BOW
TRG	HF-3	026 09.75

HF-3, RUN 342, 30 KTS ——————

LF-6, RUN 349, 30 KTS —o—o—o—

LF-7, RUN 349, 30 KTS - - - - -

FIG. 3.1.1-16

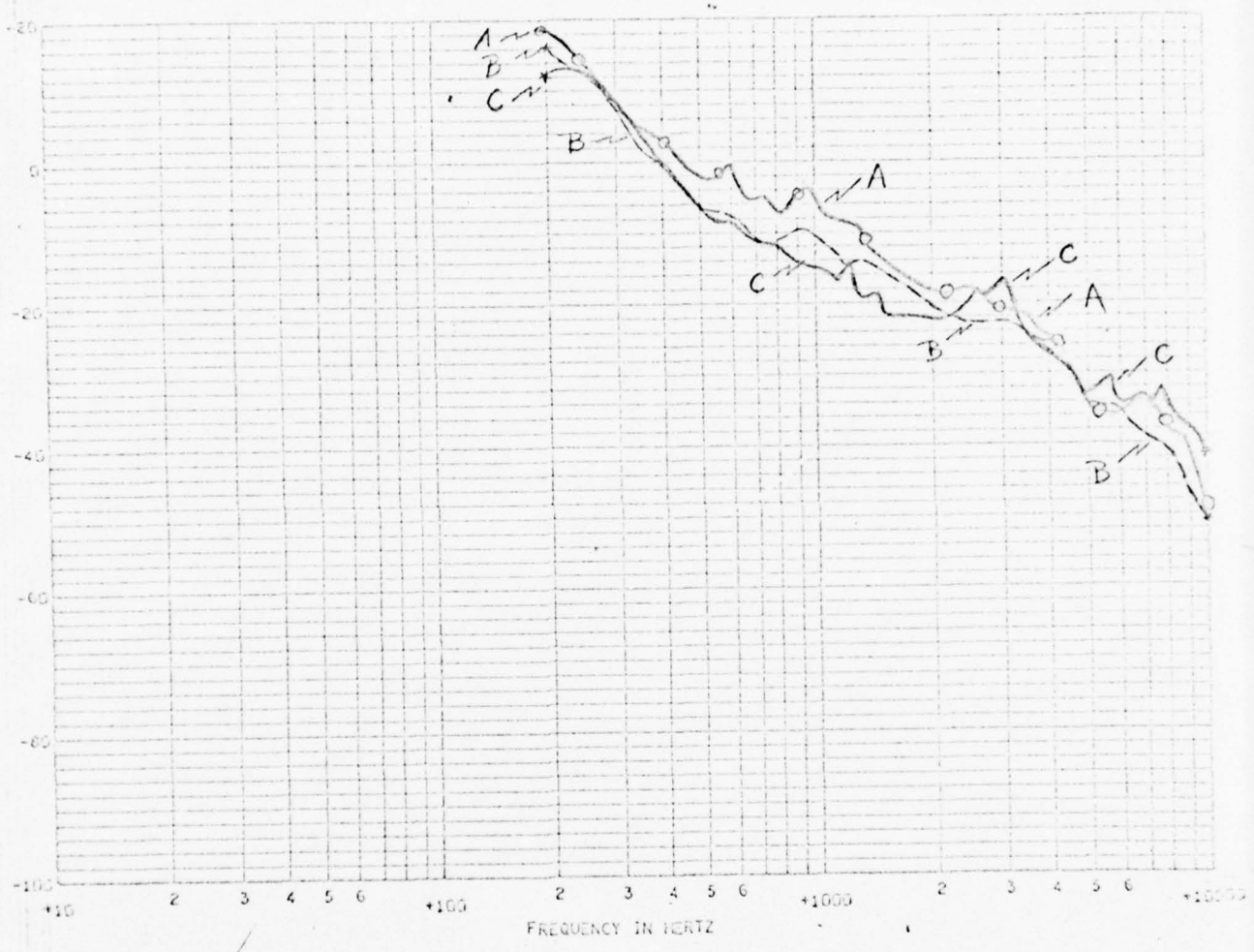

SPECTRUM DB REF 1 MICROBAR SQUARED TIMES SEC 6XX LOW BAND CF222 - 38D - HIGH BAND CF222 - 110B
RUN [redacted] START TIME 1694D930.D SPEED 2D HEADING 00D
TYPE SER NO FT FROM DOW
TRG [redacted] 093 02.75

A: LF-7, RUN 347A
B: HF-3, RUN 340A
C: 5E111, RUN 331
} 20 KNOTS

FIG. 3.1.1-16A

Fuselage A.F.-6

π_1 vs ω_1

A :	5 KTS	RUN 859
B :	10 KTS	RUN 345
C :	15 KTS	RUN 857
D :	20 KTS	RUN 347H
E :	30 KTS	RUN 347

Fig. 3.1.1-17

CONFIDENTIAL

1930

ELEMENT: LF-7

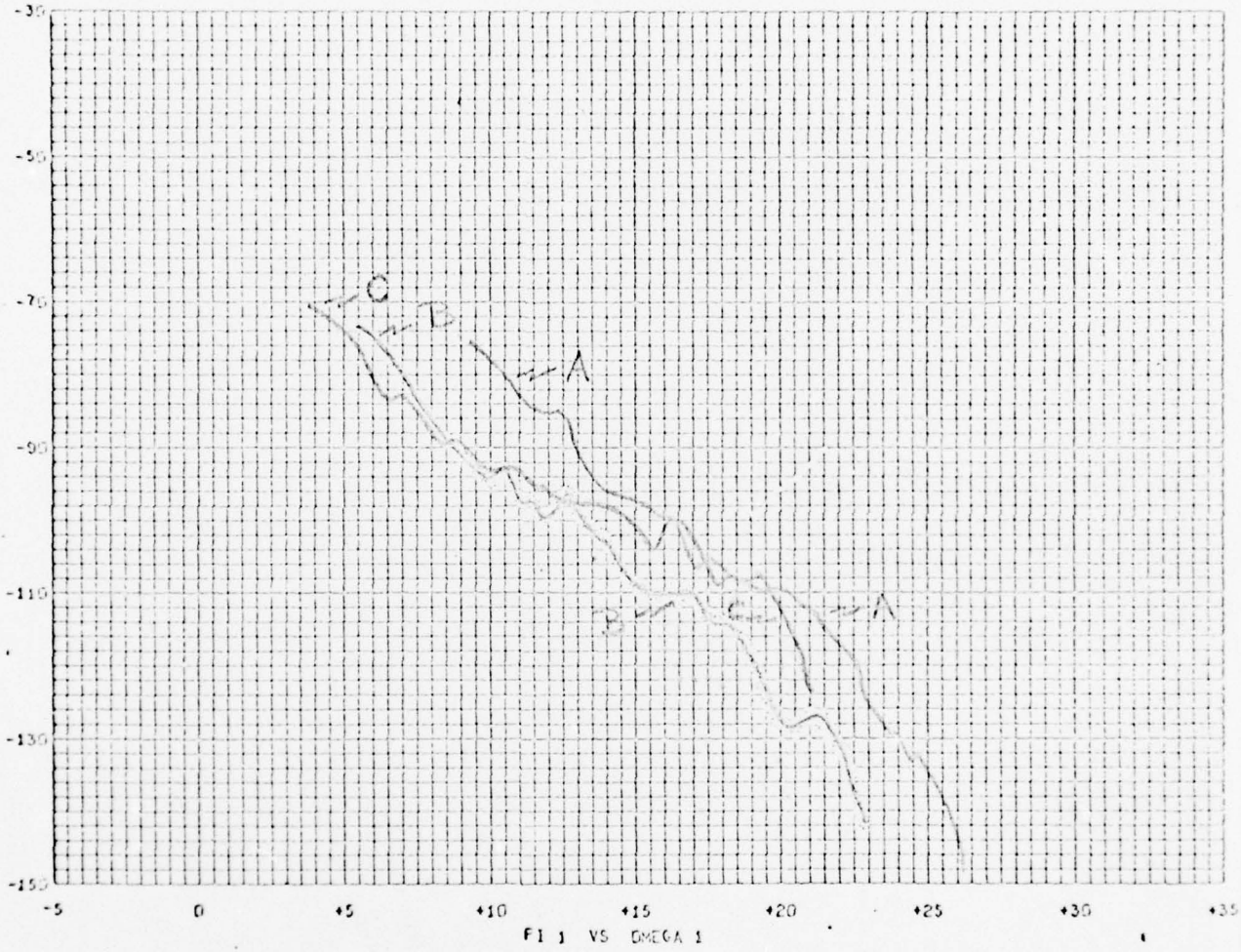

SPECTRUM LOW BAND CF222 - 38D - HIGH BAND CF222 - 110B
RUN 347A START TIME 16:40:30.0 SPEED 20 HEADING 000
TYPE SER NO FT FROM BOW
TRG LF-7 093 02.75

A: 10 KTS, RUN 345
B: 20 KTS, RUN 347A
C: 30 KTS, RUN 349

FIG. 3.1.1-18

CONFIDENTIAL

ELEMENT: LF-4

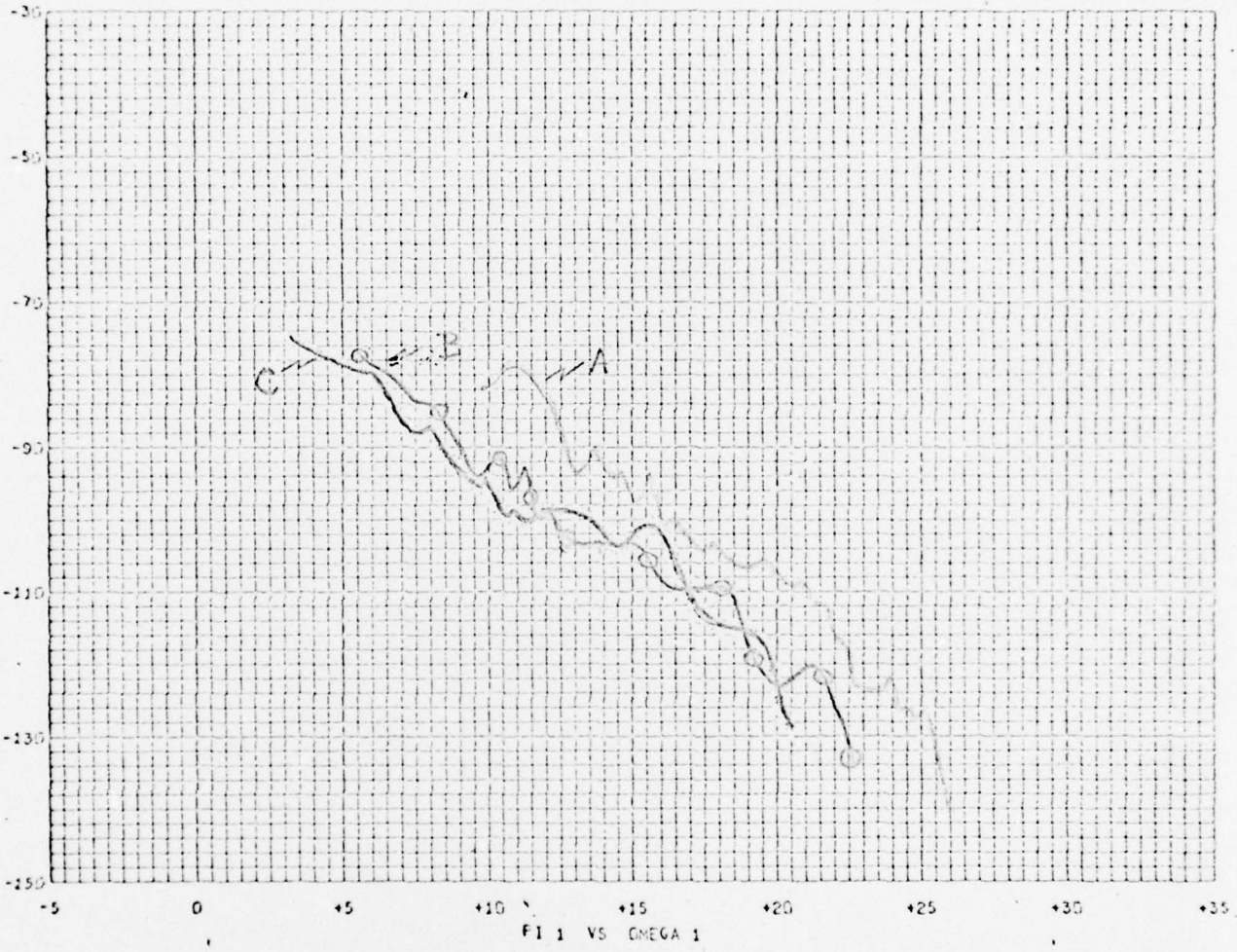

SPECTRUM LOW BAND CF222 - 44A - HIGH BAND CF222 - 46A
RUN 349 START TIME 13956400.0 SPEED 30 HEADING 000
TYPE SER NO FT FROM EOW
TRG LF-4 085 05.75

A: 10 KTS, RUN 345
B: 20 KTS, RUN 347A
C: 30 KTS, RUN 349

FIG. 3.1.1-19. CONFIDENTIAL

ELEMENT: LF-12

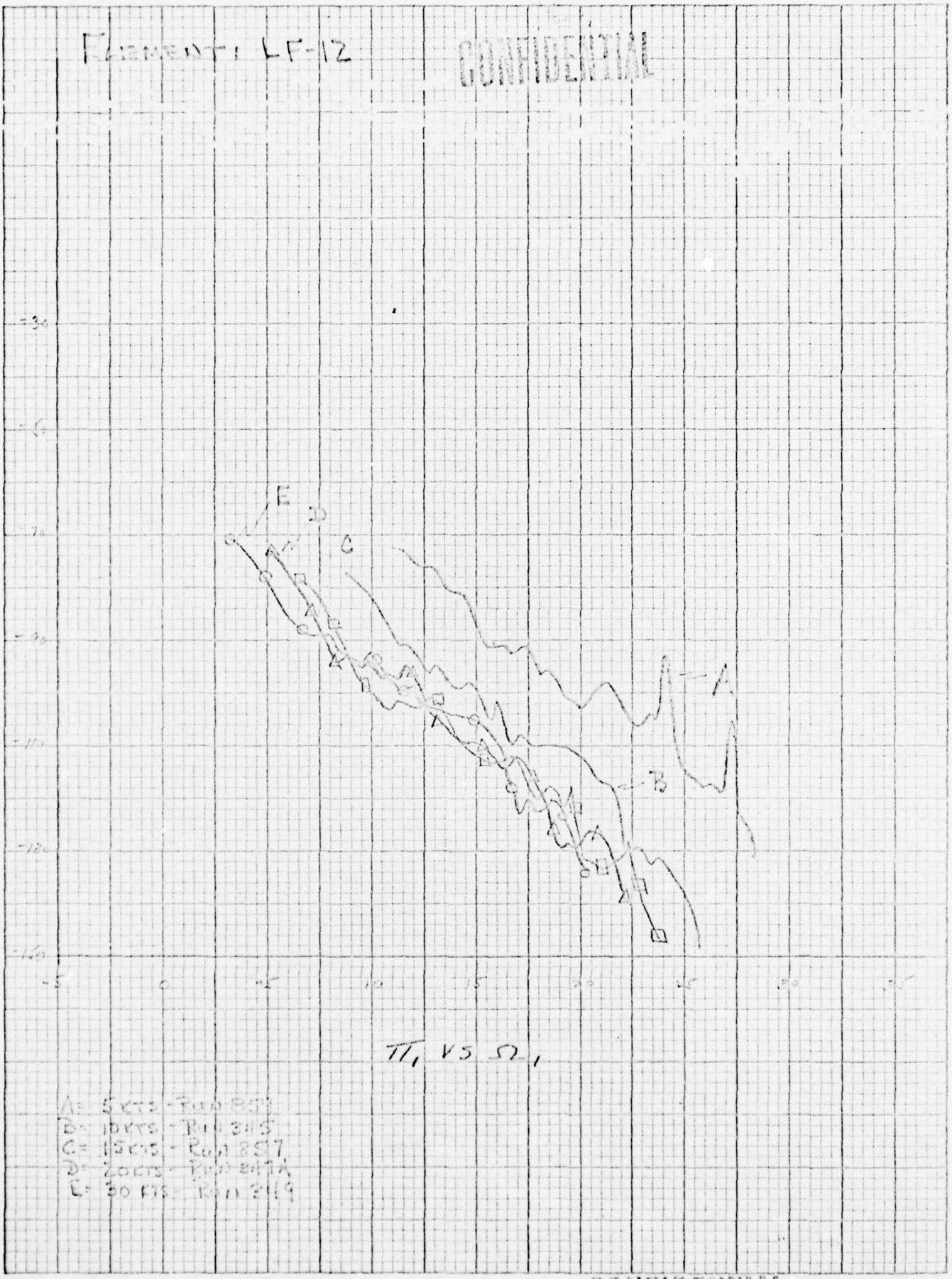

FIG. 3.1.1-20

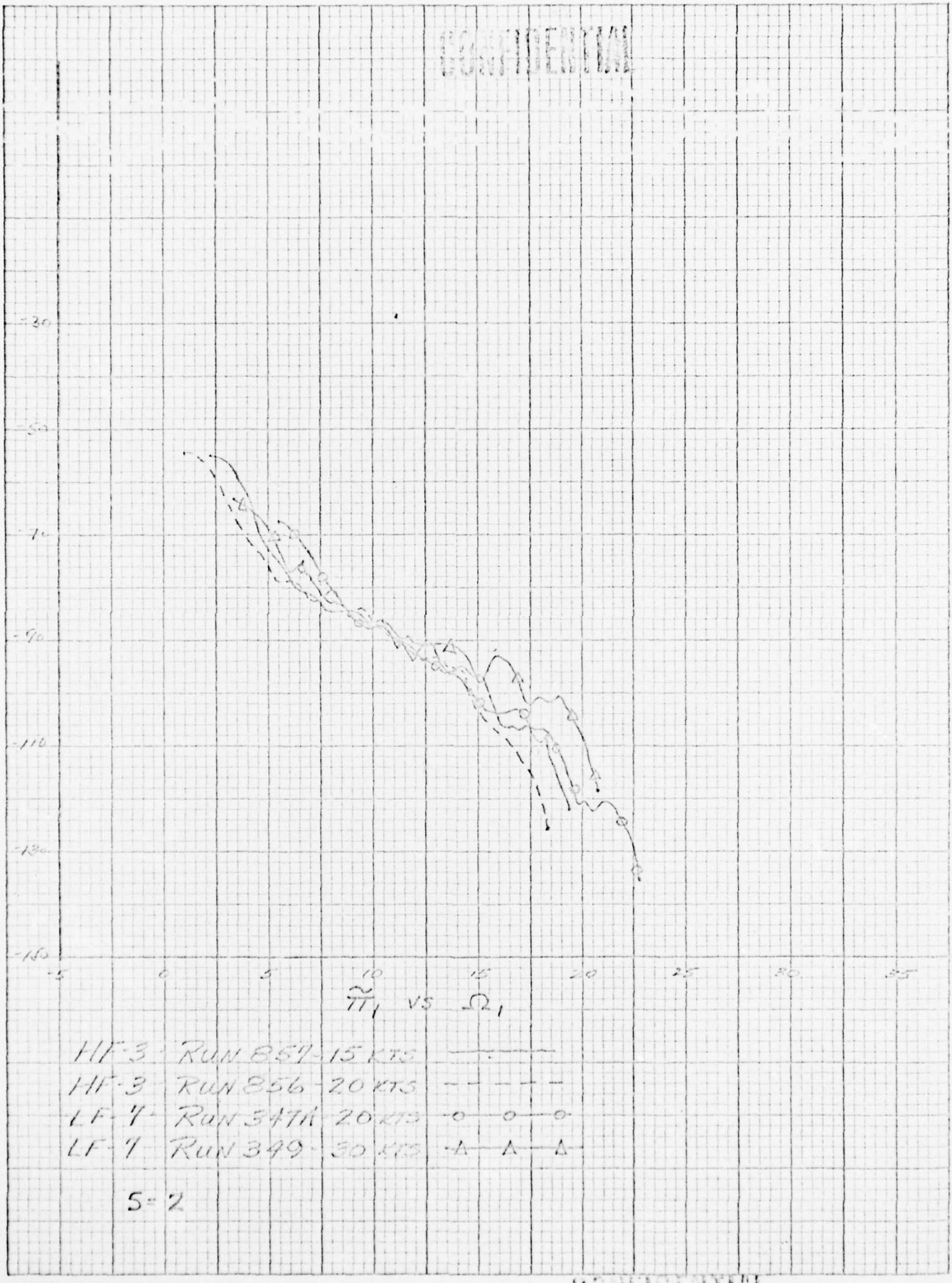

5-2

FIG. 3.1.1-21

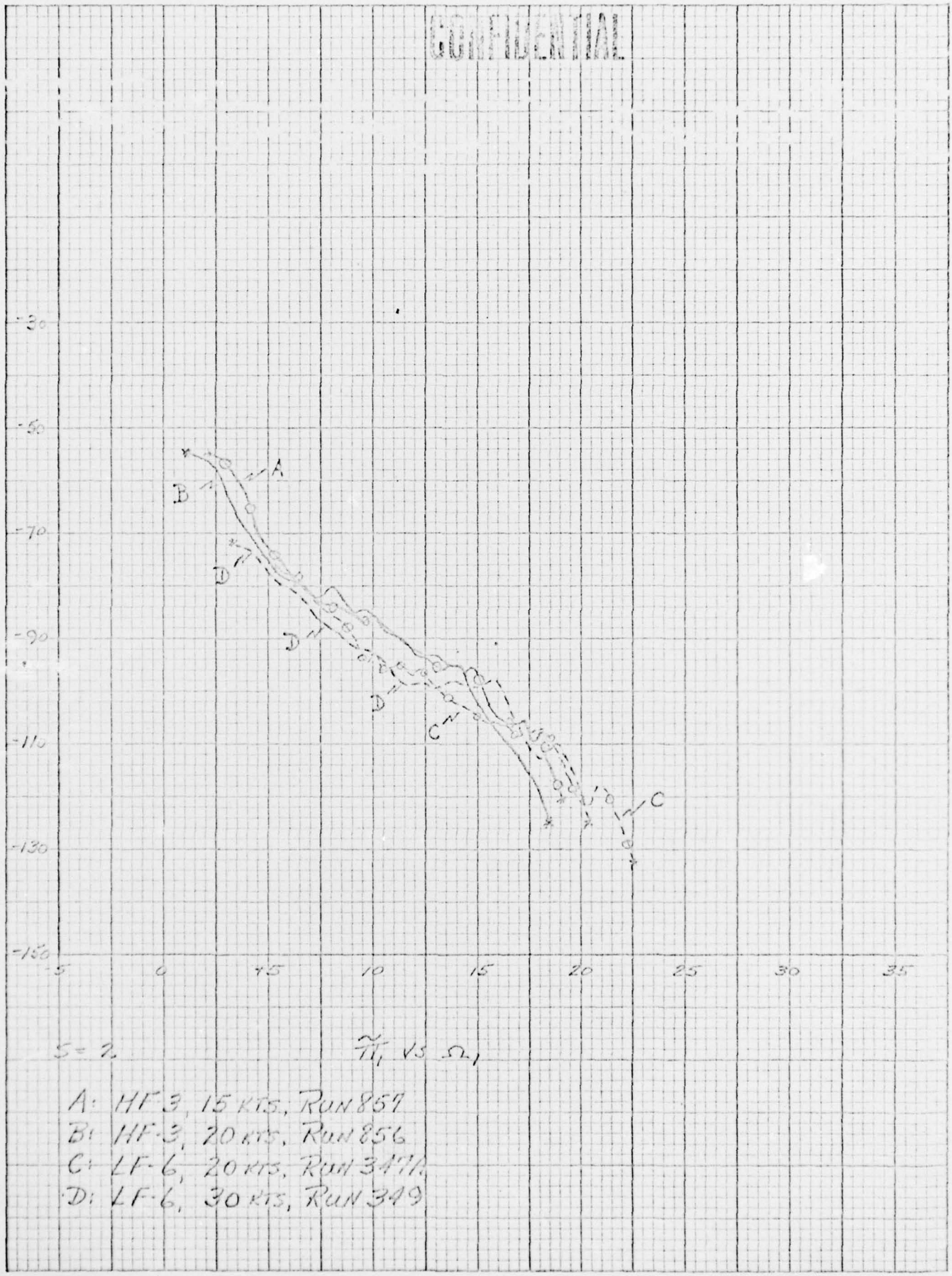

FIG. 3.1.1-22

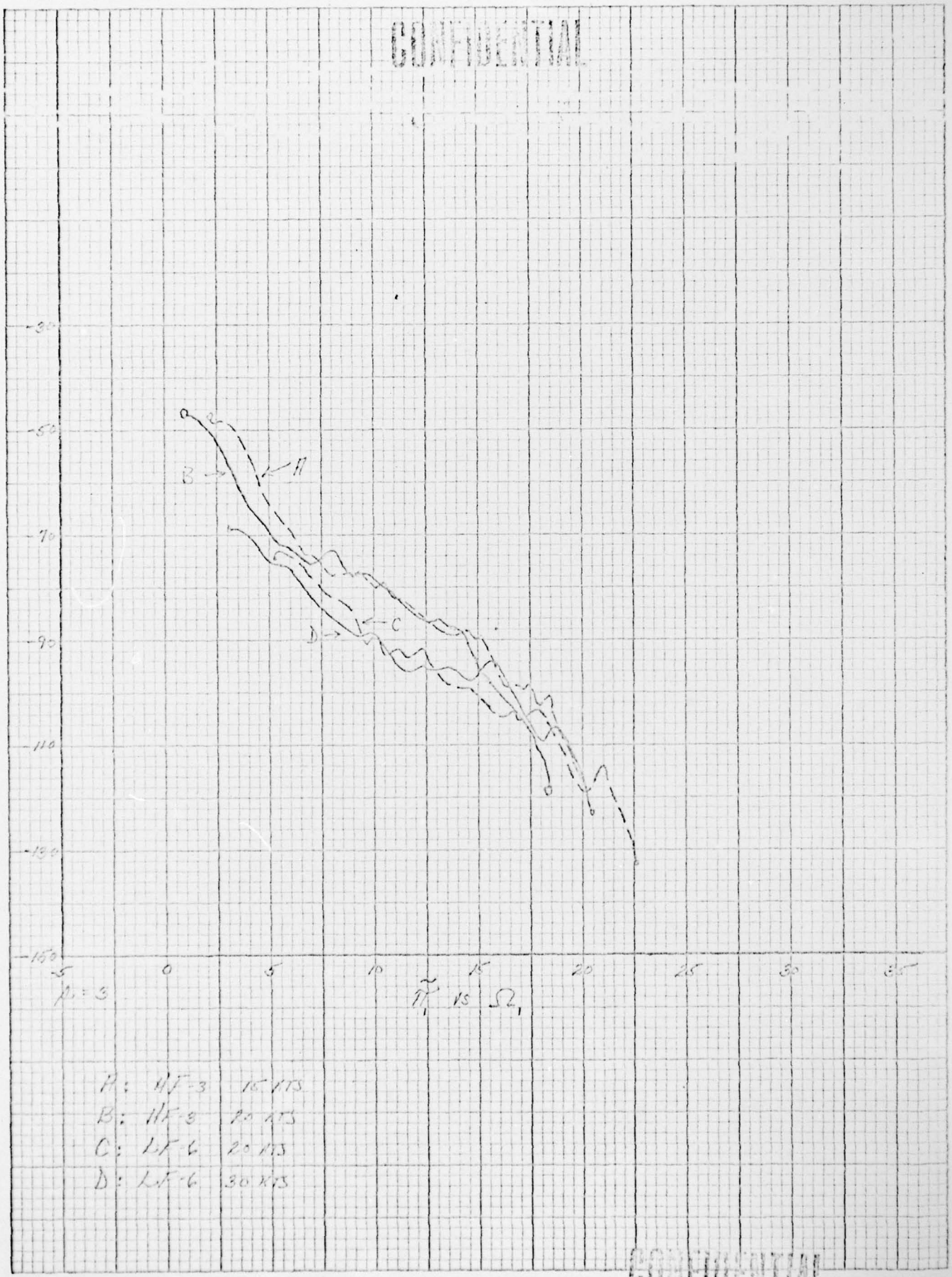

FIG. 3.1.1-23

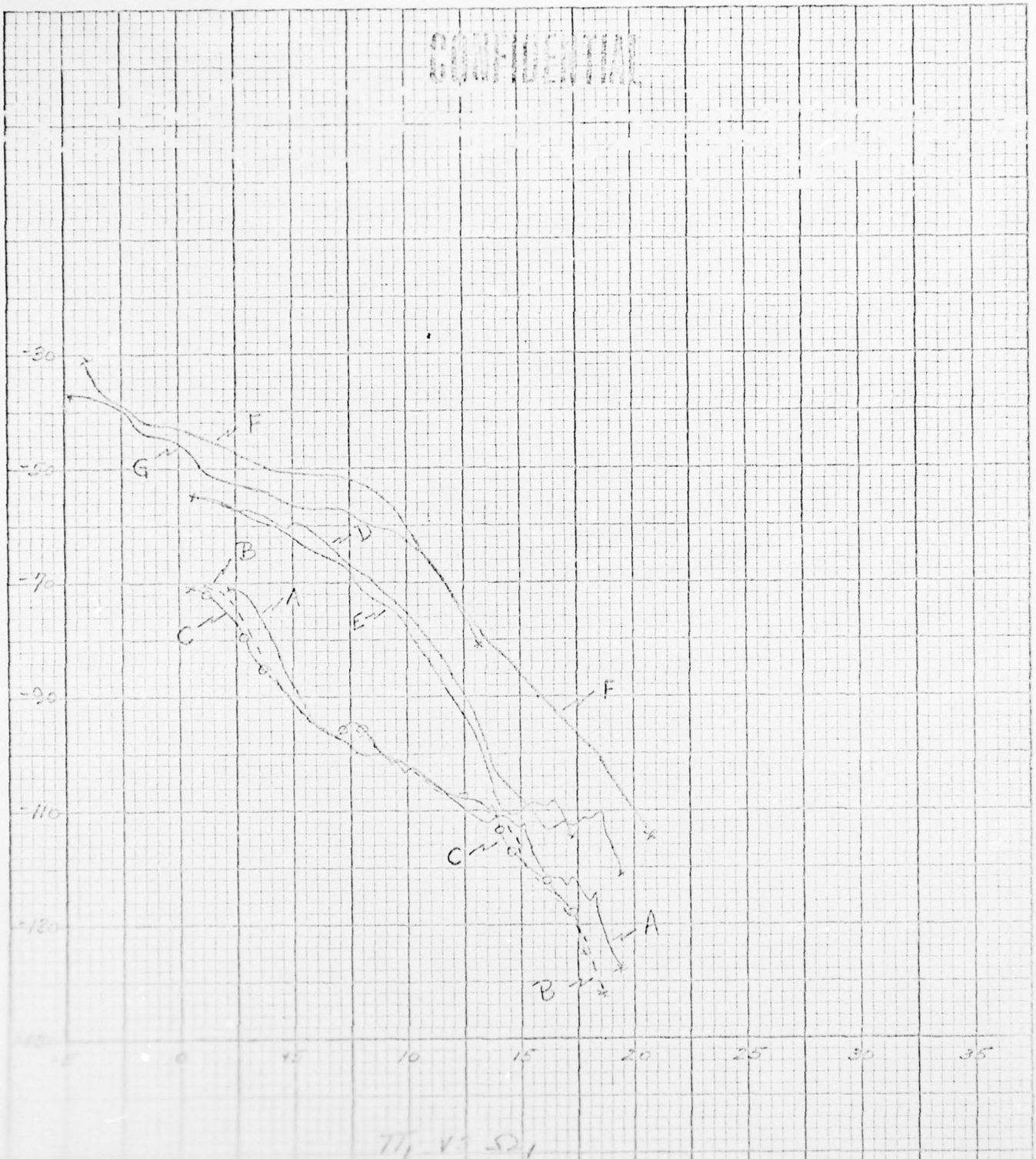

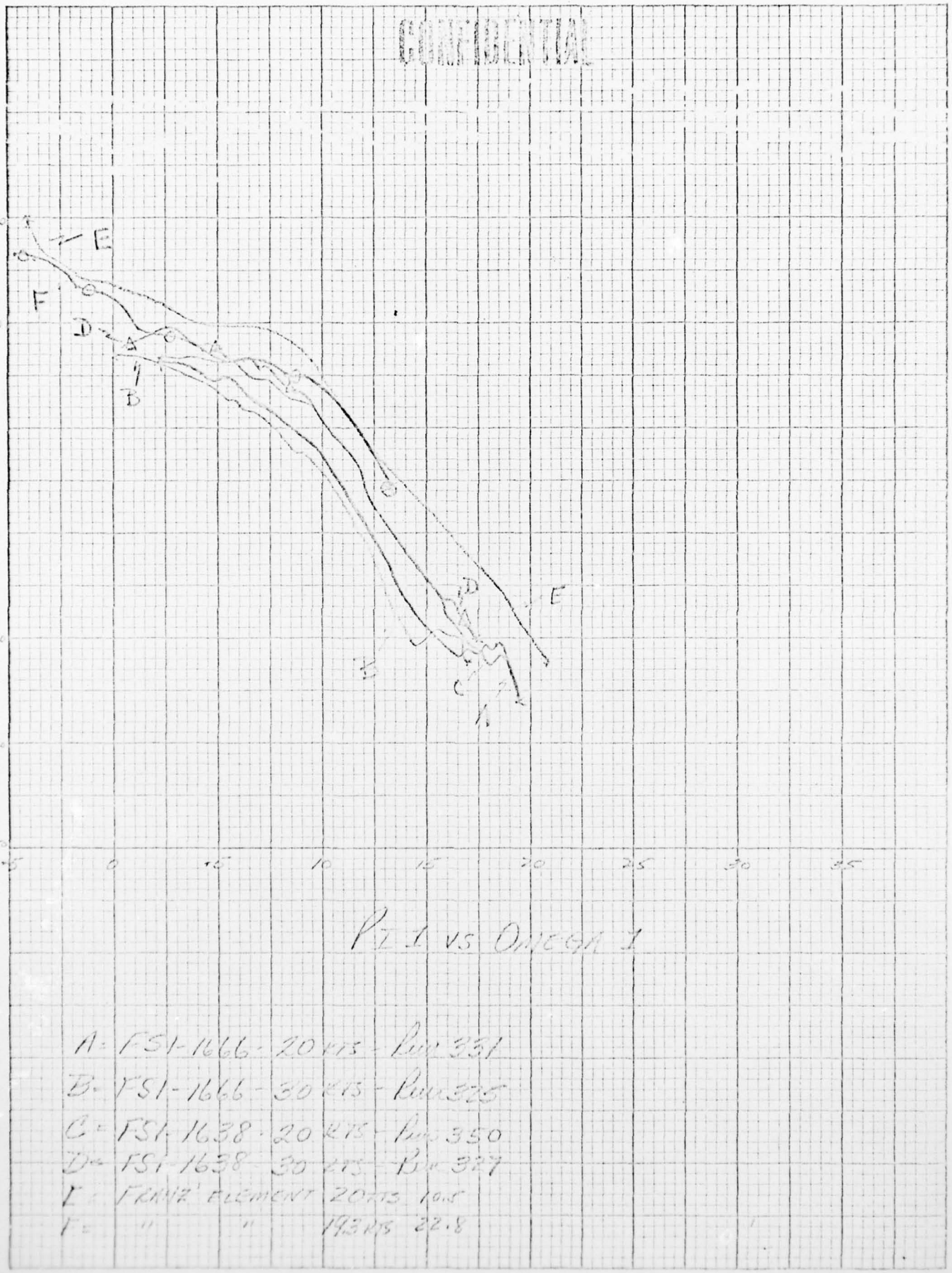

$P_{L\,I}$ vs Omega I

A = FSI-1666 - 20 KTS - Run 331
B = FSI-1666 - 30 KTS - Run 325
C = FSI-1638 - 20 KTS - Run 350
D = FSI-1638 - 30 KTS - Run 327
E = Franz' element 20 KTS 10.5
F = " " 193 KTS 22.8

FIG. 3.1.1-25

ELEMENT: H-5

1528

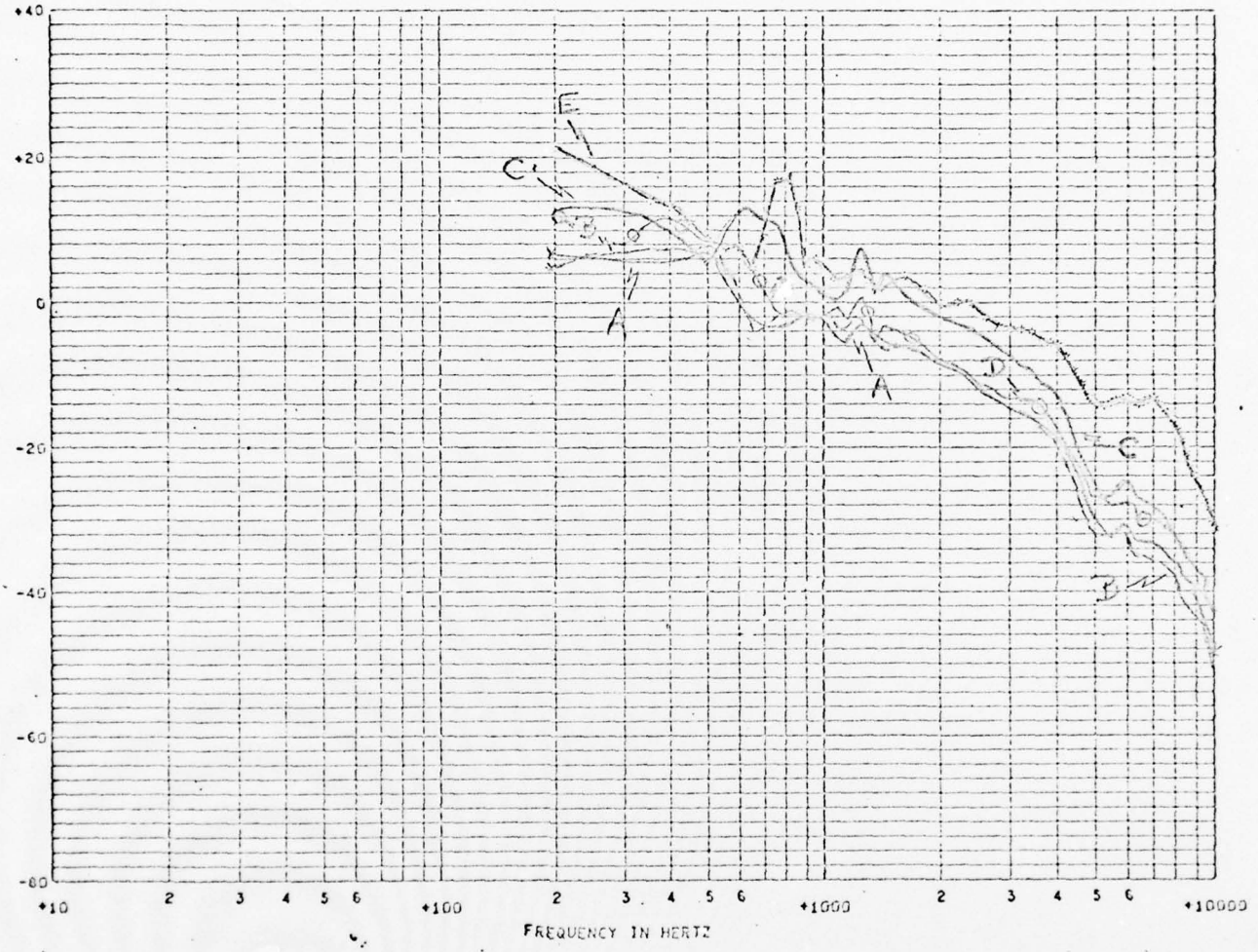

SPECTRUM DB REF 1 MICROBAR SQUARED TIMES SEC GXX LOW BAND CF56 - 66B - HIGH BAND CF56 - 64B
RUN 342 START TIME 13447:00.0 SPEED 30 HEADING 000
TYPE SER NO FT FROM BOW
TRG H-5 125 02.75

A: 0 KTS, RUN 336
B: 10 KTS, RUN 338
C: 20 KTS, RUN 340A
D: 20 KTS, RUN 340B
E: 30 KTS, RUN 342

FIG. 3.1.1-26

CONFIDENTIAL

1530

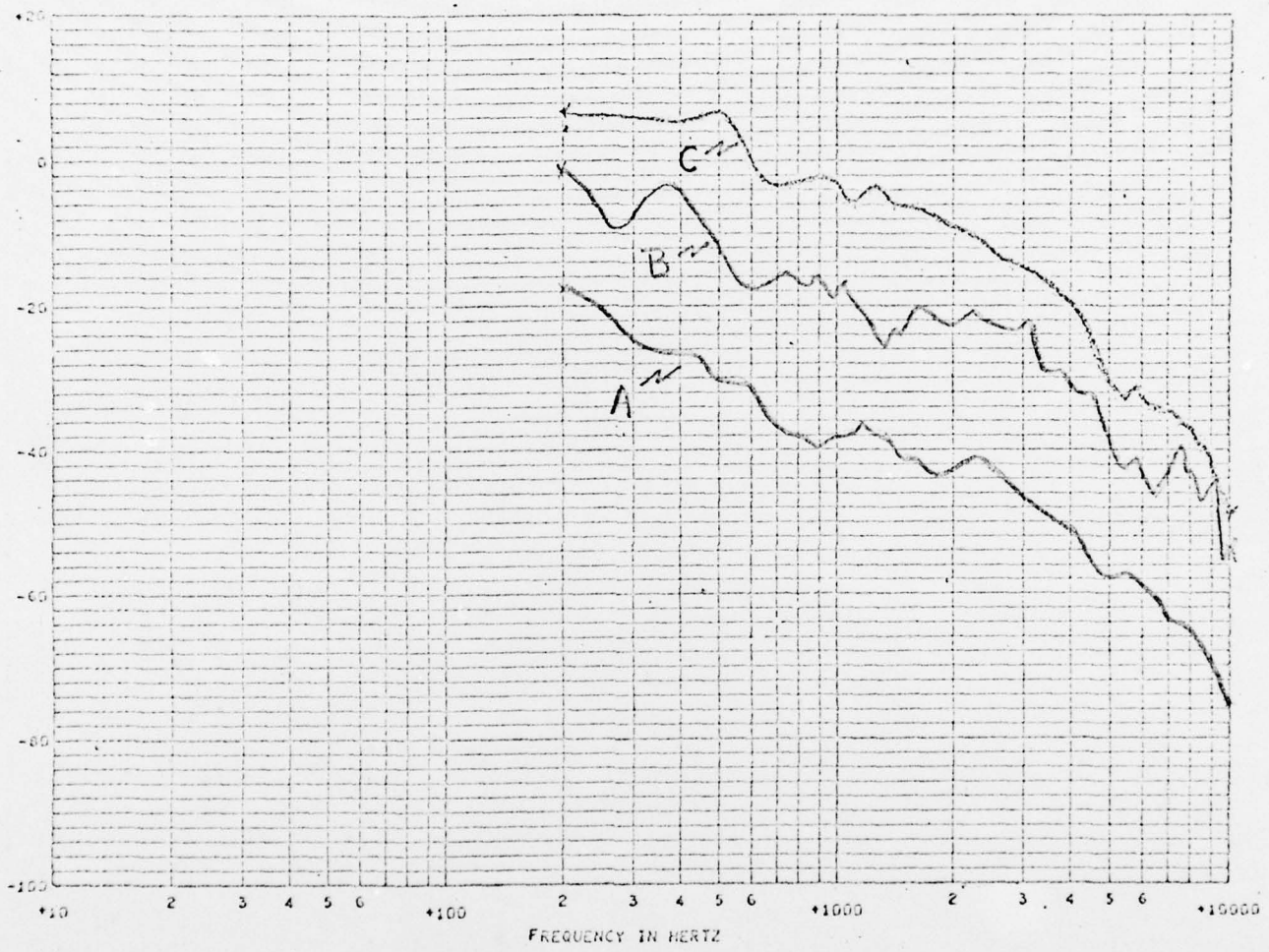

SPECTRUM DD REF 1 MICROBAR SQUARED TIMES SEC GXX LOW BAND CF56 - 88 - HIGH BAND CF56 - 68
RUN [redacted] START TIME 1400Z#10.0 SPEED 00 HEADING 000
TYPE SER NO FT FROM BOW
TRG [redacted] 125 02.75

A = HF-3 Run 336
B = LF-6 Run 343
C = H-5 Run 336
} 0 KTS

Fig. 3.1.1-27

CONFIDENTIAL

CONFIDENTIAL

1531

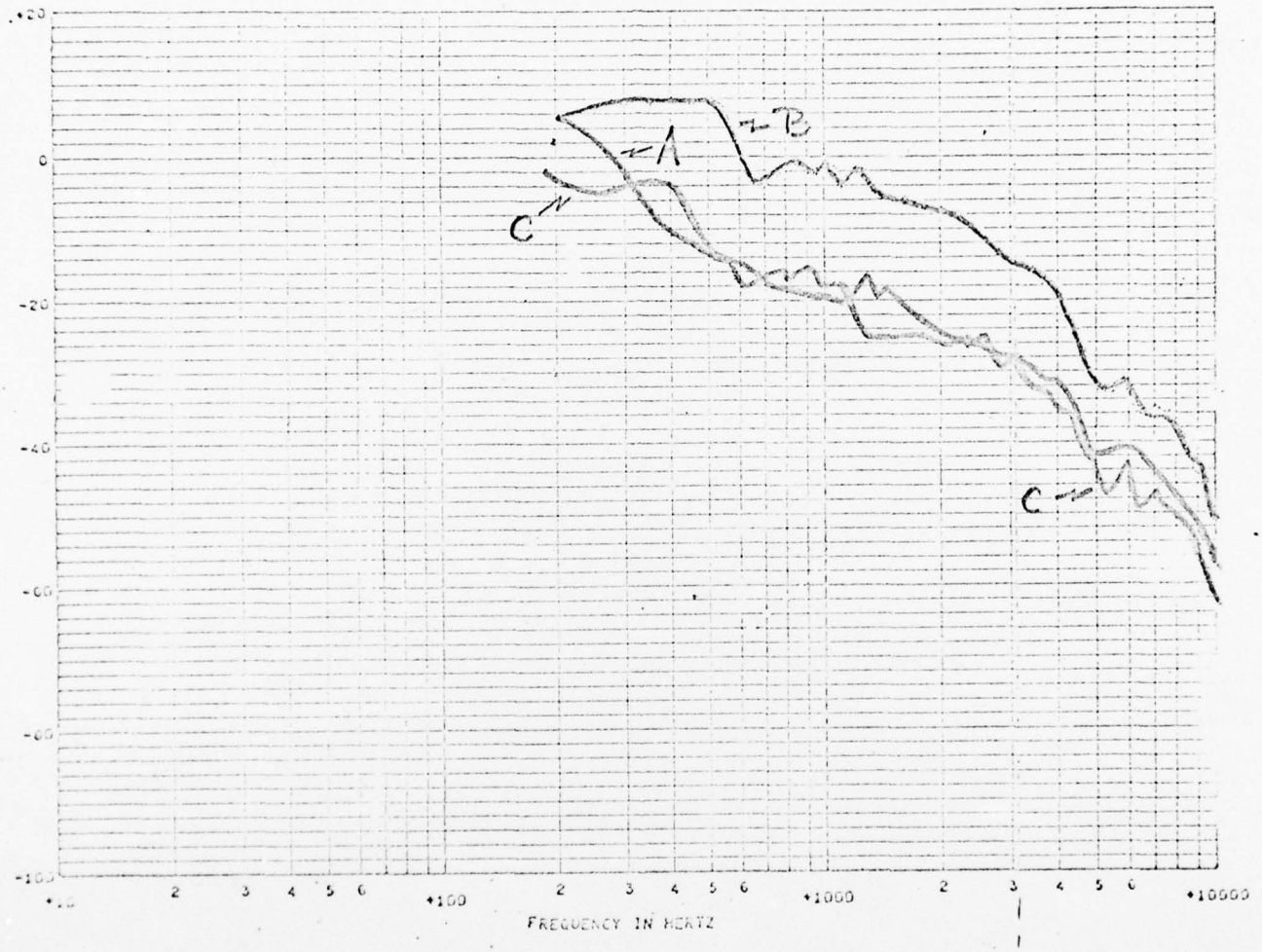

SPECTRUM DB REF 1 MICROBAR'S QUARED TIMES SEC 0XX LOW BAND CPSG - 220 - HIGH BAND CPSG - 246
RUN 338 START TIME 1645 2400.0 SPEED 10 HEADING 000
TYPE SER NO FT FROM DOW
TRG 125 02.75

A = HF-3
B = H-5
C = LF-6 - Run 345

} Run 338 } 16 KTS

Fig. 3.1.1-28

CONFIDENTIAL

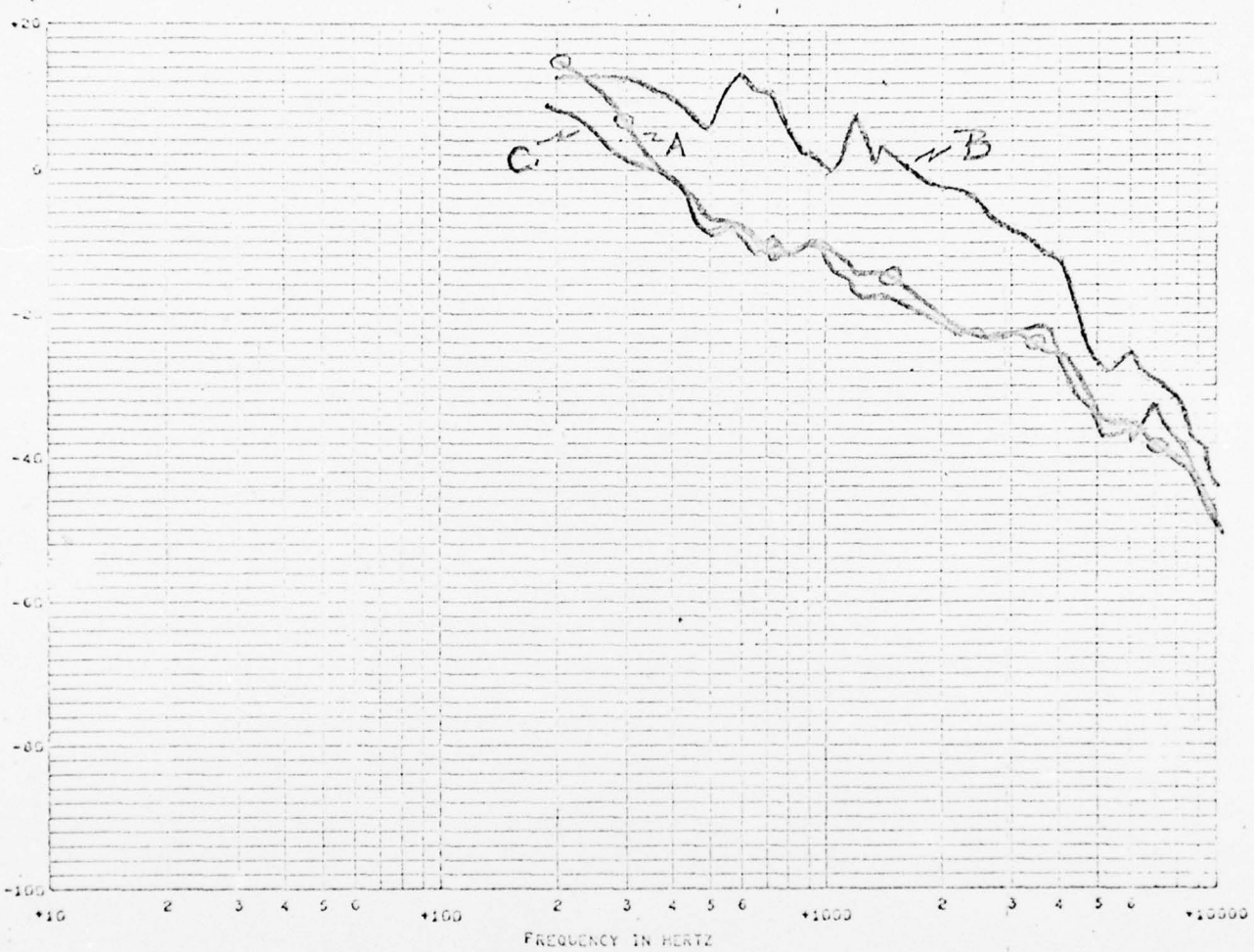

SPECTRUM DB REF 1 MICROBAR SQUARED TIMES SEC GXX LOW BAND CPSG - 540 - HIGH BAND CPSG - 525
RUN 340A START TIME 1694540.0 SPEED 20 HEADING 000

TYPE	SER NO	FT FROM BOW
TRG	H-5	125 02.75

A = HF-3
B = H-5
C = LF-6 - RUN 347A

} RUN 340A } 20 KTS

FIG. 3.1.1-29

CONFIDENTIAL

1536

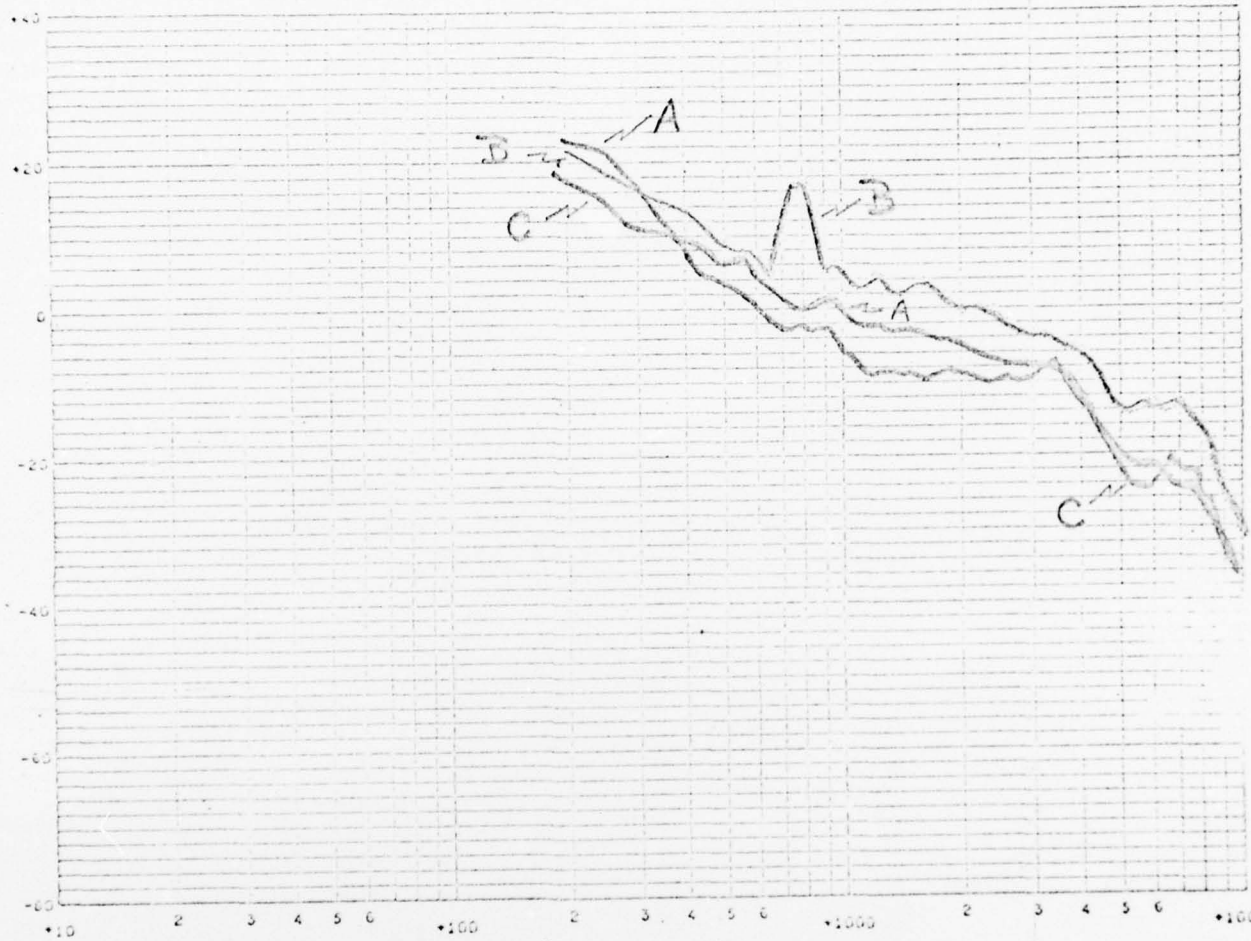

SPECTRUM DB REF 1 MICROBAR SQUARED TIMES SEC 6XX LOW BAND CPSG - 60D - HIGH BAND CPSG - 64D
RUN 34: START TIME 13947600.0 SPEED 30 HEADING 000

TYPE	SER NO	FT FROM BOW
TRC	H-5	125 02.75

A = HF-3
B = H-5 } Run 342
C = LF-6 - Run 349 } 30 KTS

FIG. 3.1.1-30

CONFIDENTIAL

CONFIDENTIAL

ELEMENT: G-5

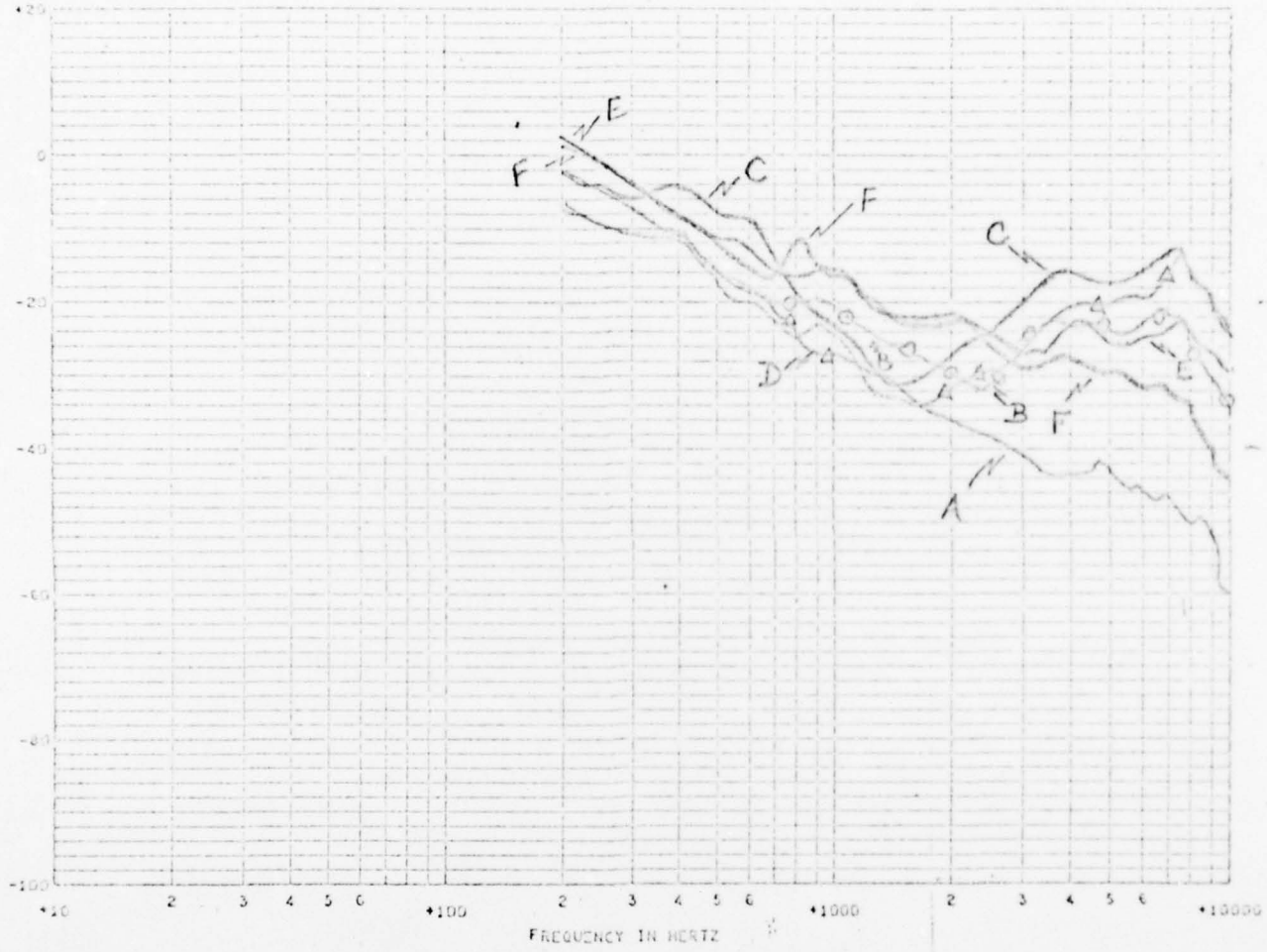

SPECTRUM DB REF 1 MICROBAR SQUARED TIMES SEC GXX LOW BAND CF100 - 79A - HIGH BAND CF100 - 81A
RUN [redacted] START TIME 12405450.0 SPEED 20 HEADING 000

TYPE	SER NO	FT FROM DOW
TAG	G-5	003 11.25

A = 0 KTS - Blue - Run 336
B = 10 KTS - Green - Run 338
C = 15 KTS - Red - Run 346A
D = 20 KTS - Purple - Run 340A
E = 25 KTS - Black - Run 348
F = 30 KTS - Orange - Run 342

} wrong; see TM-17, Fig. 3-5.

CONFIDENTIAL

Fig 5.2.1-1

CONFIDENTIAL

ELEMENT 11 G-7

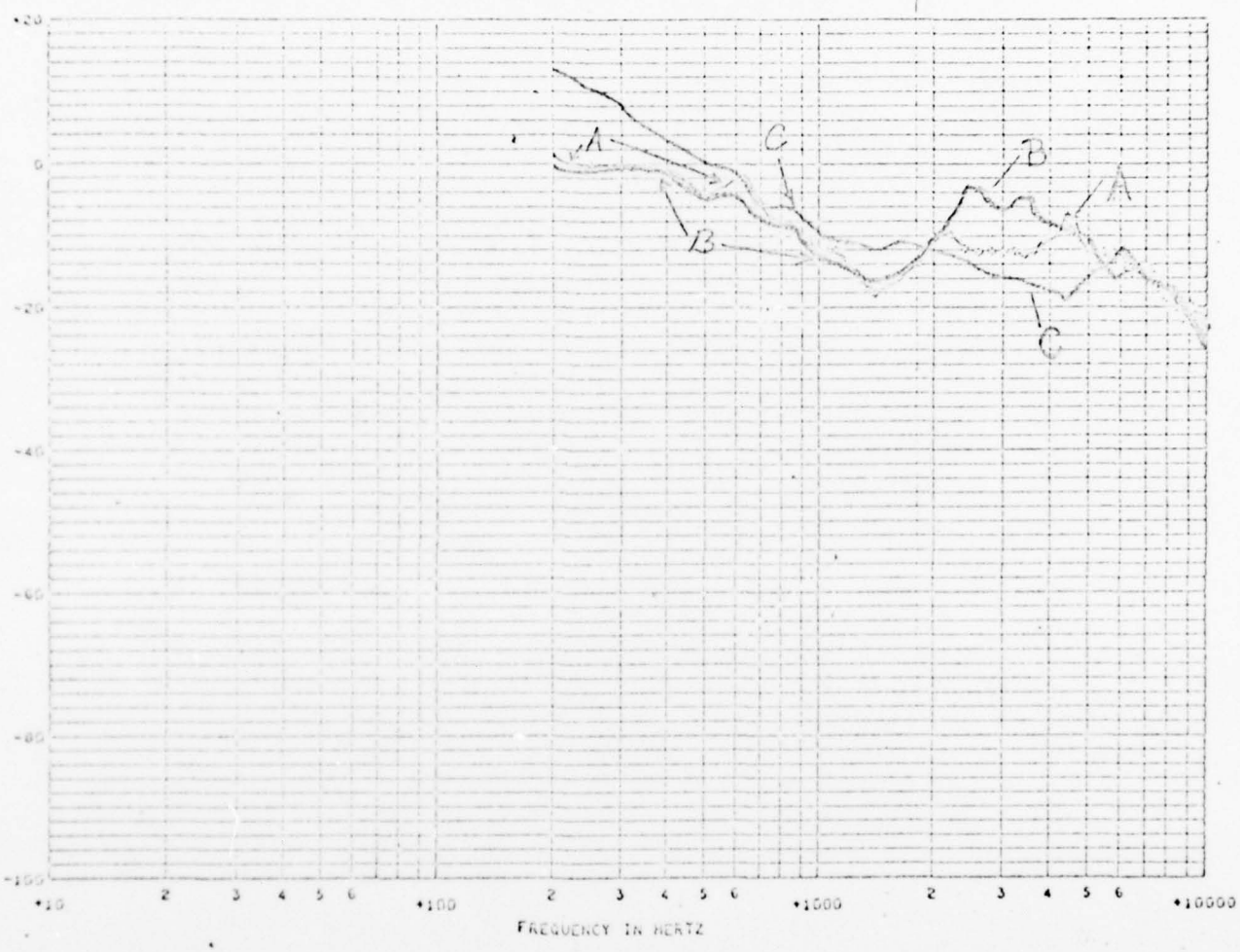

SPECTRUM DB REF 1 MICROBAR SQUARED TIMES SEC CXX LOW BAND CF100 - 70B - HIGH BAND CF100 - 68B
RUN 0660A START TIME 16027650.0 SPEED 4KT HEADING 000°
TYPE SER NO FT FROM DOW
TRG G-7 098 11.75

A= 15 KTS 0° HEADING Run 346A
B= 15 KTS 90° HEADING Run 442
C= 25 KTS 0° HEADING Run 348A
D= 25 KTS 90° HEADING - NOT SHOWN ≅ "C"

CONFIDENTIAL

Fig 321-2

1000

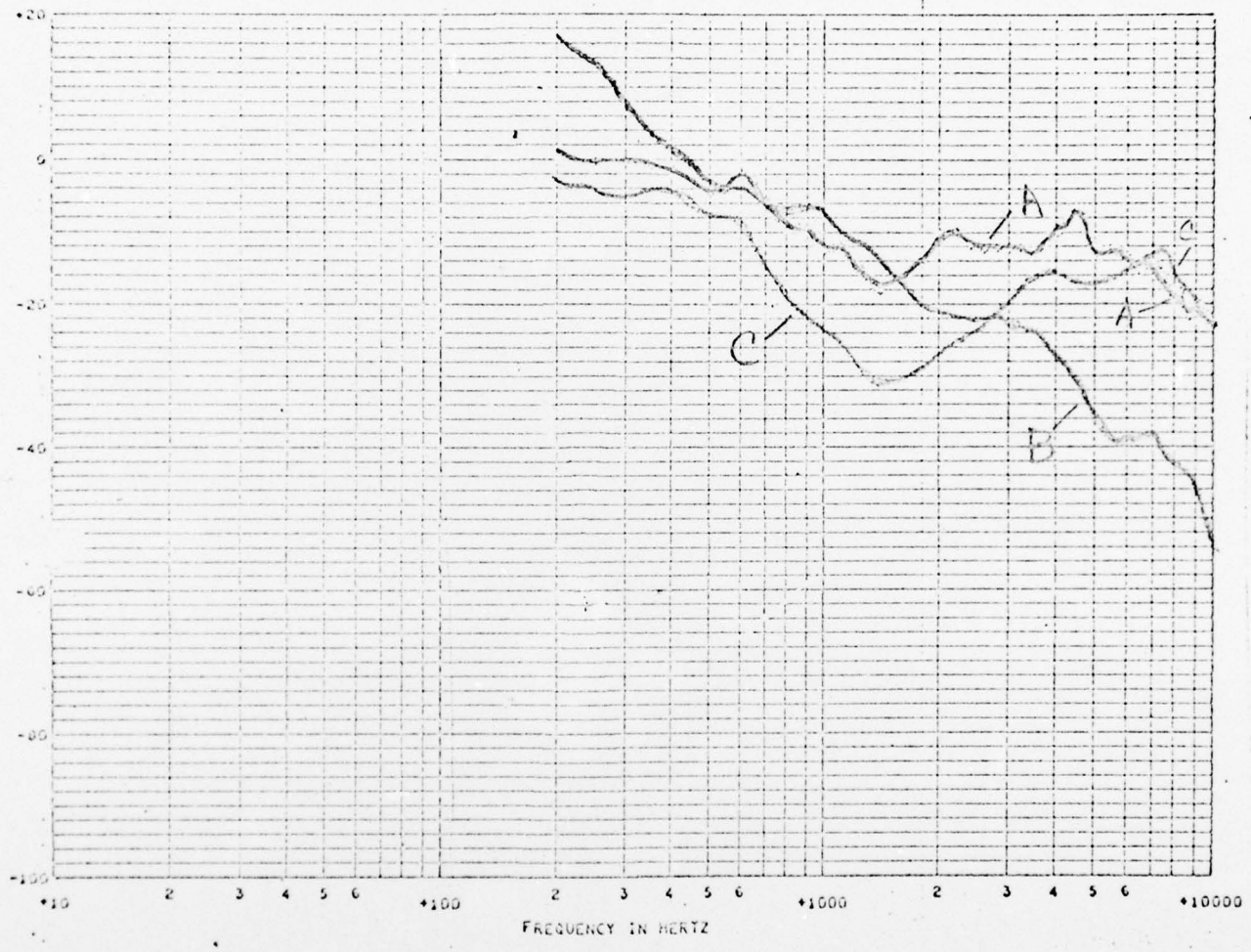

SPECTRUM DB REF 1 MICROBAR SQUARED TIMES SEC 6XX LOW BAND CF100 - 700 - HIGH BAND CF100 - 688
RUN 346A START TIME 16027050.0 SPEED 15 HEADING 000
TYPE SER NO FT FROM BOW
TRG 098 11.75

A- G-7
B- LF-7
C- G-5
} Run 346A-15 KTS

Fig 3.2.1-3

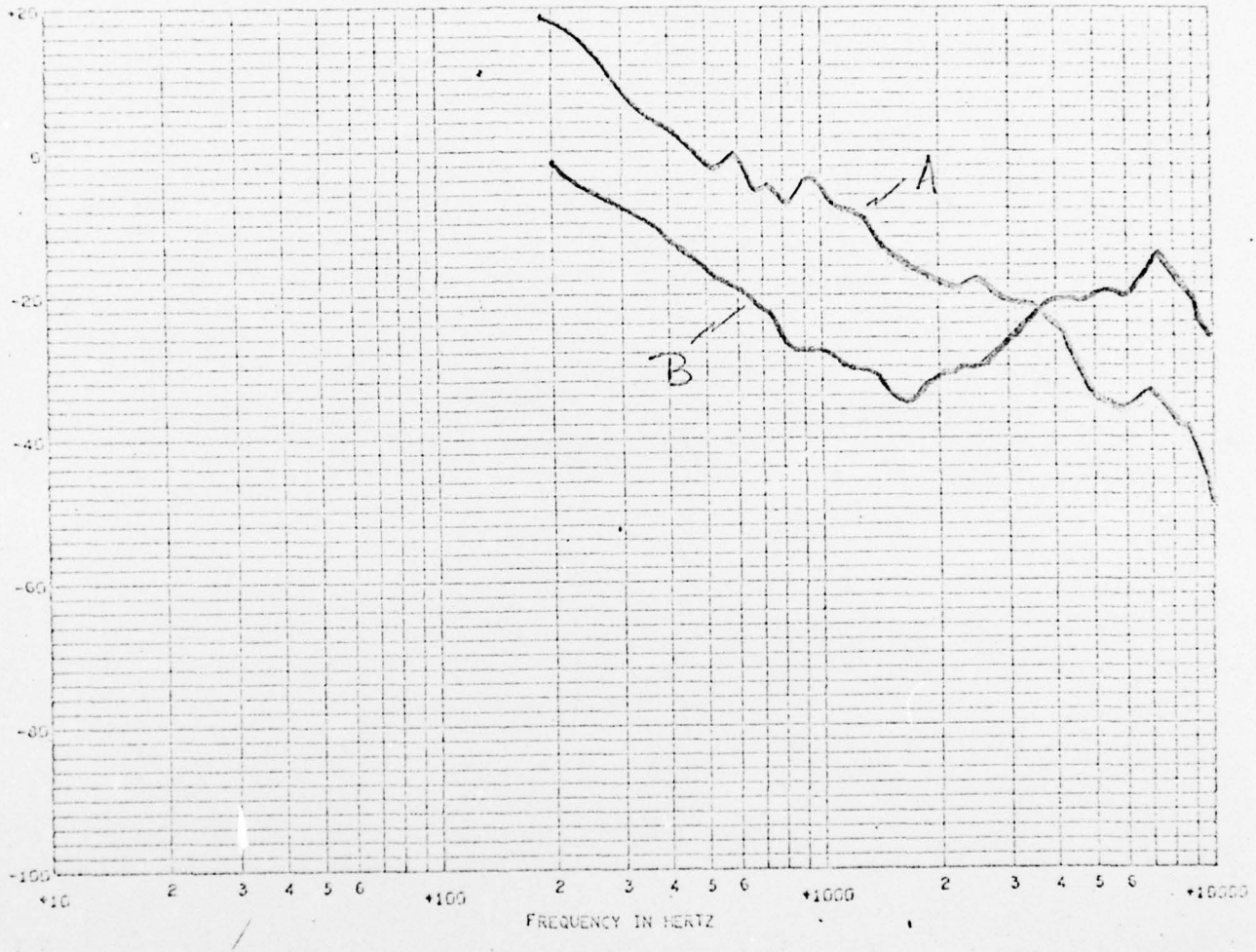

SPECTRUM DB REF 1 MICROBAR SQUARED TIMES SEC GXX LOW BAND CF222 - 38B - HIGH BAND CF222 - 110B
RUN 3[illegible] START TIME 16040930.0 SPEED 20 HEADING 000
TYPE SER NO FT FROM B.W
TRG [illegible] 093 02.75

A = LF-7 - Run 347A
B = G-5 Run 340A
} 20 KTS

Fig 5-2.1-4

CONFIDENTIAL

1083

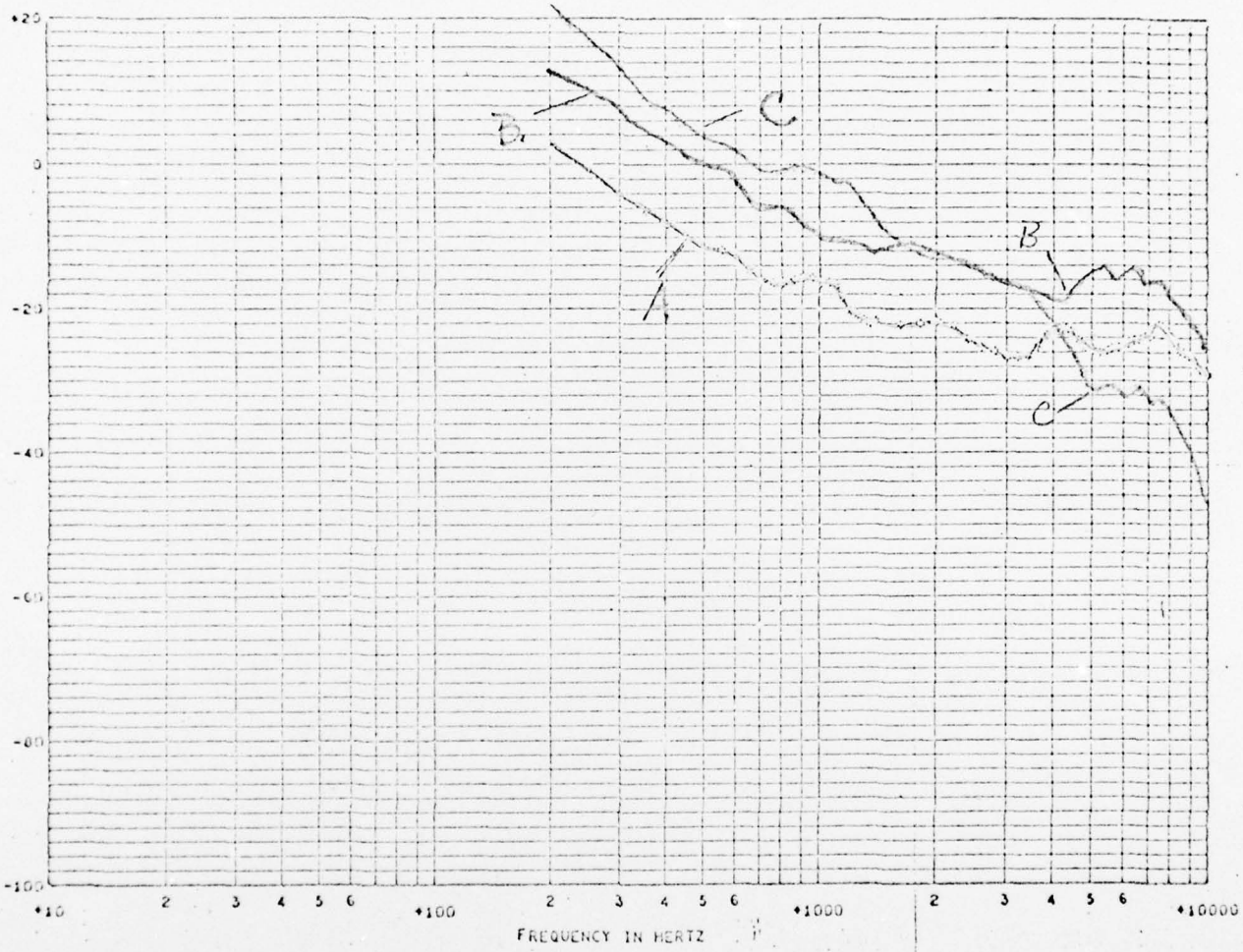

SPECTRUM DD REF 1 MICRODAR SQUARED TIMES SEC XXX LOW BAND CF100 - 79A - HIGH BAND CF100 - 81A
RUN 348A START TIME 12405630.0 SPEED 25 HEADING 000
TYPE SER NO FT FROM BOW
TRG G-5 093 11.25

A = G-5 Run 348A
B = G-7 Run 348A } 25 KTS
C = LF-7 Run 348A

CONFIDENTIAL

Fig 3.2.1-5

1100

ELEMENT-D4H

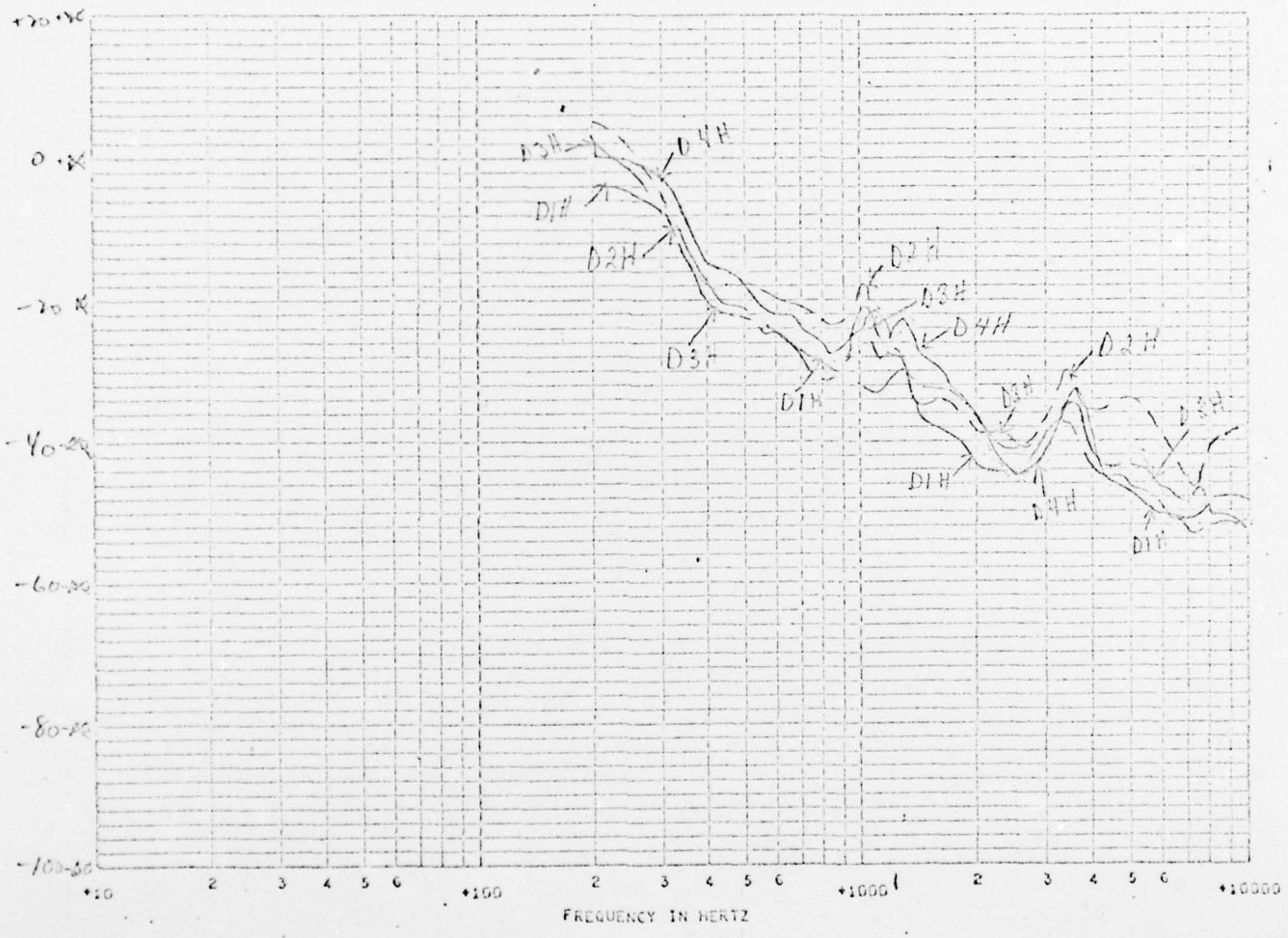

SPECTRUM DB REF 1 MICROBAR SQUARED TIMES SEC GXX LOW BAND CF56 - 108 - HIGH BAND CF56 - 148
RUN 336 START TIME 14402#10.0 SPEED 00 HEADING 000
TYPE SER NO FT FROM DOW
TRG D4H

D1H = ——— ——— ———
D2H = — — — — — —
D3H = ——— — ——— —
D4H = ———————————

} RUN 336 - 0 KTS

FIG. 3.3.1-1

3473

ELEMENT DH

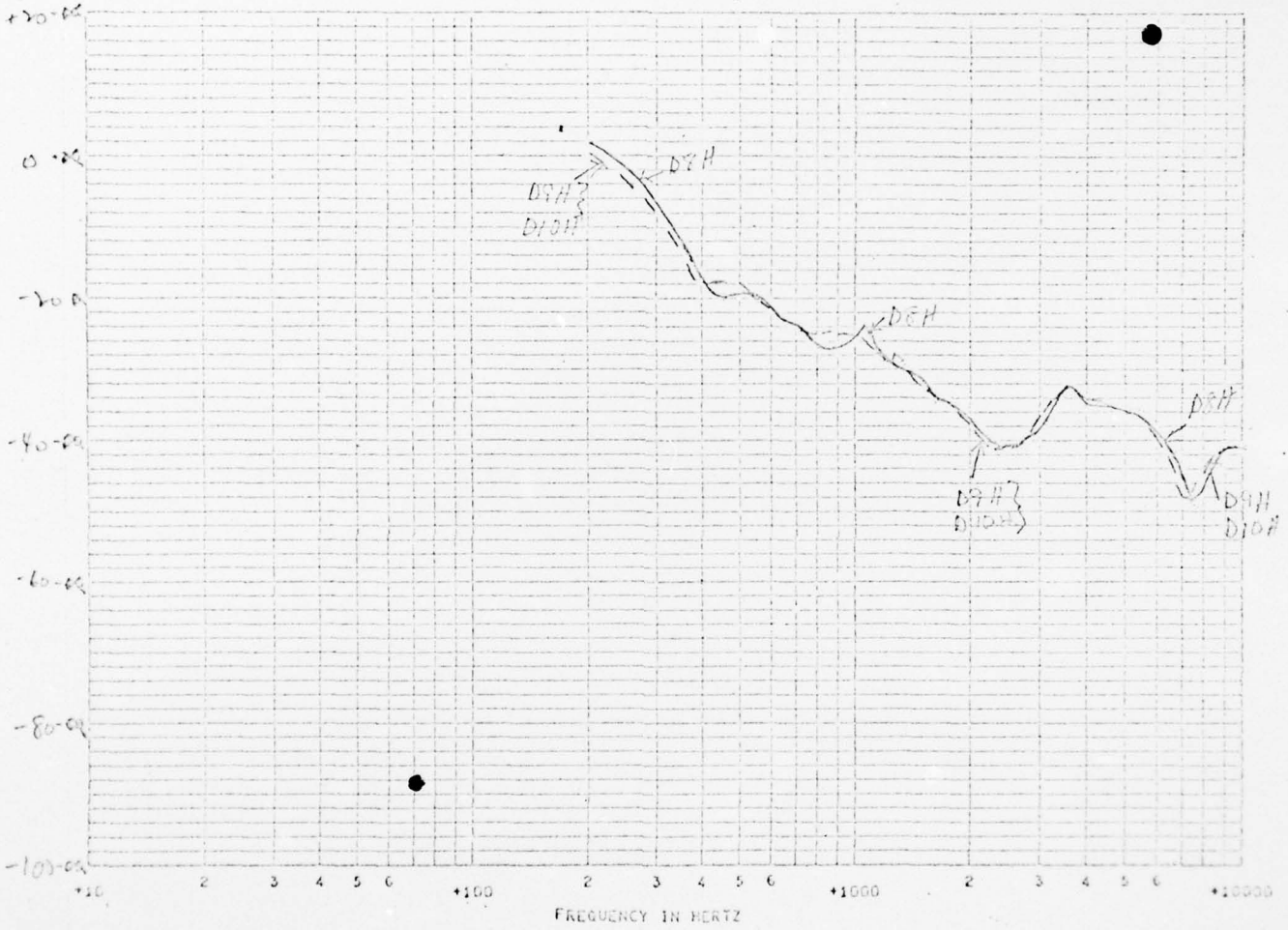

SPECTRUM DB REF 1 MICROBAR SQUARED TIMES SEC GXX LOW BAND CF56 - 110 - HIGH BAND CF56 - 150
RUN 336 START TIME 1490240.0 SPEED 00 HEADING 000
TYPE SER NO FT FROM BOW
TRG D8H

D8H =
D9H =
D10H =
RUN 336 - 0 Kts.

FIG. 3.3.1-2

AD-A044 689 CONTROL DATA CORP MELVILLE N Y TRG DIV F/G 20/1
PURVIS II SEA TRIALS PRELIMINARY DATA ANALYSIS REPORT. VOLUME I--ETC(U)
MAR 67 D CHASE, R NEWMAN NOBSR-93023
UNCLASSIFIED TRG-023-TM-67-10 NL

2 OF 2
AD
A044689

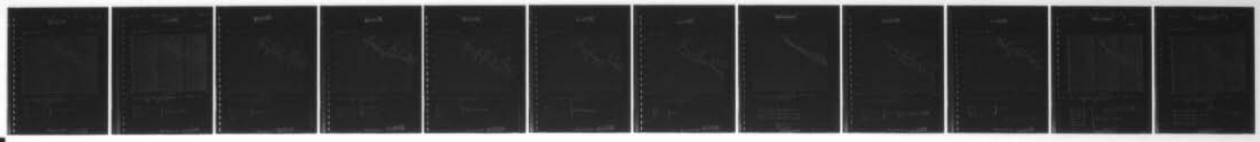

END
DATE
FILMED
10-77
DDC

D H ELEMENT - 10 Kts.

1454

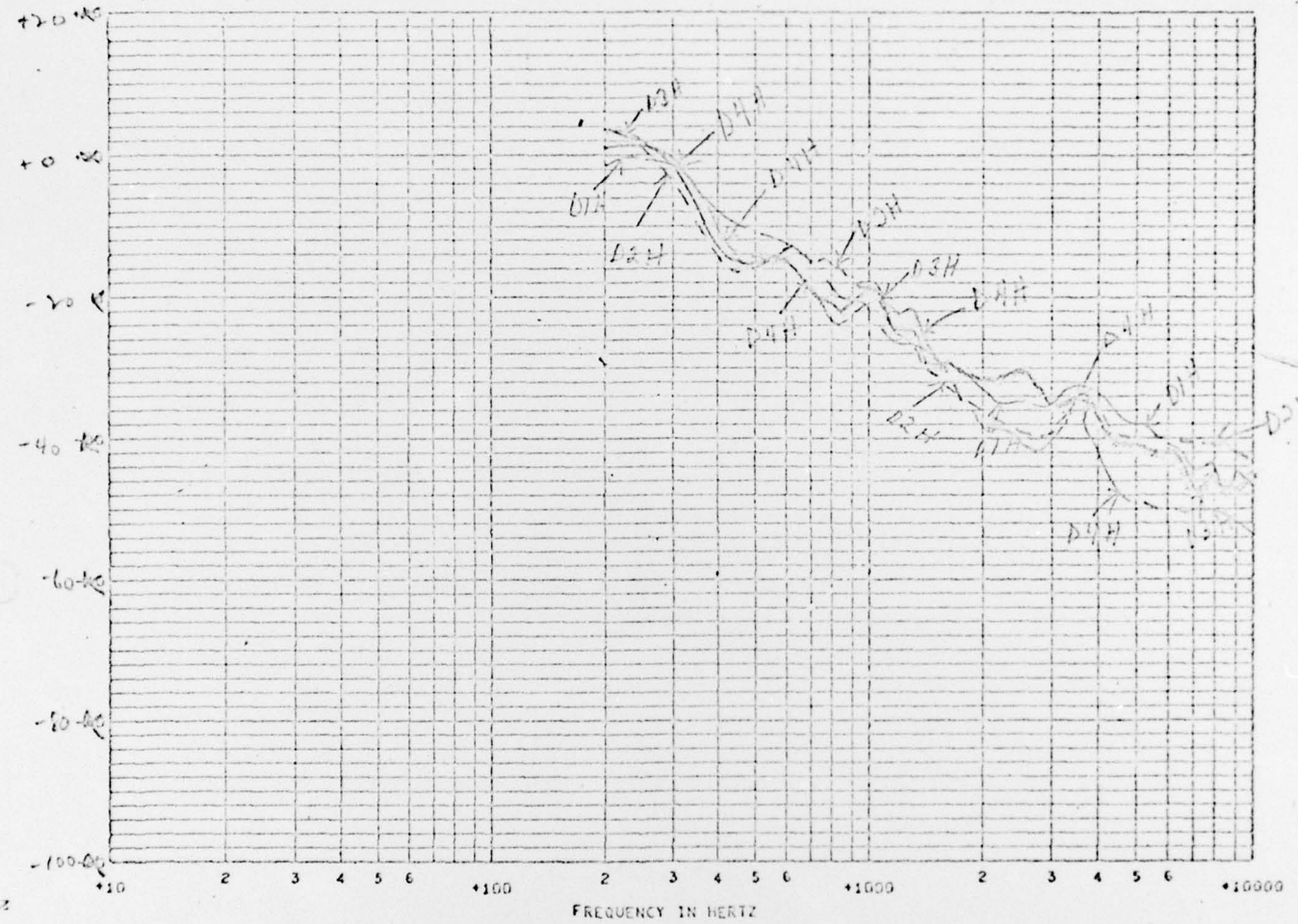

SPECTRUM DB REF 1 MICROBAR SQUARED TIMES SEC GXX LOW BAND CF56 - 30A - HIGH BAND CF56 - 20A
RUN 338 START TIME 1605:00.0 SPEED 10 HEADING 000
TYPE SER NO FT FROM BOW
TRG D3H

D1H: ——— ——— ———
D2H: - - - - - - -
D3H: ———————
D4H: ——— - ——— -

} Run 338 - 10 Kts.

FIG. 3.3.1-3

1480

DH ELEMENT - 10 Kts.

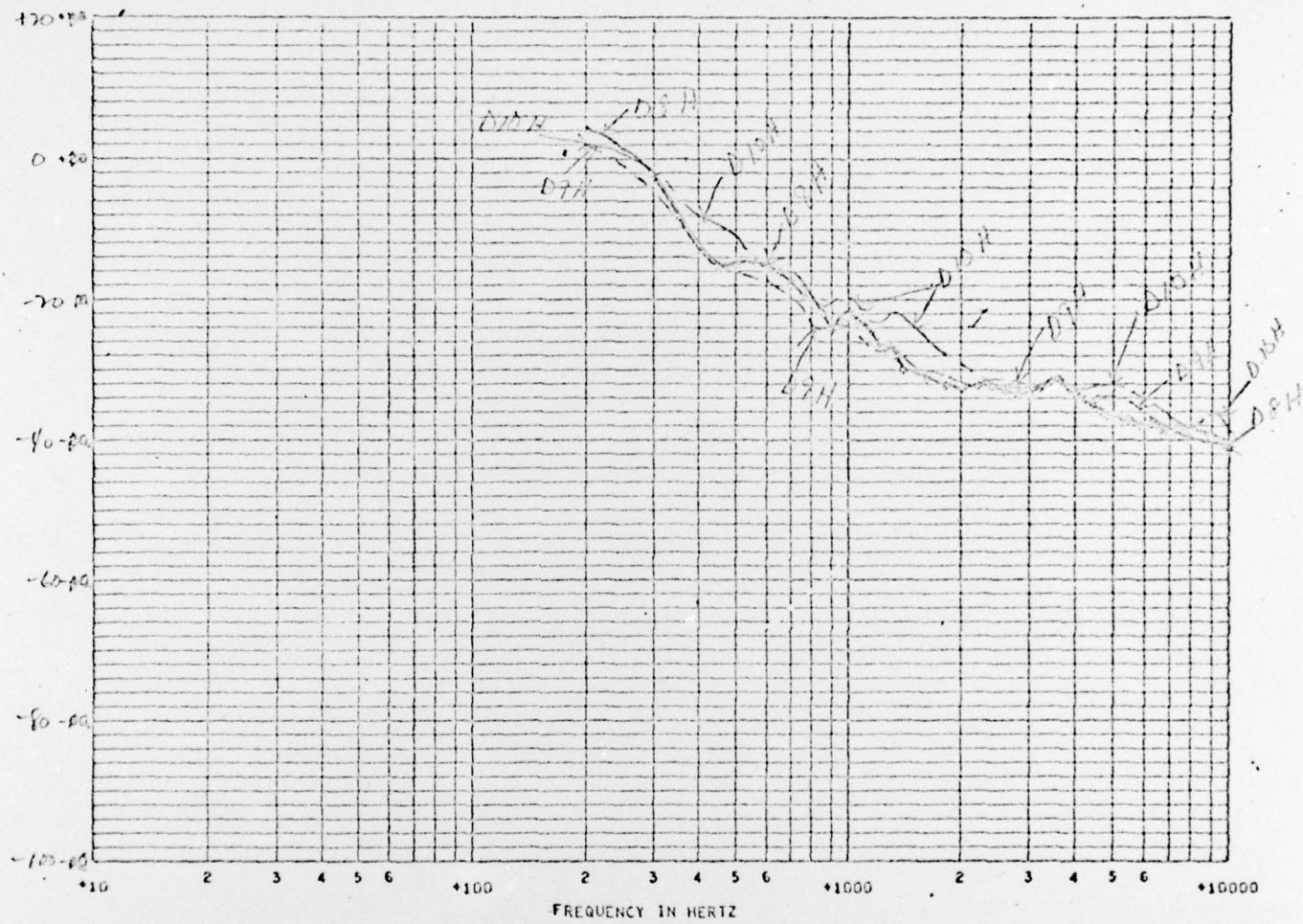

SPECTRUM DD REF 1 MICROBAR SQUARED TIMES SEC GXX LOW BAND CF56 - 31B - HIGH BAND CF56 - 27B
RUN 338 START TIME 16909400.0 SPEED 10 HEADING 000
TYPE SER NO FT FROM BOW
TRG D8H

D8H = ——————
D9H = - - - - - -
D10H = —— · ——

} Run 338 - 10 Kts.

Fig. 3.3.1-4

DH ELEMENT - 20 Kts.

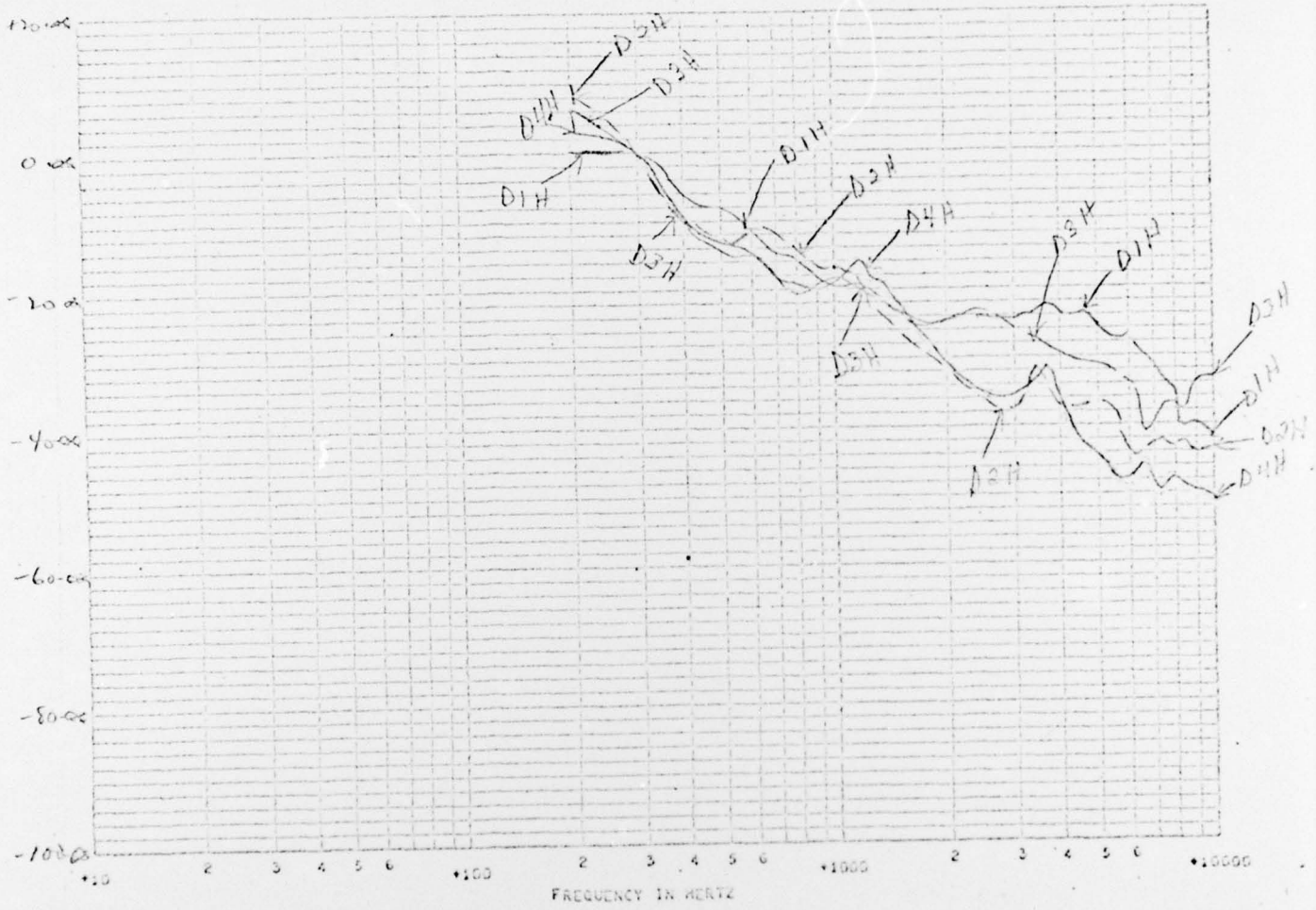

SPECTRUM DB REF 1 MICROBAR SQUARED TIMES SEC 0XX LOW BAND CPSG - 56B - HIGH BAND CPSG - 58B
RUN 340A START TIME 10946940.0 SPEED 20 HEADING 000
TYPE SER NO FT FROM BOW
TRG D4H

D1 H: ——— ———
D2 H: — — — — —
D3 H: ——— — —
D4 H: ———

RUN 340A 20 Kts

Fig. 3.3.1-5

3451

DH ELEMENT 20 KHz.

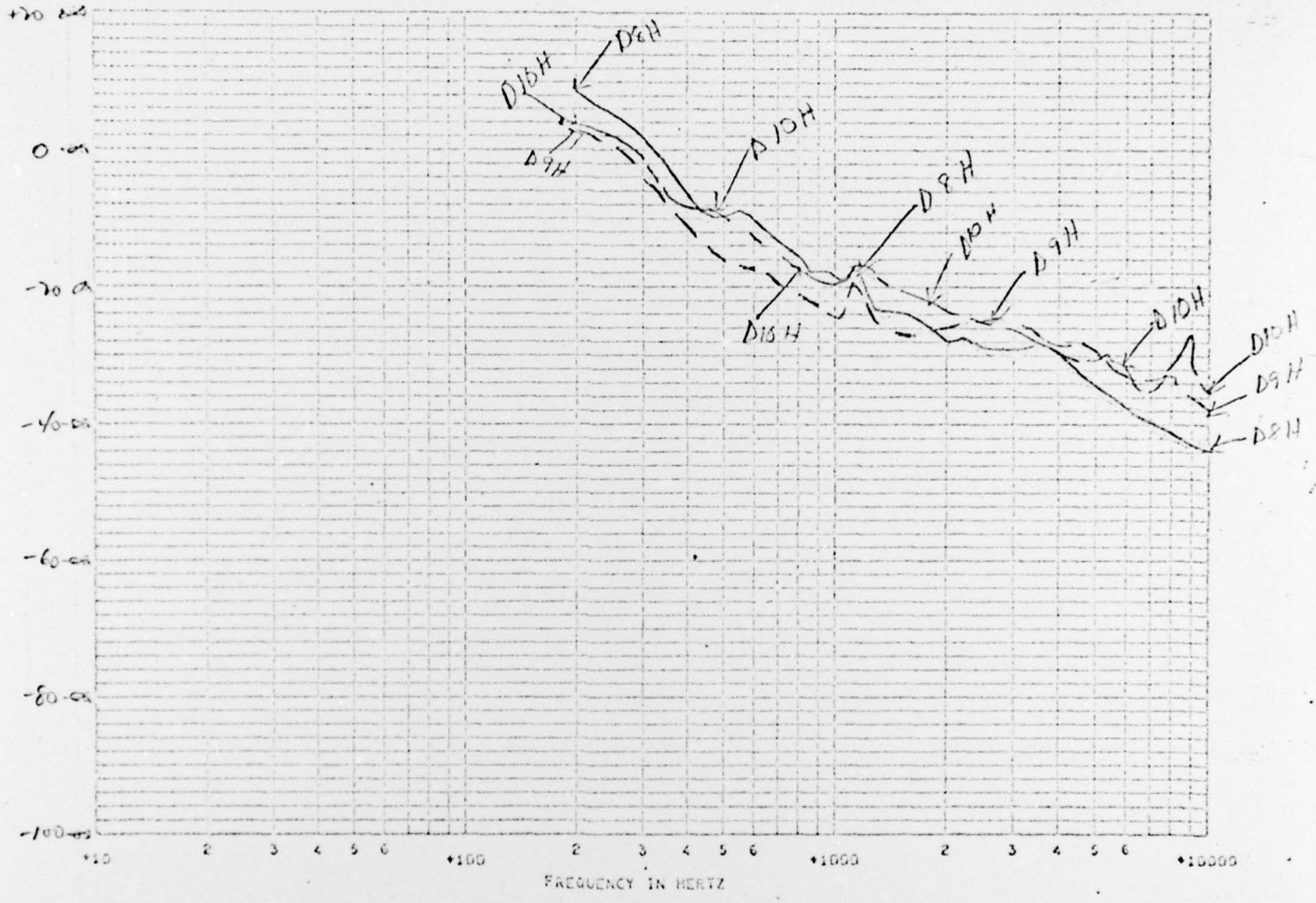

SPECTRUM DB REF 1 MICROBAR SQUARED TIMES SEC 6XX LOW BAND CF56 - 450 - HIGH BAND CF56 - 455
RUN 3400 START TIME 11050450.0 SPEED 20 HEADING 000
TYPE SER NO FT FROM DOW
TRG D8H

D8H= ——— } Run 340B
D9H= - - - -
D16H= —— - —— - } Run 340A

20 kts.

Fig. 3.3.1-6

DH ELEMENT -30 KTS

1 1403'

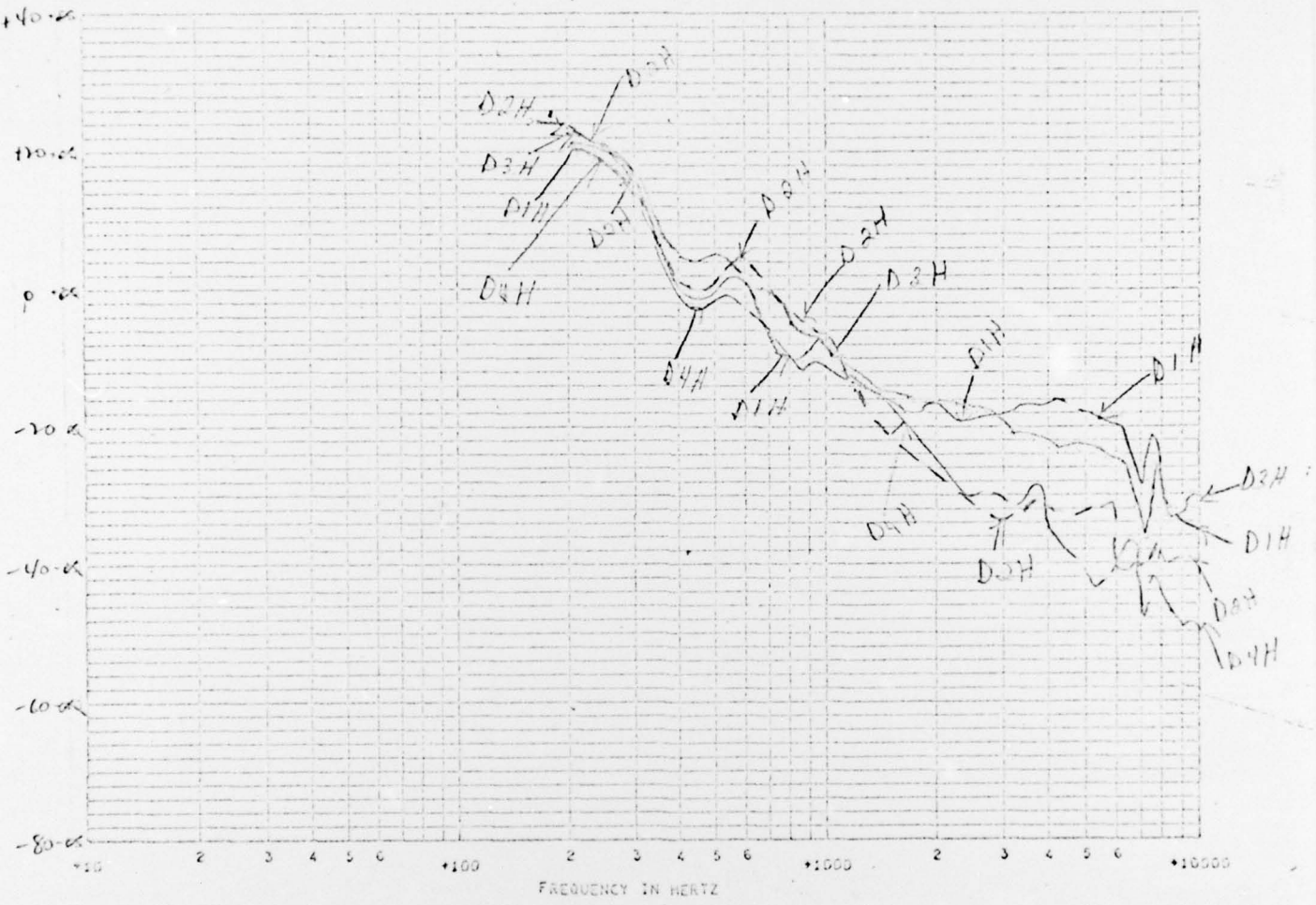

SPECTRUM DD REF 1 MICROBAR SQUARED TIMES SEC 0XX LOW BAND CP50 - 68A - HIGH BAND CP50 - 92A
RUN 342 START TIME 1544748DD.0 SPEED 30 HEADING 000
TYPE SER NO FT FROM BOW
TRG D3H

D1H =
D2H = - - - - - - - -
D3H =
D4H =

RUN 342 - 30 KTS

Fig. 3.3.1-7

DH ELEMENT - 30 KTS.

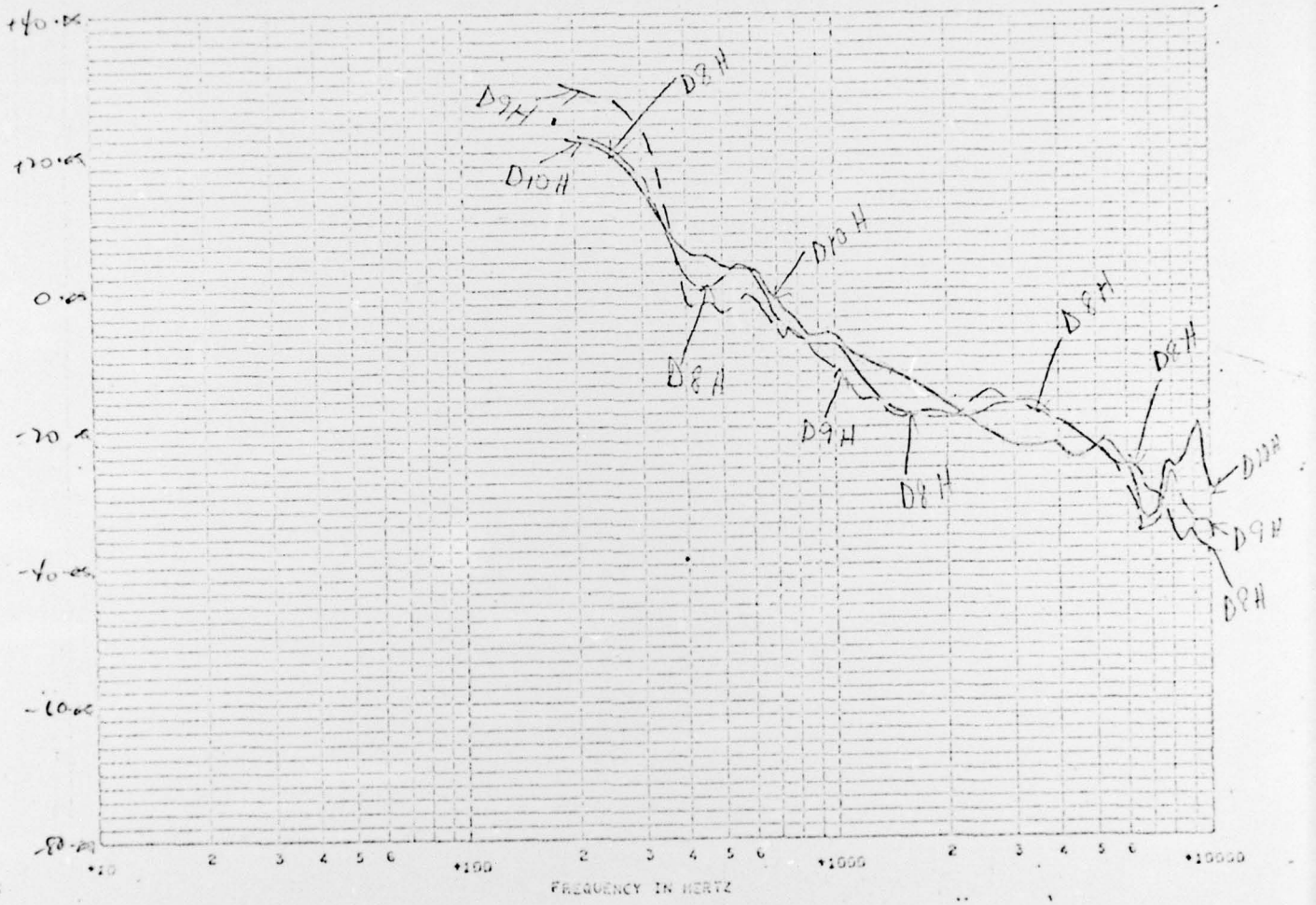

SPECTRUM DD REF 1 MICROBAR SQUARED TIMES SEC 6XX LOW BAND CF56 - 703 - HIGH BAND CF56 - 745
RUN 342 START TIME 1394700.0 SPEED 30 HEADING 000
TYPE SER NO FT FROM DOW
TRG D10H

D9H: ———— ————
D9H: — — — — —
D10H: ————————

RUN 342 - 30 KTS

Fig. 3.3.1-8

1420

ELEMENT DH

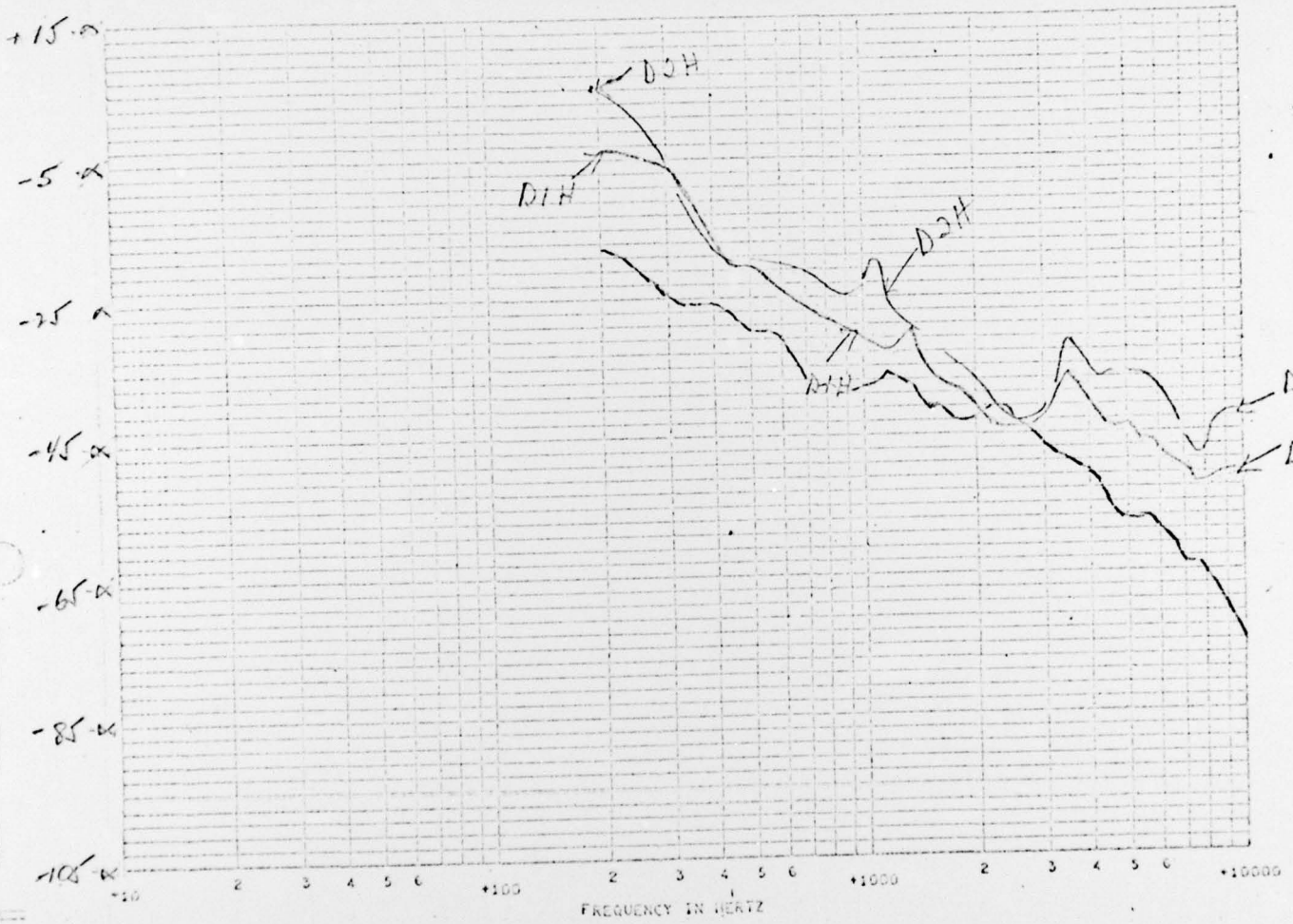

SPECTRUM DB REF 1 MICROBAR SQUARED TIMES SEC XXX LOW BAND CPSC - 90 - HIGH BAND CPSC - 130
RUN 330 START TIME 149024910.0 SPEED 00 HEADING 000
TYPE SER NO FT FROM BOW
TRG D2H D1H

D1H = ——
D2H = — — —
HF-3 = - - - -
} 0 KTS

Fig. 3.3.1-9

1791

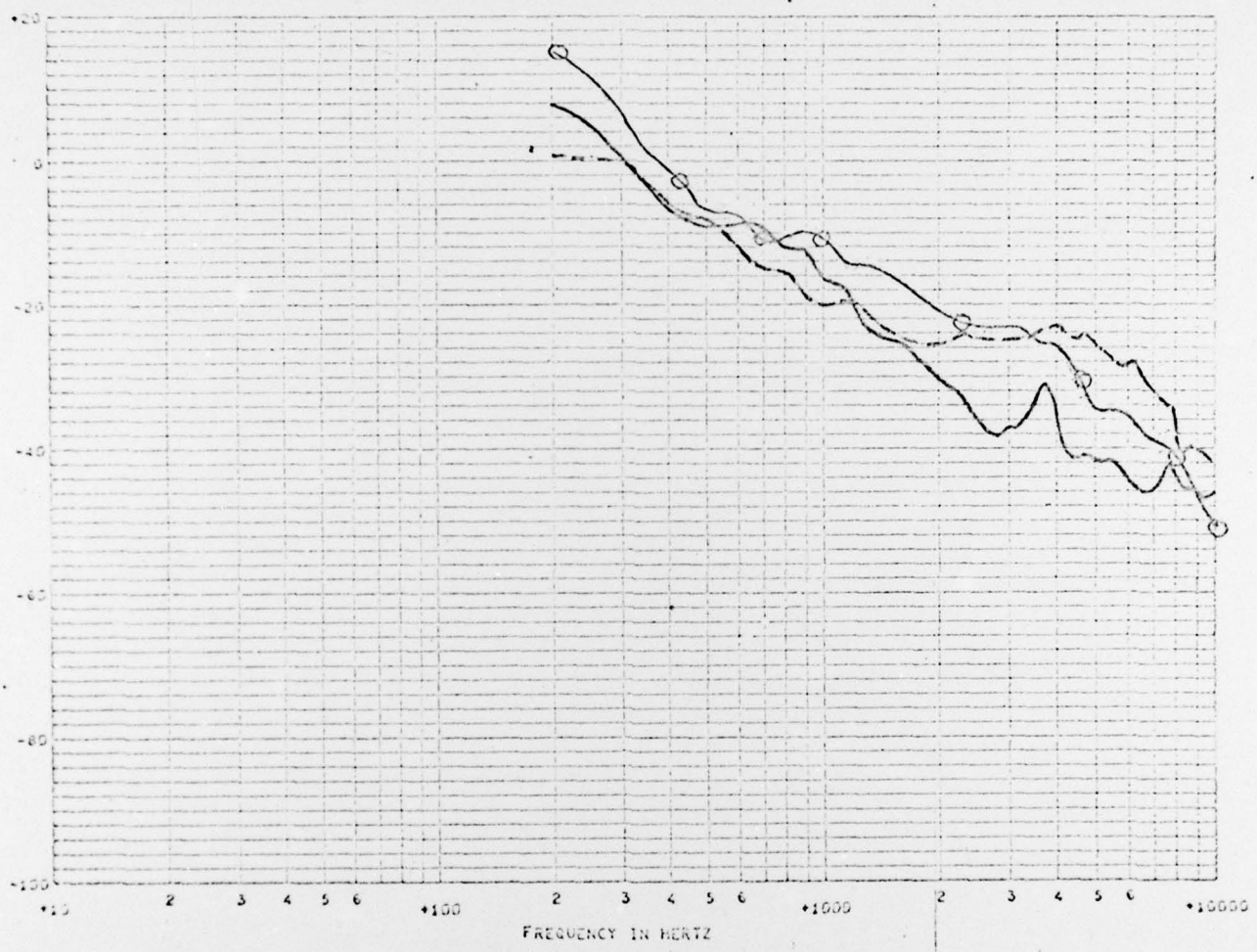

SPECTRUM DD REF 1 MICROBAR SQUARED TIMES SEC GXX LOW BAND CF56 - 330 - HIGH BAND CF56 - 348
RUN 340A START TIME 16940940.0 SPEED 20 HEADING 000

TYPE	SER NO	FT FROM DOW
TRG	HF-3	026 09.75

D1H, 20 KTS, RUN 340A - - - -
D2H, 20 KTS, RUN 340B ——
HF-3, 20 KTS, RUN 340A —o—o—

Fig. 3.3.1-10
(corrected)

1466

ELEMENT D11

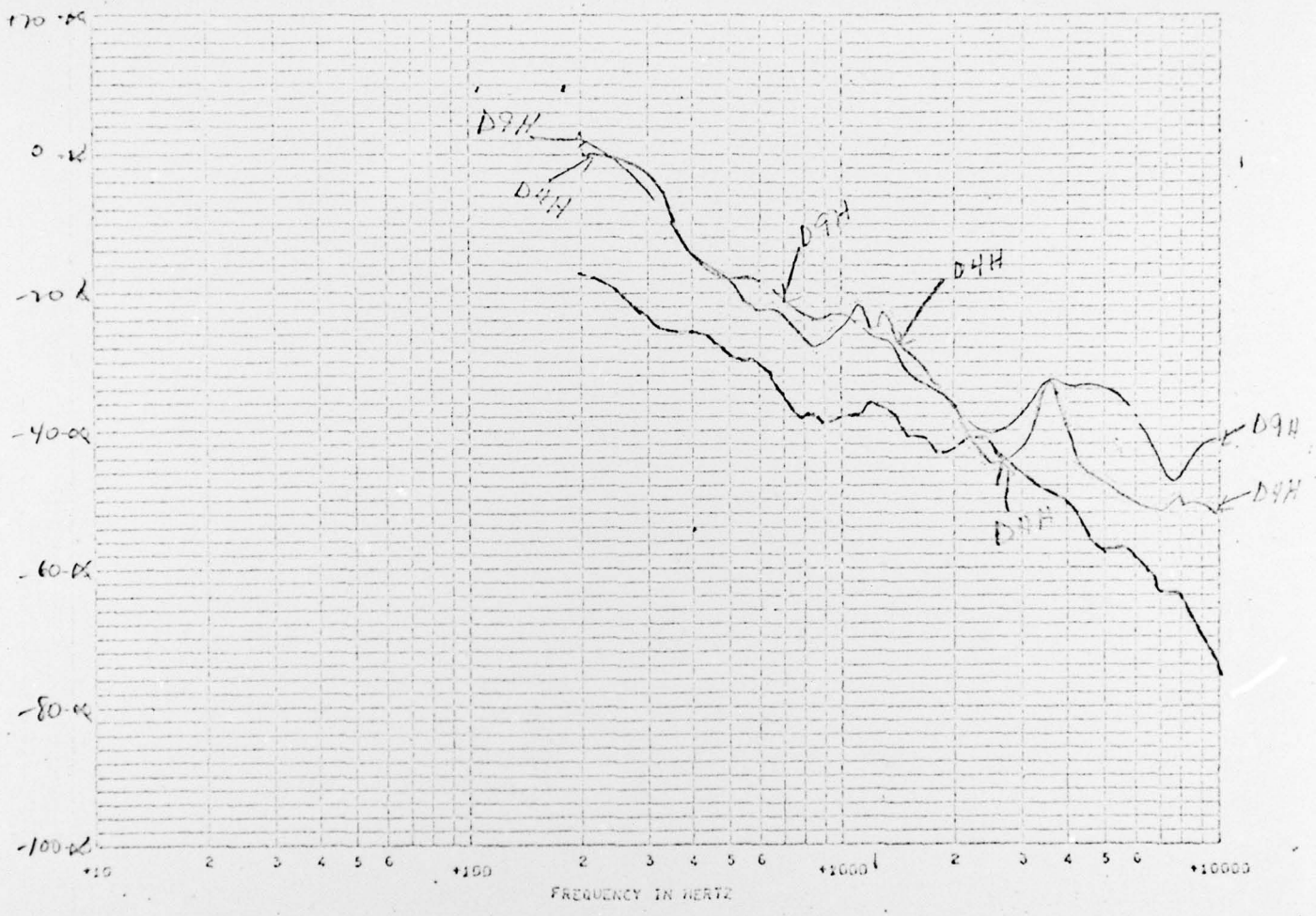

SPECTRUM DB REF 1 MICROBAR SQUARED TIMES SEC GXX LOW BAND CF56 - 100 - HIGH BAND CF56 - 140
RUN 336 START TIME 144024:10.0 SPEED 00 HEADING 000
TYPE SER NO FT FROM BOW
TRG D4H

D4H = ——————
D9H = ——————
HF-3 = - - - - - - -
} 3 Kts.

Fig. 3.3.1-11

ELEMENT DH - 20 kts

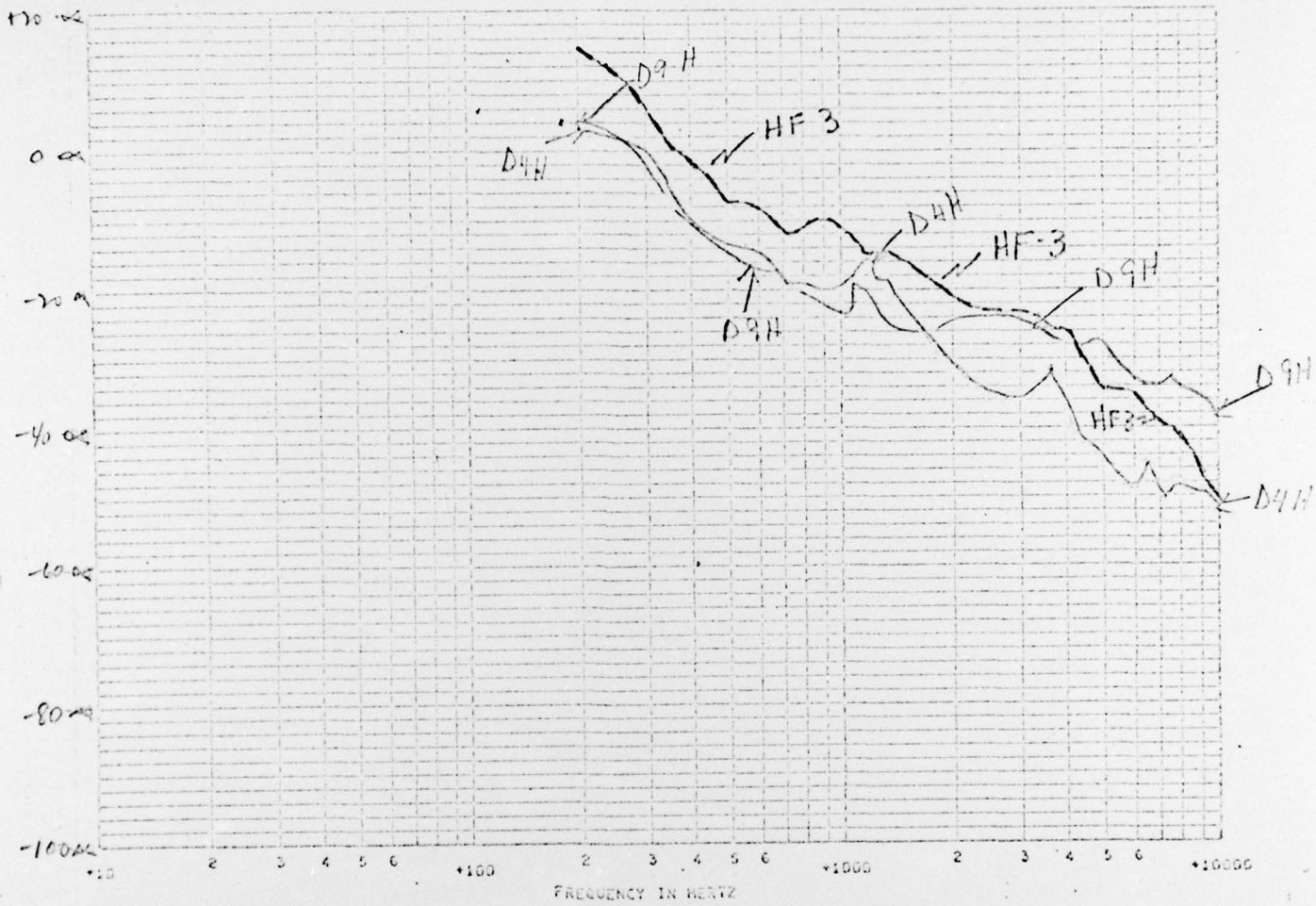

SPECTRUM DB REF 1 MICROBAR SQUARED TIMES SEC GXX LOW BAND CPSG - 560 - HIGH BAND CPSG - 500
RUN 340A START TIME 1644640.0 SPEED 20 HEADING 000
TYPE SER NO FT FROM BOW
TRC D4H

D4H : ——————
D9H : — — —
HF-3 : - - - - - -
} 20 kts

FIG. 3.3.1-12

1432

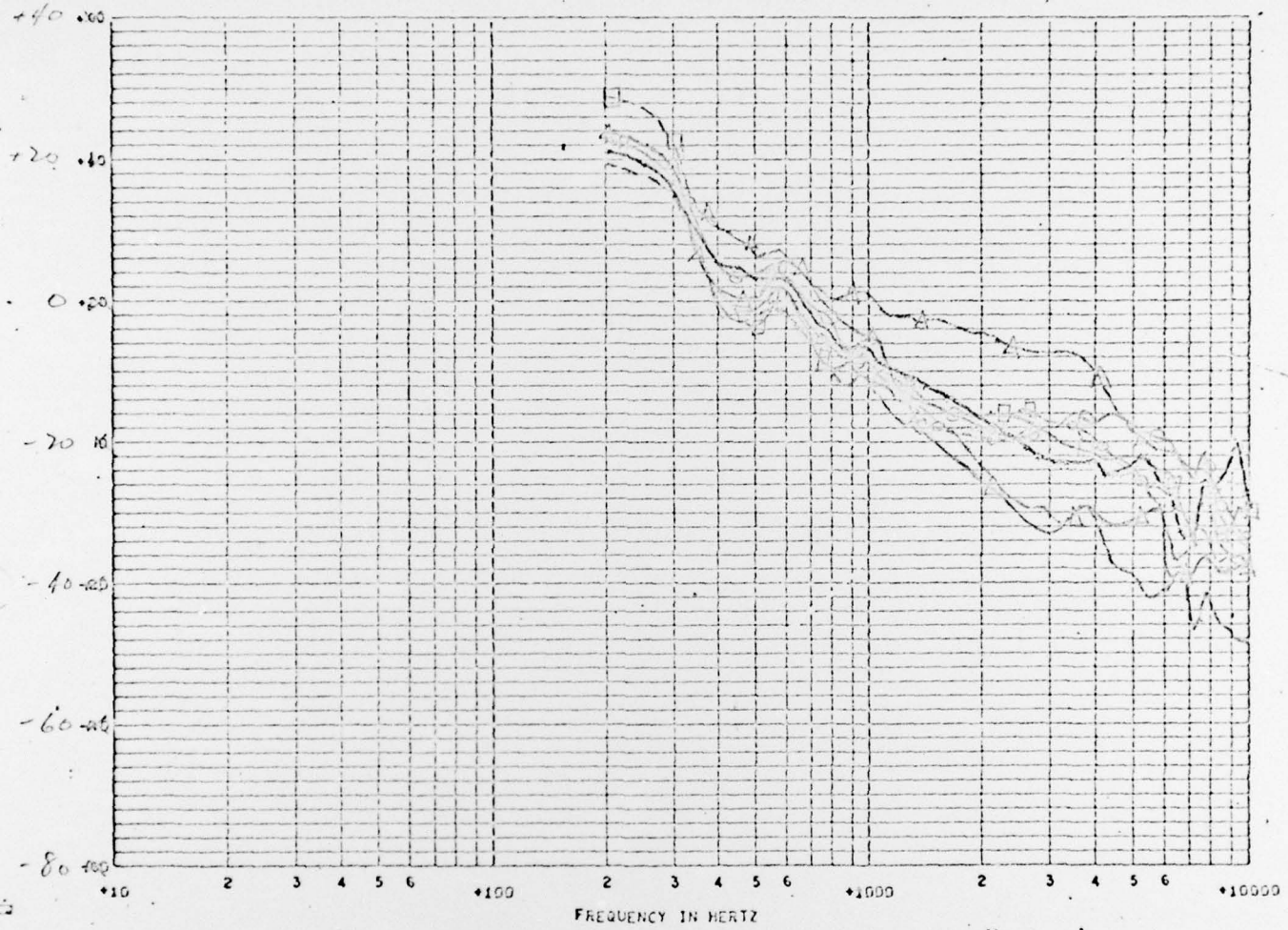

SPECTRUM DB REF 1 MICROBAR SQUARED TIMES SEC GXX LOW BAND CF56 - 70B - HIGH BAND CF56 - 74B
RUN 342 START TIME 13947400.0 SPEED 30 HEADING 000
TYPE SER NO FT FROM BOW
TRG D10H

D1H
D2H
D3H
D4H
D8H
D9H
D10H
HF-3

RUN 342 - 30 KTS

Fig. 3.3.1-13

ELEMENT: DIOH

1492

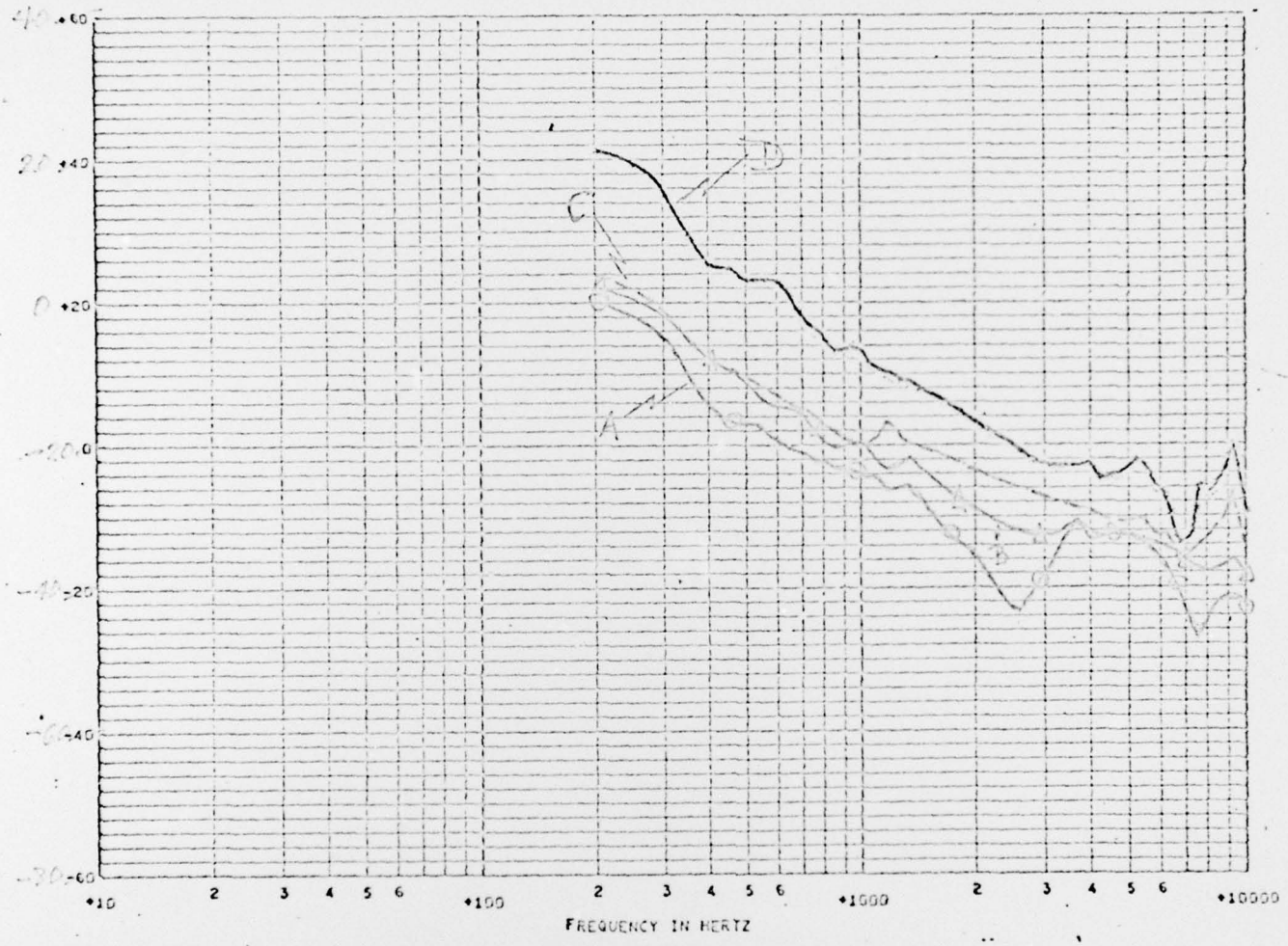

SPECTRUM DB REF 1 MICROBAR SQUARED TIMES SEC GXX LOW BAND CF56 - 70B - HIGH BAND CF56 - 74B
RUN 342 START TIME 13347400.0 SPEED 30 HEADING 000

TYPE	SER NO	FT FROM DOW
TRG	DIOH	

A: 0 KTS, RUN 336 ——o——o——

B: 10 KTS, RUN 338 ——Δ——Δ——

C: 20 KTS, RUN 340A - - - -

D: 30 KTS, RUN 342 ————

Fig. 3.3.1-14

~~CONFIDENTIAL~~ UNCLASSIFIED

1476

ELEMENT: D4H

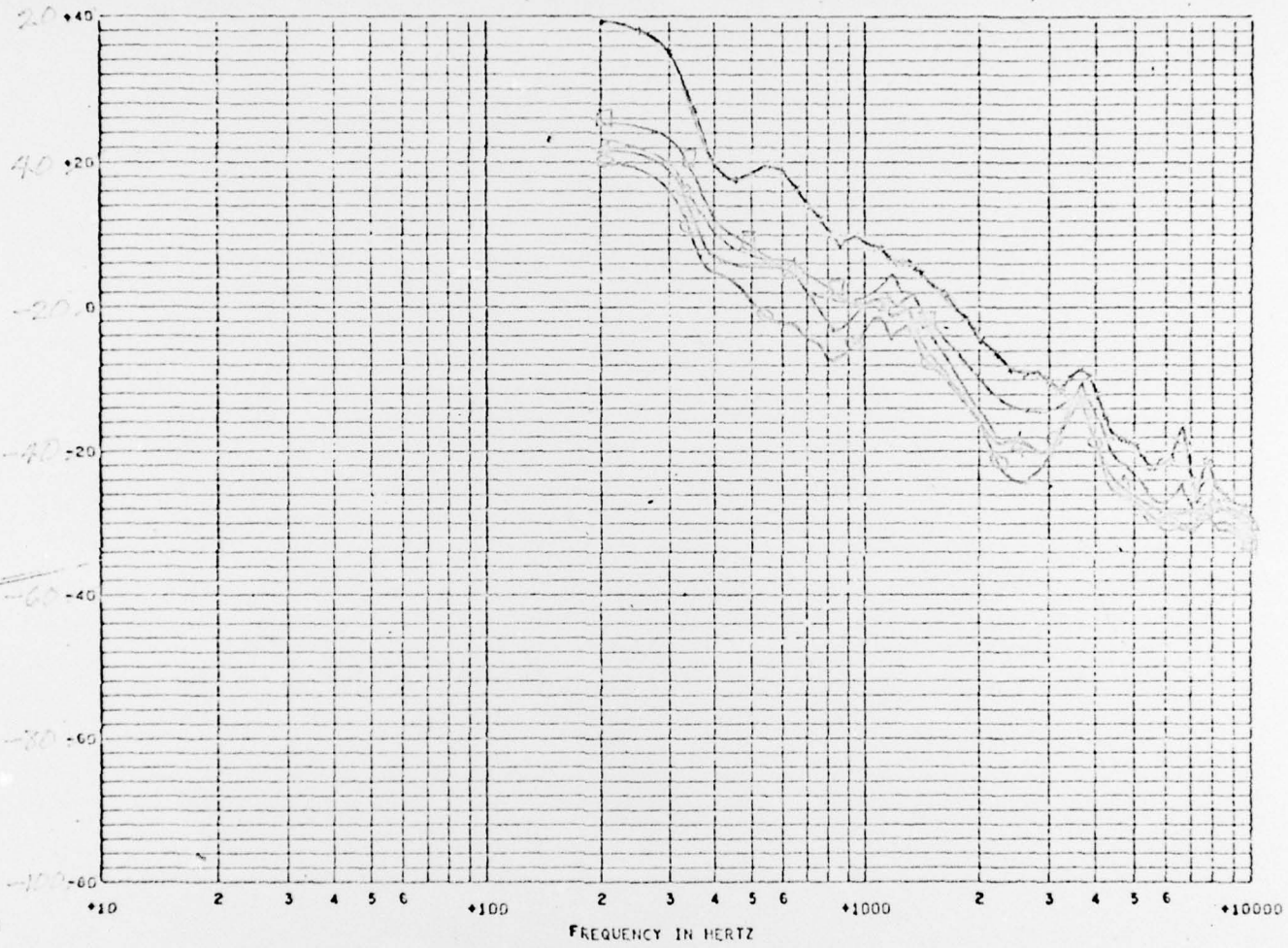

SPECTRUM DB REF 1 MICROBAR SQUARED TIMES SEC GXX LOW BAND CF56 - 68D - HIGH BAND CF56 - 72B
RUN 342 START TIME 13947400.0 SPEED 30 HEADING 000
TYPE SER NO FT FROM BOW
TRG D4H

A: 0 KTS, RUN 336
B: 10 KTS, RUN 338
C: 15 KTS, RUN 339A
D: 20 KTS, RUN 340A
E: 30 KTS, RUN 342

UNCLASSIFIED

Fig. 3.3.1-15

~~CONFIDENTIAL~~

~~CONFIDENTIAL~~ UNCLASSIFIED

ELEMENT: D9H

1487

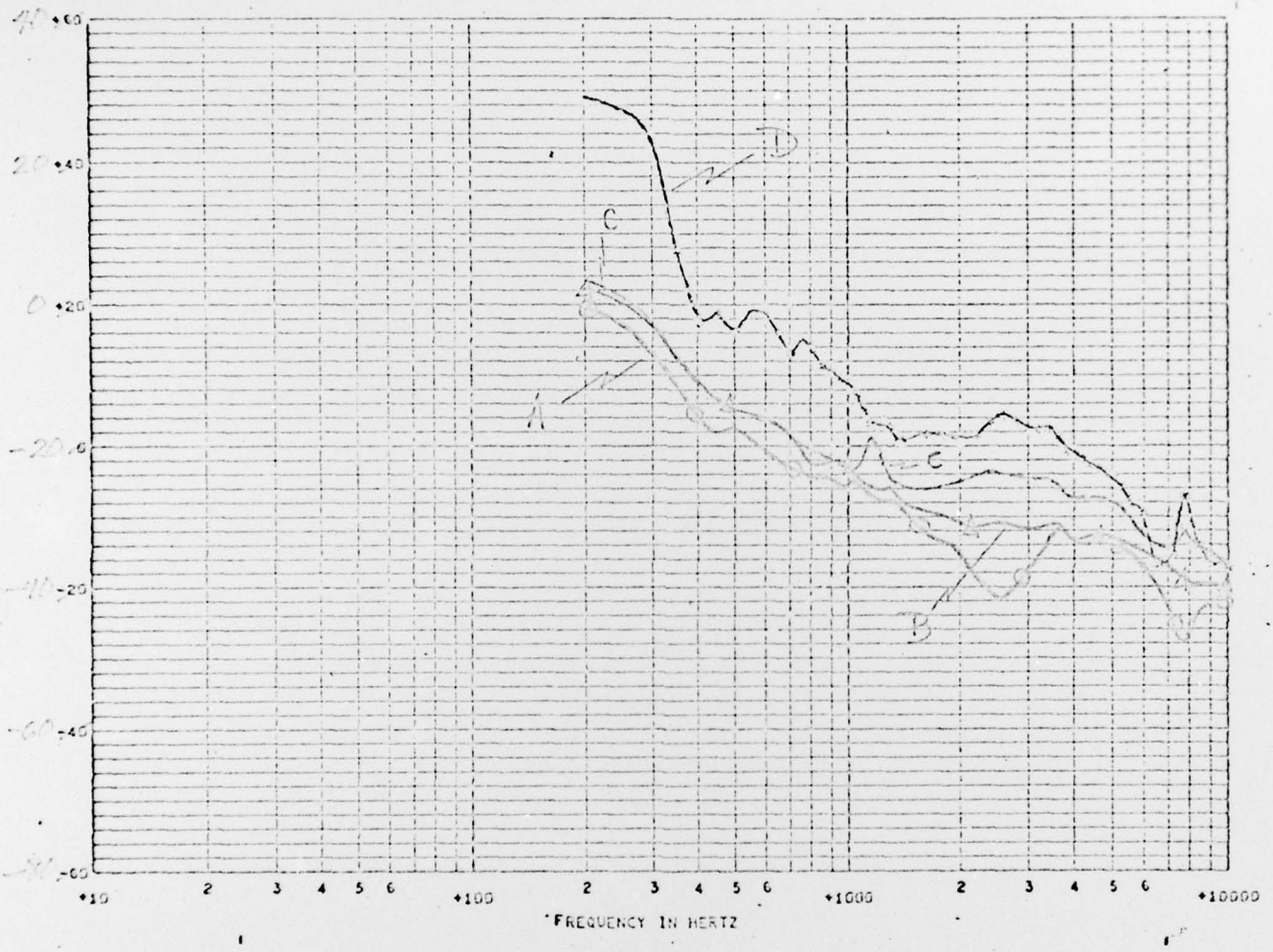

SPECTRUM DB REF 1 MICROBAR SQUARED TIMES SEC 0XX LOW BAND CP56 - 70A - HIGH BAND CP56 - 74A
RUN 342 START TIME 1347900.0 SPEED 30 HEADING 000
TYPE SER NO FT FROM BOW
TRG D9H

A: 0 KTS, Run 336 ——o——o——

B: 10 KTS, Run 338 ——Δ——Δ——

C: 20 KTS, Run 340A — — — —

D: 30 KTS, Run 342. ————————

UNCLASSIFIED

Fig 3.3.1-16

~~CONFIDENTIAL~~